AD NUMBER

AD514934

CLASSIFICATION CHANGES

TO: unclassified

FROM: confidential

LIMITATION CHANGES

TO:

Approved for public release, distribution unlimited

FROM:

AUTHORITY

DTRA ltr, 6 May 99; DTRA ltr, 6 May 99

(1)

CONFIDENTIAL

DASA 2627
TRW-16118-6002-R7-00
APRIL 1971

AN ANALYSIS OF BLAST WAVE LAMINAR BOUNDARY LAYERS AND PARTICLE ENTRAINMENT (U)

by

VICTOR QUAN
RICHARD M. TRACI
JOHN L. FARR

Prepared for

DEFENSE ATOMIC SUPPORT AGENCY
WASHINGTON, D.C. 20305
UNDER CONTRACT DASA01-70-C-0135

CONFIDENTIAL

When this report is no longer needed, Department of Defense organizations will destroy it in accordance with appropriate procedures. Contractors will destroy the report according to the requirements of the Industrial Security Manual for Safeguarding Classified Information.

CONFIDENTIAL

DASA 2627
TRW-16118-6002-R7-00
Total Pages: 160

AN ANALYSIS OF BLAST WAVE LAMINAR BOUNDARY LAYERS AND PARTICLE ENTRAINMENT (U)

This work was sponsored by
DEFENSE ATOMIC SUPPORT AGENCY
under NWER Subtask SA 001

by

VICTOR QUAN
RICHARD M. TRACI
JOHN L. FARR

APRIL 1971

Prepared for

DEFENSE ATOMIC SUPPORT AGENCY
WASHINGTON, D.C. 20305
UNDER CONTRACT DASA01-70-C-0135

TRW SYSTEMS GROUP

ONE SPACE PARK · REDONDO BEACH, CALIFORNIA 90278

CONFIDENTIAL

This report is classified CONFIDENTIAL, Group 3
based on the aggregate contents of the document

(THIS PAGE IS UNCLASSIFIED)

FOREWORD

The analyses described in this report were performed by TRW Systems Group for the Defense Atomic Support Agency under Contract DASA01-70-C-0135, Blast Wave Boundary Layers and Particle Entrainment. This final report consists of two separate parts. Part I contains the results of the boundary layer study, and Part II describes the results of the particle entrainment investigation. The first part is independent of the second, while the second part occasionally refers to the first.

V. Quan was the project engineer, and R.M. Traci and J.F. Farr, Jr. contributed significantly to this study. J.E. Melde and V.R. Hyman also contributed to the numerical results. The interest and support of H.J. Carpenter and C.W. Busch in this work are acknowledged. The DASA technical monitor was C.B. McFarland.

PART I

BLAST WAVE LAMINAR BOUNDARY LAYERS

(Reverse of Page is Blank)

ABSTRACT

The laminar boundary layer flowfields generated by plane, cylindrical, and spherical strong blast waves are studied. Solutions are obtained using two different methods. In the first method, the governing equations are reduced to ordinary differential equations by using a similarity transformation and a parametric integral technique. In the second method, the assumptions of quasi-steady state and local similarity are invoked. Results obtained using each method are presented. A method of solving the turbulent boundary layer equations is also outlined in detail in this report.

CONTENTS OF PART I

ILLUSTRATIONS

ILLUSTRATIONS (Continued)

ILLUSTRATIONS (Continued)

NOMENCLATURE

A = constant defined by Equation (3-3)

c_p = specific heat at constant pressure

C = constant related to explosion strength

F = function given by Equation (A-5)

h = specific enthalpy

k = conductivity

ℓ = distance in η at which the velocity reaches $(1-e^{-1})$ of the local free-stream value.

ℓ_t = distance in η at which the temperature reaches $(1-e^{-1})$ of the local free-stream value.

m = geometry factor, = $2/(3+\bar{\sigma})$

p = pressure

Pr = Prandtl number, = $\mu c_p/k$

q_w = heat flux to the wall

Q = time scaling factor defined by Equation (5-4)

R = function given by Equation (A-4)

t = time

u = velocity in x-direction

u_s = shock velocity

v = velocity in y-direction

V = function defined by Equation (A-6)

W = time scaling factor defined by Equation (5-7)

x = distance along surface from explosion point

x_s = distance between shock and explosion point

y = distance normal to surface

y_δ = boundary layer velocity thickness

NOMENCLATURE (Continued)

y_{δ_t} = boundary layer temperature thickness

α = geometry factor, = (m-1)/m

γ = specific heat ratio

δ = distance in η at which local free-stream velocity is reached

δ_t = distance in η at which local free-stream temperature is reached

η = transformed coordinate defined by Equation (3-2b)

μ = viscosity

ξ = transformed coordinate defined by Equation (3-2a)

ρ = density

τ = transformed coordinate defined by Equation (3-2c)

τ_w = shear stress at the wall

σ = 0 for two-dimensional boundary layer and 1 for axisymmetric boundary layer

$\bar{\sigma}$ = 0, 1, and 2 for plane, cylindrical, and spherical shock, respectively.

ϕ = function given by Equation (A-3)

ψ = stream function defined by Equation (3-1)

Subscripts

e = free-stream (at edge of boundary layer)

w = wall condition

η = derivative with respect to η

ξ = derivative with respect to ξ

∞ = ambient condition

(Reverse of Page is Blank)

1. INTRODUCTION

The occurence of an intense explosion at or near the earth's surface results in a complex fluid-surface interaction. The main characteristics of such an explosion are indicated in Figure 1-1. The intensely hot, low density region of air and vaporized earth form what is known as the fireball shortly after burst. Within seconds the fireball begins to rise due to its buoyancy, carrying with it large amounts of vaporized and pulverized surface material. As it rises it is cooled by entraining ambient air and by radiation to the surrounding air and surface. In the meantime the explosion is communicated to the surrounding air by the advancing shock front. A more extensive description of the explosion phenomena is given by Brode.[1*] The fluid-surface interaction can result in large amounts of ground material being lifted into the air. Several such lofting mechanisms, including vaporization, crater splashing, thermal expansion, elastic rebound, jetting from cracks, and aerodynamic entrainment, have been identified by Trulio and others.[2]

Of prime interest to this study is the boundary layer produced by the spherically expanding shock wave flowfield. In order to assess the aerodynamic entrainment of surface materials, it is necessary to determine the boundary layer shear stress on the surface. Also, boundary layer properties are required for the design of surface and subsurface installations which are hardened to the thermal and dynamic environment of the blast wave. Antennas, silo closures, and air entrainment systems are examples of such facilities. Knowing the boundary layer properties such as the velocity and temperature profiles, one can calculate the aerodynamic forces on the facilities. Test techniques such as (proposed) NEST

*Superscripts indicate references.

(Nuclear Explosion Simulation Technique) require information about the boundary layer characteristics to properly evaluate the test technique and to interpret test data. To adequately determine the degradation of underground facilities caused by the blast environment, the flow properties of air which enters weapon system ducts are required. In addition, the rate of heat transfer to exposed surfaces can be estimated. The total heat transfer consists of the heat convected from the hot boundary layer gases and the heat radiated from the fireball. Of particular importance to the calculation of the heat transfer is the generation of airborne dust by entrainment into the boundary layer. The dust cloud so generated may block a significant portion of the fireball's thermal radiation by absorption or dispersion, thus decreasing the total heat rate to exposed surfaces.

In the present study, the boundary layer behind a strong shock moving into a stationary fluid is investigated. The solution is presented as a model for the blast wave boundary layer caused by an explosion at or near the earth's surface. Although the primary interest here is on spherical blast waves, the solutions are formulated such that they are applicable to plane and cylindrical as well as spherical shocks. Since the boundary layer flow is laminar within a short distance from the shock front in which the shear stress and heat transfer are high and since it is of interest to assess the character of the boundary layer if it were to remain laminar throughout the blast wave, the major effort of the present study is devoted to laminar flow. However, a method of solving the turbulent boundary layer equations has been conceived and formulated and is included in the present report.

The equations governing the two-dimensional transient flow in a laminar boundary layer are presented in Section 2 of this report and are solved using two distinct methods. The first method involves a similarity transformation coupled with a parametric integral technique and is described in detail in Section 3. This method is believed to yield accurate boundary layer solutions for strong-shock conditions (i.e., when the

ambient pressure is negligible compared to the shock overpressure). This condition is satisfied for early time blast waves which are of most practical and theoretical interest. The second solution method involves the assumption of quasi-steady state and local similarity and is discussed in Section 4. This method is being investigated because the solution can be extended to non-ideal blast waves including weak shocks. Results obtained using the present analyses are illustrated in Section 5, and a discussion of the present work and conclusions are given in Section 6.

A complete definition of the flowfield involves determining the inviscid flow and the boundary layer flow. The inviscid flowfield, calculated by neglecting the presence of the boundary layer, has been analyzed by a number of investigators and is rather well defined. For ideal gas and strong shock conditions, Taylor[3] obtained an exact numerical solution and an approximate closed-form solution while Sedov[4] obtained an exact closed-form solution. Sedov's inviscid solution is used in the present study and is presented in Appendix A.

The laminar boundary layer associated with strong shocks has been investigated by Mirels and Hamman;[5] however, their solution is limited to the region very close to the shock. The method of analysis, results, and region of applicability of this solution is described in Appendix B. This solution provides the only rigorous source of comparison to the results of the present study, and such a comparison is discussed in Sections 3 and 4. Mirels[6] and Murdock[7] have applied integral techniques to obtain solutions to the boundary layer behind shocks of constant velocity. Such a shock has a uniform flowfield behind it, whereas the flowfield for a blast wave is far from uniform. Thus, those solutions do not apply to the problem of interest here. To adequately define the blast wave boundary layer, a more comprehensive solution than those presently available in the literature is needed. The need is for a boundary layer solution valid throughout the region of the influence of the blast wave, from the explosive source to the shock front. The purpose of this study is to present such a solution for the laminar case. Although

the actual blast wave boundary layer probably becomes turbulent very near the shock front and boundary layer theory probably is invalid near the explosion point where the density is extremely low, it is believed that the laminar solution is a necessary first step in the description of the physical problem. For turbulent boundary layers, a method of solution as derived by Quan[8] is shown in Appendix C. The actual numerical results for turbulent flow will be computed at a later date.

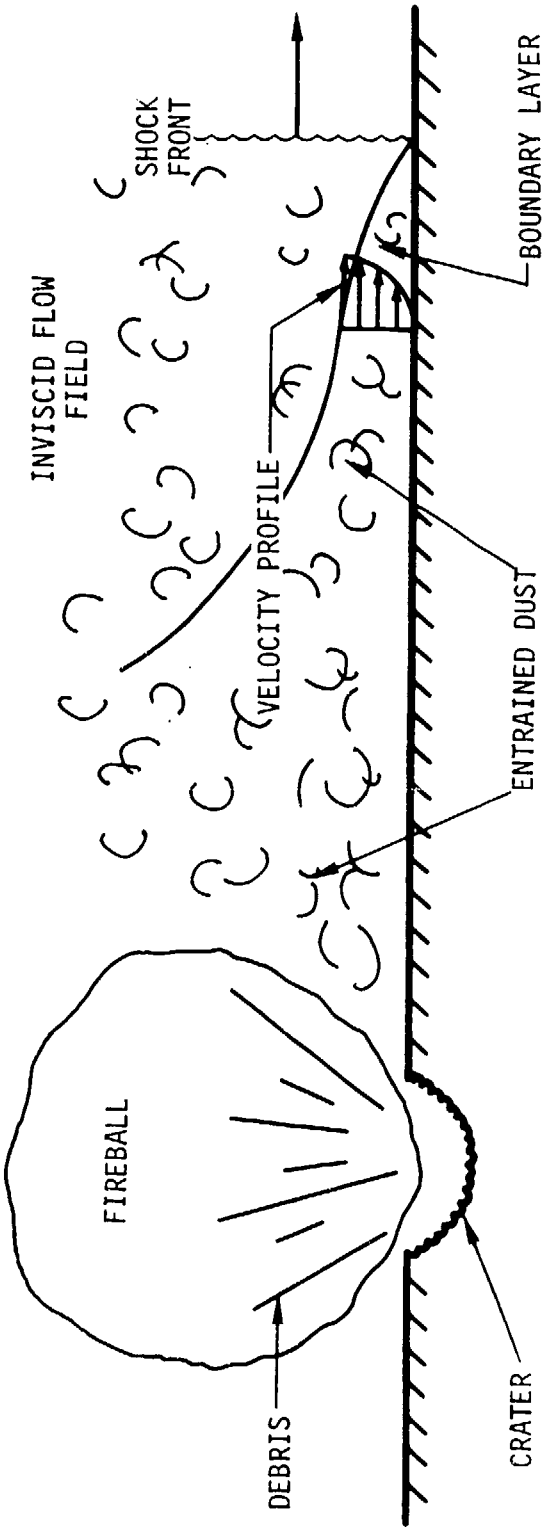

FIGURE 1-1 BLAST CONFIGURATION

(Reverse of Page is Blank)

2. GOVERNING EQUATIONS

A blast wave is by nature unsteady and produces a high temperature, high velocity flowfield. Thus, transient and compressibility effects must be necessarily be considered in the solution of its associated boundary layer. The unsteady, compressible laminar boundary layer equations form the starting point for the solution performed in this report, and are presented in this section. A schematic of the boundary layer which defines the parameters used is given in Figure 2-1. Both two-dimensional (σ=0) and axisymmetric (σ=1) boundary layers are considered. The y coordinate is measured perpendicular to the surface and the x coordinate is measured along the surface from the point of origin of the blast. A point explosion generates an axisymmetric boundary layer, a plane explosion generates a two-dimensional boundary layer, and a line explosion can generate either an axisymmetric or a two-dimensional boundary layer.

The boundary layer equations applicable to both cases are:[5,9]

Continuity

$$\frac{\partial \rho}{\partial t} + \frac{1}{x^{\sigma}} \frac{\partial (\rho u x^{\sigma})}{\partial x} + \frac{\partial (\rho v)}{\partial y} = 0 \qquad (2\text{-}1)$$

Momentum

$$\rho \frac{Du}{Dt} = - \frac{\partial p_e}{\partial x} + \frac{\partial}{\partial y} \left(\mu \frac{\partial u}{\partial y} \right) \qquad (2\text{-}2)$$

Energy

$$\rho \frac{Dh}{Dt} - \frac{Dp_e}{Dt} = \frac{1}{Pr} \frac{\partial}{\partial y} \left(\mu \frac{\partial k}{\partial y} \right) + \mu \left(\frac{\partial u}{\partial y} \right)^2 \qquad (2\text{-}3)$$

where u and v are flow velocities in the x and y directions respectively, t is time, p is pressure, ρ is density, h is enthalpy, μ is viscosity, and Pr is Prandtl number. The subscript e denotes free-stream properties, the subscript ∞ denotes ambient fluid properties, and

$$\frac{D}{Dt} = \frac{\partial}{\partial t} + u\frac{\partial}{\partial x} + v\frac{\partial}{\partial y} \tag{2-4}$$

Air is assumed to be an ideal gas with an equation of state given by

$$p = [(\gamma-1)/\gamma]\rho h \tag{2-5}$$

where γ is the ratio of specific heats. In Equation (2-3) it is assumed that the constant pressure specific heat (c_p) and Prandtl number ($\mu c_p/k$) are constant where k is the fluid conductivity. The general boundary conditions for the governing equations are:

$$\begin{aligned} &u(x,0,t) = v(x,0,t) = 0, \quad h(x,0,t) = h_w(x,t) \quad \text{at} \quad y = 0 \\ &u(x,\infty,t) = u_e(x,t), \quad h(x,\infty,t) = h_e(x,t) \qquad \text{at} \quad y = \infty \end{aligned} \tag{2-6}$$

where the subscript w refers to the flow properties at the wall (y=0).

The location and velocity of a strong shock are given by

$$x_s = Ct^m, \quad u_s = Cmt^{m-1} \tag{2-7}$$

where the constant C is related to the energy liberated during the explosion (see Appendix A) and the constant m is given by $m=2/(3+\bar{\sigma})$ where $\bar{\sigma}$=0, 1, and 2 for a plane, cylindrical, and spherical shock, respectively (see Figure 2-2).

If a similarity variable is defined by $\xi=1-x/x_s$, the inviscid flow properties can be express as

$$\begin{aligned} &p_e/\rho_\infty = u_s^2 F(\xi), \quad \rho_e/\rho_\infty = R(\xi) \\ &u_e = u_s\,\phi(\xi), \quad h_e = \frac{\gamma}{\gamma-1}\frac{p_e}{\rho_e} = \frac{\gamma}{\gamma-1}u_s^2\frac{F(\xi)}{R(\xi)} \end{aligned} \tag{2-8}$$

where the functions F, R, and ϕ depend on $\bar{\sigma}$ and γ as well as on ξ and they are given in Appendix A.

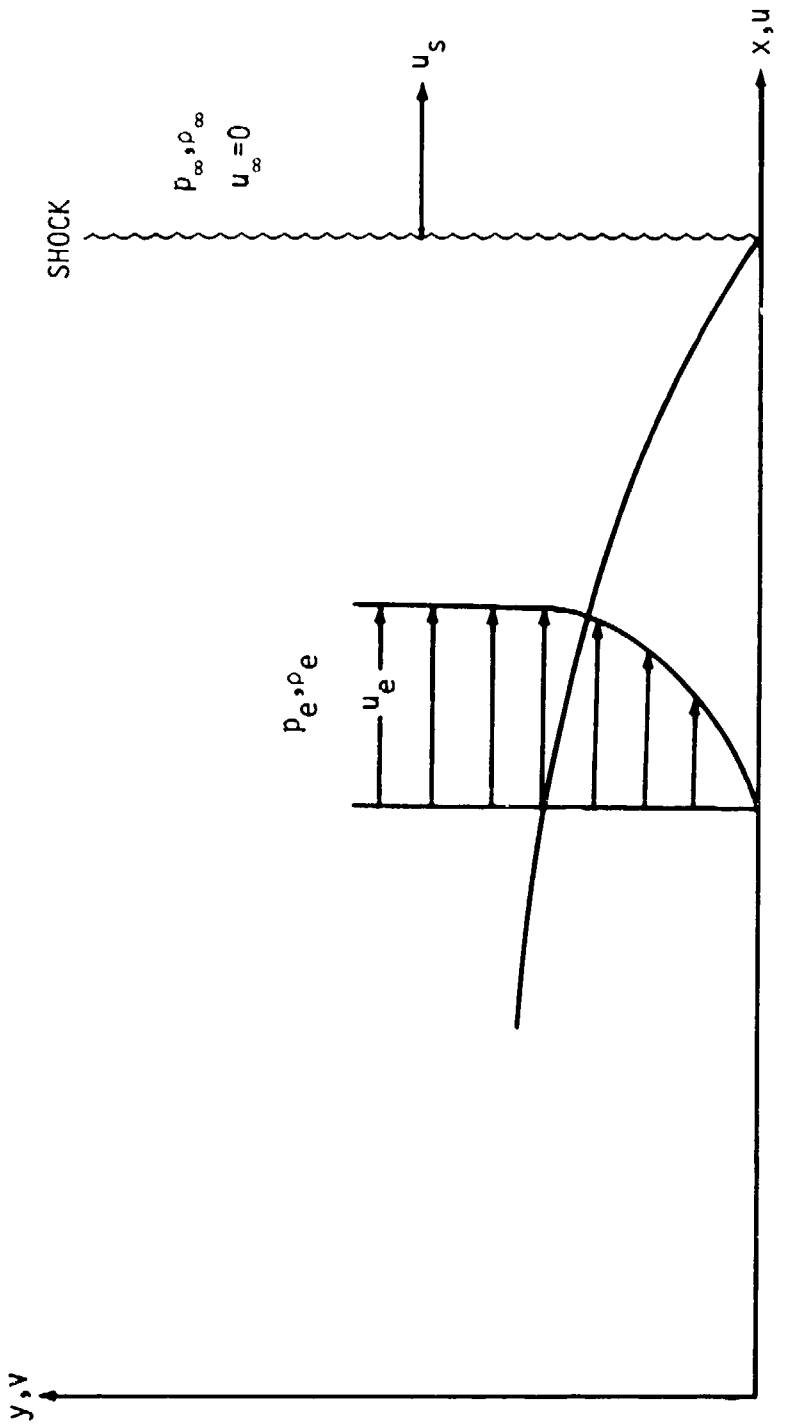

FIGURE 2-1 BOUNDARY LAYER BEHIND MOVING SHOCK

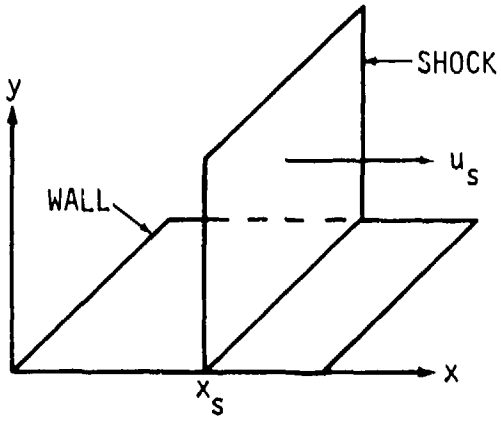

PLANE SHOCK
($\bar{\sigma}=\sigma=0$)

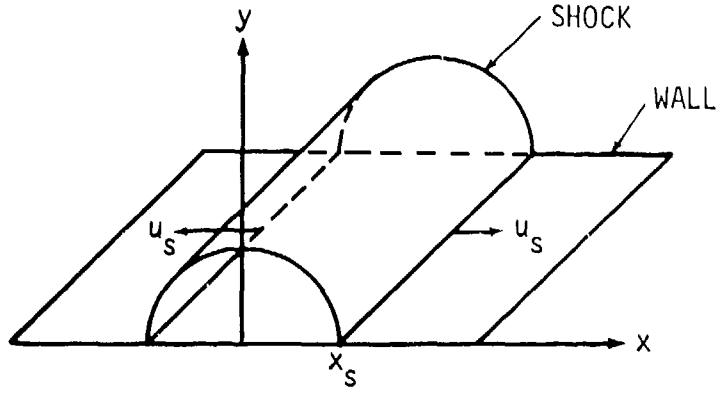

CYLINDRICAL SHOCK
($\bar{\sigma}=1$, $\sigma=0$)

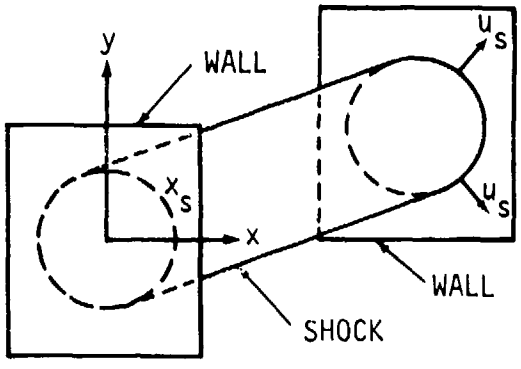

CYLINDRICAL SHOCK
($\bar{\sigma}=\sigma=1$)

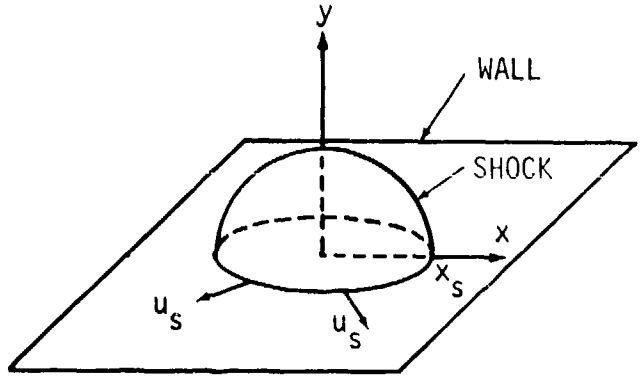

SPHERICAL SHOCK
($\bar{\sigma}=2$, $\sigma=1$)

FIGURE 2-2 PLANE, CYLINDRICAL, AND SPHERICAL MOVING SHOCKS IN VICINITY OF PLANE WALLS

3. INTEGRAL SOLUTION

The equations given in Section 2 which describe the laminar boundary layer behind a shock have been reduced by Mirels and Hamman[5] to two partial differential equations involving two dependent and two independent variables. Equation (2-1) is satisfied by a function ψ such that

$$u = \frac{\rho_\infty}{\rho x^\sigma}\frac{\partial \psi}{\partial y}, \quad v = -\frac{\rho_\infty}{\rho x^\sigma}\left(\frac{\partial \psi}{\partial x} + \frac{\partial}{\partial t} x^\sigma \int_0^y \frac{\rho}{\rho_\infty}\, d\bar{y}\right) \tag{3-1}$$

The following independent variables are introduced:

$$\xi = 1 - x/Ct^m \tag{3-2a}$$

$$\eta = \frac{x^\sigma \int_0^y \frac{\rho}{\rho_\infty}\, d\bar{y}}{\left[At^{2m(\sigma+1)-1}(1-x/Ct^m)\right]^{1/2}} \tag{3-2b}$$

$$\tau = t \tag{3-2c}$$

where A is a constant defined by

$$A = 2mF_o C^{2(\sigma+1)}\mu_\infty/p_\infty \tag{3-3}$$

The independent variables are assumed to have the following form

$$\psi = u_e\left[A\tau^{2m(\sigma+1)-1}\xi\right]^{1/2} f(\xi,\eta) \tag{3-4a}$$

$$h/h_e = \rho_e/\rho = g(\xi,\eta) \tag{3-4b}$$

and the boundary conditions are taken as

$$f(\xi,0) = f_\eta(\xi,0) = 0, \quad f_\eta(\xi,\infty) = 1 \tag{3-5a}$$

$$g(\xi,0) = 0, \quad g(\xi,\infty) = 1 \tag{3-5b}$$

Similar to the treatment in Reference 5, the wall temperature has been assumed to be negligible compared to the free-stream temperature.

Using the equations given above, Equations (2-2) and (2-3) reduce to

$$(1-\xi)^{2\sigma}\frac{F}{F_o}f_{\eta\eta\eta}+(\eta-\phi f)f_{\eta\eta}=2\xi\left\{\left[f\phi_\xi+\phi f_\xi-\frac{1}{2}(2\sigma+\alpha)\eta\right]f_{\eta\eta}\right.$$

$$\left.+\left[\alpha+(1-\xi-\phi f_\eta)\left(\frac{\phi_\xi}{\phi}+\frac{f_{\eta\xi}}{f_\eta}\right)\right]f_\eta-\frac{F_\xi g}{R\phi}\right\} \qquad (3\text{-}6a)$$

$$(1-\xi)^{2\sigma}\left(\frac{1}{Pr}\frac{F}{F_c}g_{\eta\eta}+\frac{\gamma-1}{\gamma}\frac{R\phi^2}{F_o}f_{\eta\eta}^{\,2}\right)+(\eta-\phi f)g_\eta$$

$$=2\xi\left\{\left[f\phi_\xi+\phi f_\xi-\frac{1}{2}(2\sigma+\alpha)\eta\right]g_\eta+\left[\frac{2\alpha}{\gamma}+(1-\xi-\phi f_\eta)\left(\frac{g_\xi}{g}+\frac{F_\xi}{\gamma F}-\frac{R_\xi}{R}\right)\right]g\right. \qquad (3\text{-}6b)$$

where $\alpha=(m-1)/m$. In deriving Equations (3-6a) and (3-6b) it is assumed that viscosity is proportional to temperature. Equations (3-6a) and (3-6b) must be solved simultaneously for f and g in terms of ξ and η. It is noted that the independent variable τ has been eliminated.

The shear and heat transfer at the wall can be calculated from

$$\tau_w=\mu_w\left(\frac{\partial u}{\partial y}\right)_w$$

$$=\left[\frac{\mu_\infty}{2F_o p_\infty u_s(x_s-x)}\right]^{1/2}\left(\frac{x}{x_s}\right)^\sigma p_e\,u_e\,f_{\eta\eta}(\xi,0) \qquad (3\text{-}7a)$$

$$q_w=k_w\left(\frac{\partial T}{\partial y}\right)_w$$

$$=\frac{1}{Pr}\left[\frac{\mu_\infty}{2F_o p_\infty u_s(x_s-x)}\right]^{1/2}\left(\frac{x}{x_s}\right)^\sigma p_e\,h_e\,g_\eta(\xi,0) \qquad (3\text{-}7b)$$

The wall temperature, which has been neglected in computing the coefficients of drag and heat transfer, can be determined by the procedure outlined by Mirels and Hamman.[5]

Mirels and Hamman obtained a solution by expanding the variables f and g in power series of ξ (see Appendix B). Their solution, however, is valid only within a short distance from the shock front. The purpose of employing the integral technique is to obtain a solution that may be valid, under the assumption of laminar flow, for all distances from the shock front.

3.1 POLYNOMIAL PROFILES

The integral method of obtaining approximate solutions to boundary layer problems has been explained in textbooks (e.g., Reference 10). In the present analysis, f and g are represented by polynomials in η. The coefficients of the polynomials are chosen to satisfy the boundary conditions. Equations (3-6a) and (3-6b) are integrated from $\eta=0$ to $\eta=\infty$. This results in two first-order ordinary differential equations describing δ and δ_t as functions of ξ where δ and δ_t are the distances of η at which $f \to 1$ and $g \to 1$, respectively. It should be pointed out that δ and δ_t are not the physical boundary layer thicknesses. The actual boundary layer thicknesses are the distances in y at which $\eta \to \delta$ and $\eta \to \delta_t$ and can be found from Equation (3-2b) once δ and δ_t are determined.

In the present analysis, fourth-degree polynomials are chosen to represent f_η and g

$$\frac{u}{u_e} = f_\eta(\xi,\eta) = a_1 z + a_2 z^2 + a_3 z^3 + a_4 z^4 \qquad (3\text{-}8a)$$

$$\frac{h}{h_e} = g(\xi,\eta) = b_1 w + b_2 w^2 + b_3 w^3 + b_4 w^4 \qquad (3\text{-}8b)$$

where $z=\eta/\delta$ and $w=\eta/\delta_t$. The a_1, b_1, δ, and δ_t are functions of ξ.

Equations (3-8a) satisfies the condition of $f_\eta(\xi,0)$. Upon integration, Equation (3-8a) yields an additional constant which, to satisfy the condition of $f(\xi,0)=0$, turns out to be zero. The four coefficients a_i are determined by the four conditions of $f_\eta(\xi,\delta)=1$, $f_{\eta\eta}(\xi,\delta)=0$, $f_{\eta\eta\eta}(\xi,\delta)=0$, and $f_{\eta\eta\eta}(\xi,0)=0$. The second and third conditions are consistent with the definition of δ, i.e., all derivatives of f_η vanish at $\eta=\delta$, and the fourth condition is obtained by satisfying Equation (3-6a) at $\eta=0$.

Similarly, Equation (3-8b) satisfies the condition of $g(\xi,0)=0$. The four coefficients b_i are determined by the four conditions of $g(\xi,\delta_t)=1$, $g_\eta(\xi,\delta_t)=0$, $g_{\eta\eta}(\xi,\delta_t)=0$, and $g_{\eta\eta}(\xi,0)= -Pr(\gamma-1)R\phi^2 f_{\eta\eta}^2(\xi,0)/\gamma F$ where the fourth condition is derived by evaluating Equation (3-6b) at $\eta=0$.

The resulting expressions for f and g are

$$f = \delta(z^2 - \frac{1}{2} z^4 + \frac{1}{5} z^5) \qquad (3\text{-}9a)$$

$$g = 2w - 2w^3 + w^4 - \frac{1}{3} b_2(w - 3w^2 + 3w^3 - w^4) \qquad (3\text{-}9b)$$

where

$$b_2 = - \frac{2Pr(\gamma-1)R\phi^2\Delta^2}{\gamma F} \qquad (3\text{-}10)$$

and

$$z = \eta/\delta(\xi), \quad w = \eta/\delta_t(\xi), \quad \Delta(\xi) = \delta_t/\delta \qquad (3\text{-}11)$$

Integrating Equations (3-6a) and (3-6b) from $\eta=0$ to $\eta=\infty$ and using Equation (3-9a) and (3-9b), one obtains two coupled first-order ordinary differential equations governing δ and δ_t. These equations, after simplification by a vast amount of algebra, are given by

$$\frac{d\delta}{d\xi} = \frac{B\delta - \frac{1}{2\xi} D}{\frac{3}{10}(1-\xi) - \frac{37}{315}\phi} \qquad (3\text{-}12a)$$

$$\frac{d\delta_t}{d\xi} = \frac{G + \delta_t K\left[\frac{1}{3}\phi N - \frac{1}{60}(1-\xi)\right] - \frac{1}{2\xi}\beta}{(1-\xi)\left(\frac{3}{10} + \frac{1}{20}b_2\right) + \phi M\left(1 + \frac{1}{6}b_2\right)} \qquad (3\text{-}12b)$$

where

$$B = \frac{74}{315}\phi_\xi - \frac{3}{20}(2\sigma+\alpha) - \left(\frac{3}{10} - \frac{3}{10}\Delta - \frac{1}{60}b_2\Delta\right)\frac{F_\xi}{R\phi} \qquad (3\text{-}13a)$$

$$D = -(1-\xi)^{2\sigma}\frac{2}{\delta}\frac{F}{F_o} + \left(\frac{3}{10} - \frac{37}{315}\phi\right)\delta \qquad (3\text{-}13b)$$

$$G = \phi_\xi \delta H + \phi\frac{d\delta}{d\xi}I - \frac{2\sigma+\alpha}{2}\delta_t\left(\frac{3}{10} + \frac{1}{60}b_2\right)$$

$$- \phi\left(\frac{F_\xi}{\gamma F} - \frac{R_\xi}{R}\right)\delta_t\left(\frac{3}{10} - \frac{3}{10\Delta} + \frac{1}{60}b_2 - \frac{1}{\Delta}H\right) \qquad (3\text{-}13c)$$

$$K = b_2\left(-\frac{2}{\delta}\frac{d\delta}{d\xi} + \frac{R_\xi}{R} + \frac{2\phi_\xi}{\phi} - \frac{F_\xi}{F}\right) \qquad (3\text{-}13d)$$

$$\beta = (1-\xi)^{2\sigma}\frac{1}{Pr}\frac{F}{F_o}\frac{1}{\delta_t}\left[-2 + \left(\frac{1}{3} - \frac{26}{35\Delta}\right)b_2\right] + \delta_t\left(\frac{3}{10} + \frac{1}{60}b_2\right) - \phi\delta H \qquad (3\text{-}13e)$$

and

$$H = \frac{2}{15}\Delta^2 - \frac{3}{140}\Delta^4 + \frac{1}{180}\Delta^5 + \frac{1}{3}b_2\Delta N \qquad \text{for } \Delta \leq 1 \qquad (3\text{-}14a)$$

$$H = -\frac{3}{10} + \frac{3}{10}\Delta + \frac{2}{150} - \frac{3}{140\Delta^3} + \frac{1}{180\Delta^4} + \frac{1}{3}b_2\Delta N \qquad \text{for } \Delta \geq 1$$

$$I = -\frac{2}{15}\Delta^2 + \frac{9}{140}\Delta^4 - \frac{1}{45}\Delta^5 - \frac{1}{3}b_2\Delta\left(\frac{1}{30}\Delta - \frac{3}{140}\Delta^3 + \frac{1}{126}\Delta^4\right) \text{ for } \Delta \leq 1 \qquad (3\text{-}14\text{-}b)$$

$$I = -\frac{3}{10} + \frac{4}{15\Delta} - \frac{3}{35\Delta^3} + \frac{1}{36\Delta^4} - \frac{1}{3}b_2\left(\frac{2}{15\Delta} - \frac{3}{14\Delta^2} + \frac{9}{70\Delta^3} - \frac{1}{36\Delta^4}\right) \text{for } \Delta \geq 1$$

$$M = -\frac{4}{15}\Delta + \frac{3}{35}\Delta^3 - \frac{1}{36}\Delta^4 \qquad \text{for } \Delta \leq 1$$

$$M = -\frac{3}{10} + \frac{2}{15\Delta^2} - \frac{9}{140\Delta^4} + \frac{1}{45\Delta^5} \qquad \text{for } \Delta \geq 1 \qquad (3\text{-}14c)$$

$$N = \frac{1}{30}\Delta - \frac{1}{140}\Delta^3 + \frac{1}{504}\Delta^4 \qquad \text{for } \Delta \leq 1$$

$$N = \frac{1}{20} - \frac{1}{15\Delta^2} + \frac{1}{14\Delta^3} - \frac{9}{280\Delta^4} + \frac{1}{180\Delta^5} \qquad \text{for } \Delta \geq 1 \qquad (3\text{-}14d)$$

Equations (3-12a) and (3-12b) along with Equations (3-13a) to (3-14d) are programmed for numerical solution using a standard Runge-Kutta-Adams-Moulton method. The initial values of δ and δ_t are obtained by requiring $d\delta/d\xi$ and $d\delta_t/d\xi$ to be finite at $\xi=0$. The free-stream properties (F, R, and ϕ) used are those given in Appendix A; F_ξ, R_ξ, and ϕ_ξ are derivatives of F, R, and ϕ, respectively, with respect to ξ. The results for Pr=0.72 and γ=1.4 have been obtained for all four geometries illustrated in Figure 2-2. The results of δ and δ_t, along with other results to be obtained in the following section, are shown in Figures 3-1 through 3-4. It should be noted that once δ and δ_t are determined, any physical property in the laminar boundary layer can be computed using the appropriate equations.

3.2 EXPONENTIAL PROFILES

In Section 3.1, the velocity and temperature profiles are represented by fourth-degree polynomials. It is highly useful to obtain an alternate solution, which is probably less accurate but is simpler to derive, by employing profiles of another form. A simple representation that satisfies the boundary conditions is an exponential profile. If the results to be obtained using the exponential representation resemble those obtained using the polynomial representation, then one may infer that the integral solution is probably not too sensitive to the particular profile representation employed as long as they are physically realistic.

The exponential forms of the velocity and temperature profiles are

$$f_\eta = 1 - \exp(-\eta/\ell) \tag{3-15a}$$

$$g = 1 - \exp(-\eta/\ell_t) \tag{3-15b}$$

where ℓ and ℓ_t are functions of ξ and are the distances in η at which the velocity and temperature, respectively, reach $(1-e^{-1})$ of the local free-stream values. It should be noted that ℓ and ℓ_t are measures of, but have values less than, the transformed velocity and temperature boundary layer thicknesses, respectively.

Integrating Equations (3-6a) and (3-6b) from y=0 to y=∞ and using Equations (3-15a) and (3-15b), one obtains two coupled first-order differential equations governing ℓ and ℓ_t. These equations are given by

$$(1 - \xi - \frac{1}{2}\phi)\frac{d\ell}{d\xi} = \ell\left[\phi_\xi - \frac{2\sigma+\alpha}{2} - \frac{F_\xi}{R\phi}(1-\Omega)\right] + \frac{\ell}{2\xi}\left[(1-\xi)^{2\sigma}\frac{F}{F_o}\frac{1}{\ell^2} - 1 + \frac{1}{2}\phi\right] \tag{3-16a}$$

$$\left[1 - \xi - \phi + \phi\left(\frac{1}{1+\Omega}\right)^2\right]\frac{d\ell_t}{d\xi} = \ell\left[\phi_\xi\left(\frac{\Omega^2}{1+\Omega}\right) - \frac{2\sigma+\alpha}{2}\Omega + \phi\left(\frac{F_\xi}{\gamma F} - \frac{R_\xi}{R}\right)\frac{1}{1+\Omega}\right] - \phi\frac{d\ell}{d\xi}\frac{1+\Omega^2}{(1+\Omega)^2} - \frac{1}{2\xi}\left[(1-\xi)^{2\sigma}\left(-\frac{1}{Pr}\frac{F}{F_o}\frac{1}{\ell_t} + \frac{\gamma-1}{\gamma}\frac{R\phi^2}{F_o}\frac{1}{2\ell}\right) + \ell_t\left(1-\phi\frac{\Omega}{1+\Omega}\right)\right] \tag{3-16b}$$

where $\Omega=\ell_t/\ell$.

Equations (3-16a) and (3-16b) are programmed for numerical solution using the Runge-Kutta method. The initial values of ℓ and ℓ_t are obtained by requiring $d\ell/d\xi$ and $d\ell_t/d\xi$ to be finite at ξ=0. The free-stream

properties used are those given in Appendix A. The results for Pr=0.72 and γ=1.4 have been obtained for all four geometries illustrated in Figure 2-2. The results of ℓ and ℓ_t, which are sufficient to determine all boundary layer properties, are shown in Figures 3-1 through 3-4.

3.3 DISCUSSION OF INTEGRAL SOLUTION

The integral solution for laminar boundary layer has been obtained using two distinct representations for the flowfield. The exponential profile representation is simpler for computation than the polynomial representation; but based on experience with simple problems such as flat plate flow, the former is also expected to be less accurate. The velocity and temperature profiles obtained using the two methods are compared in Figures 3-5 to 3-8, respectively, for ξ=0, 0.02, 0.1, and 0.5 and spherical shock. Mirels and Hamman's solution,[5] which is exact as $\xi \to 0$, is also included for comparison in Figures 3-5 and 3-6. Beyond ξ=0.02, however, the accuracy of their solution is questionable (see Appendix B) and is therefore not shown for comparison in Figures 3-7 and 3-8. The factors that determine the shear stress and heat transfer at the wall, $f_{\eta\eta}(\xi,0)$ and $g_\eta(\xi,0)$, for spherical shock are plotted in Figure 3-9. They are magnified and compared to Mirels and Hamman's solution in Figure 3-10 for small values of ξ. Also, $f_{\eta\eta}(0,0)$, $g_\eta(0,0)$, $[df_{\eta\eta}(\xi,0)/d\xi]_o$ and $[dg_\eta(\xi,0)/d\xi]_o$ for plane, cylindrical, and spherical shocks are tabulated in Table 3-1 below; the results of Mirels and Hamman's are included for comparison. The values of $f_{\eta\eta}(0,0)$ and $g_\eta(0)$ are independent of σ and α.

From Figures 3-5 through 3-10 and Table 3-1, it is seen that the exponential profile solution agrees closely with the polynomial profile solution. It is also seen that the polynomial solution yields better overall agreement with Mirels and Hamman's solution in the region where their solution is applicable.

TABLE 3-1

COMPARISON OF SHEAR STRESS AND HEAT TRANSFER FACTORS

NEAR SHOCK FRONT FOR Pr = 0.72 AND γ = 1.4

			Mirels and Hamman	Integral-Polynomial	Integral-Exponential
$f_{\eta\eta}(0,0)$			0.66141	0.63579	0.76376
$g_{\eta}(0,0)$			0.89693	0.88779	0.89032
	σ	α			
$\left[\frac{df_{\eta\eta}(\xi,0)}{d\xi}\right]_o$	0	-1/2	1.1819	1.1167	1.6487
	0	-1	1.7201	1.6139	2.2971
	1	-1	2.5051	2.4036	3.3336
	1	-3/2	3.0432	2.9008	3.9820
$\left[\frac{dg_{\eta}(\xi,0)}{d\xi}\right]_o$	0	-1/2	-1.2891	-1.3824	-1.4124
	0	-1	-2.7270	-2.8319	-3.1753
	1	-1	-1.6291	-1.7548	-2.0089
	1	-3/2	-3.0671	-3.2044	-3.7718

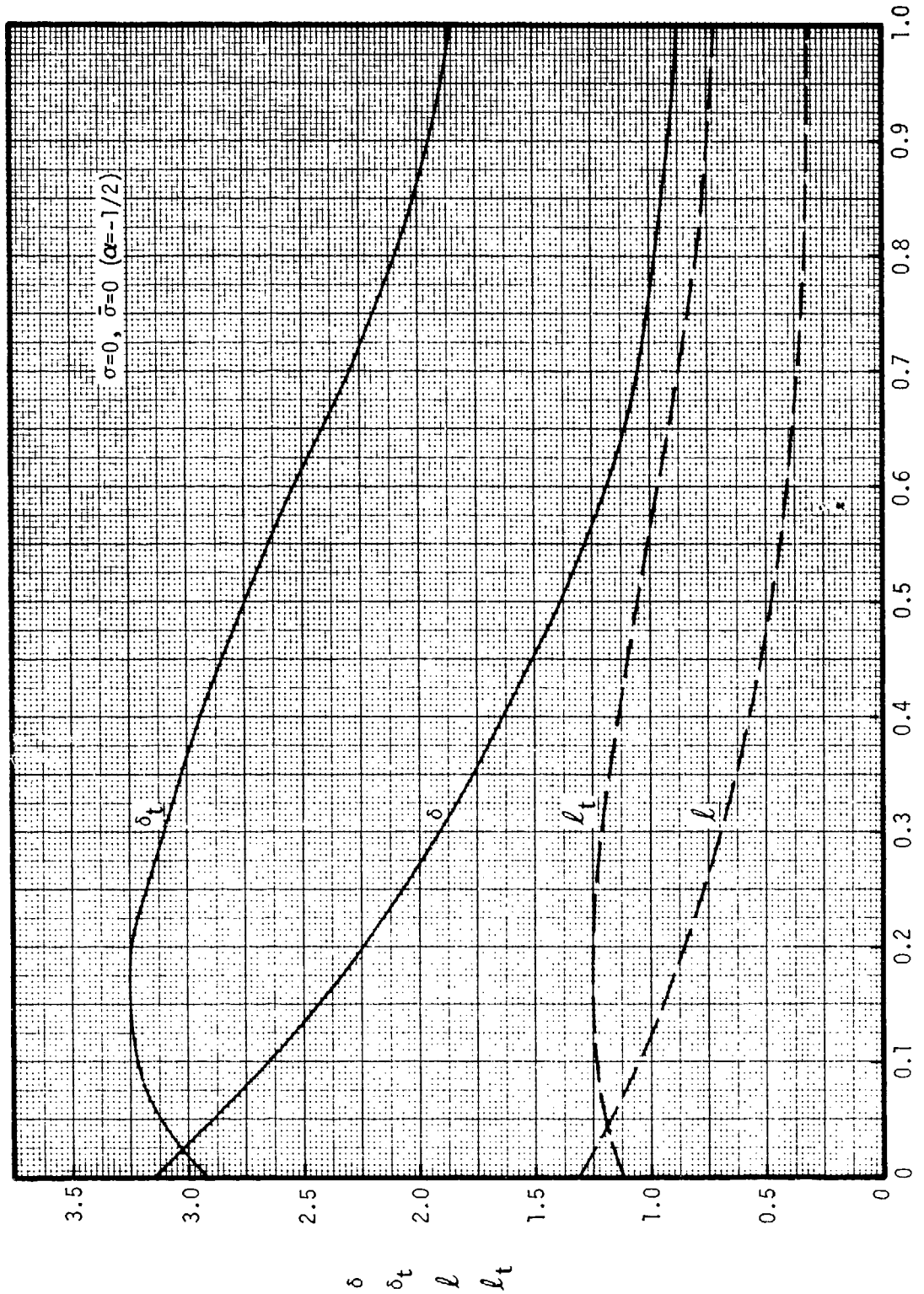

FIGURE 3-1 BOUNDARY LAYER PARAMETERS FOR TWO-DIMENSIONAL FLOW BEHIND PLANE SHOCK

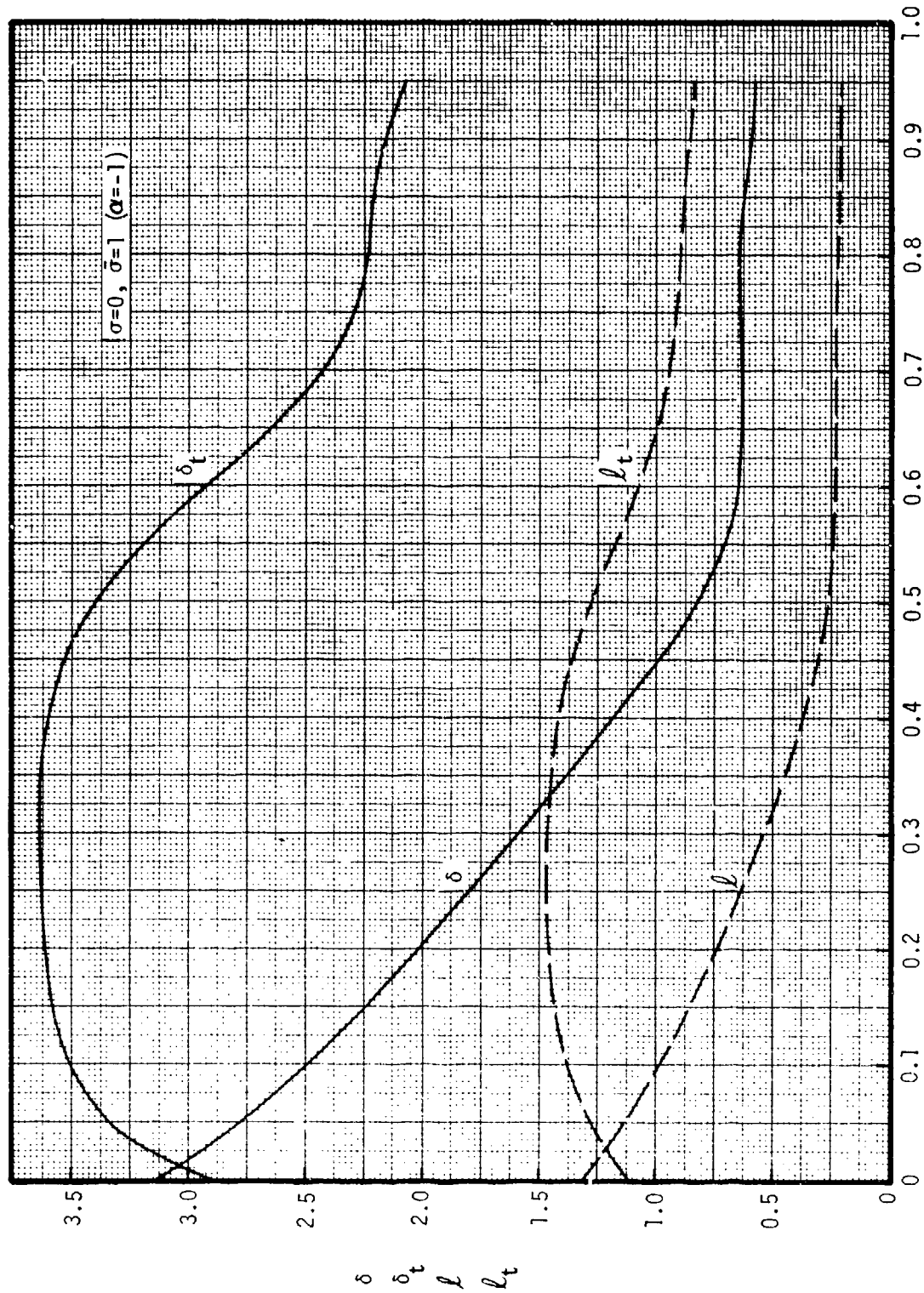

FIGURE 3-2 BOUNDARY LAYER PARAMETERS FOR TWO-DIMENSIONAL FLOW BEHIND CYLINDRICAL SHOCK

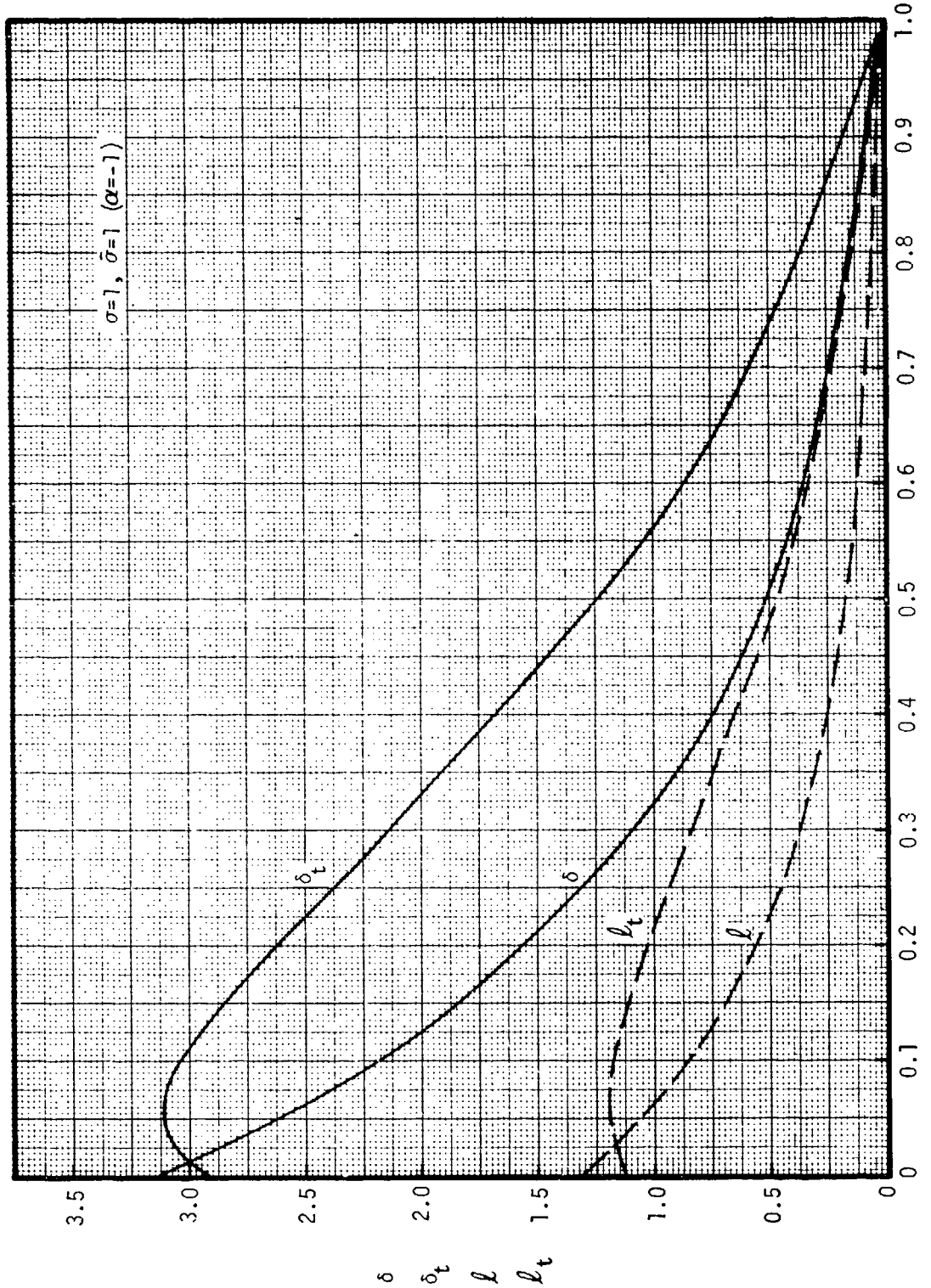

FIGURE 3-3 BOUNDARY LAYER PARAMETERS FOR AXISYMMETRIC FLOW BEHIND CYLINDRICAL SHOCK

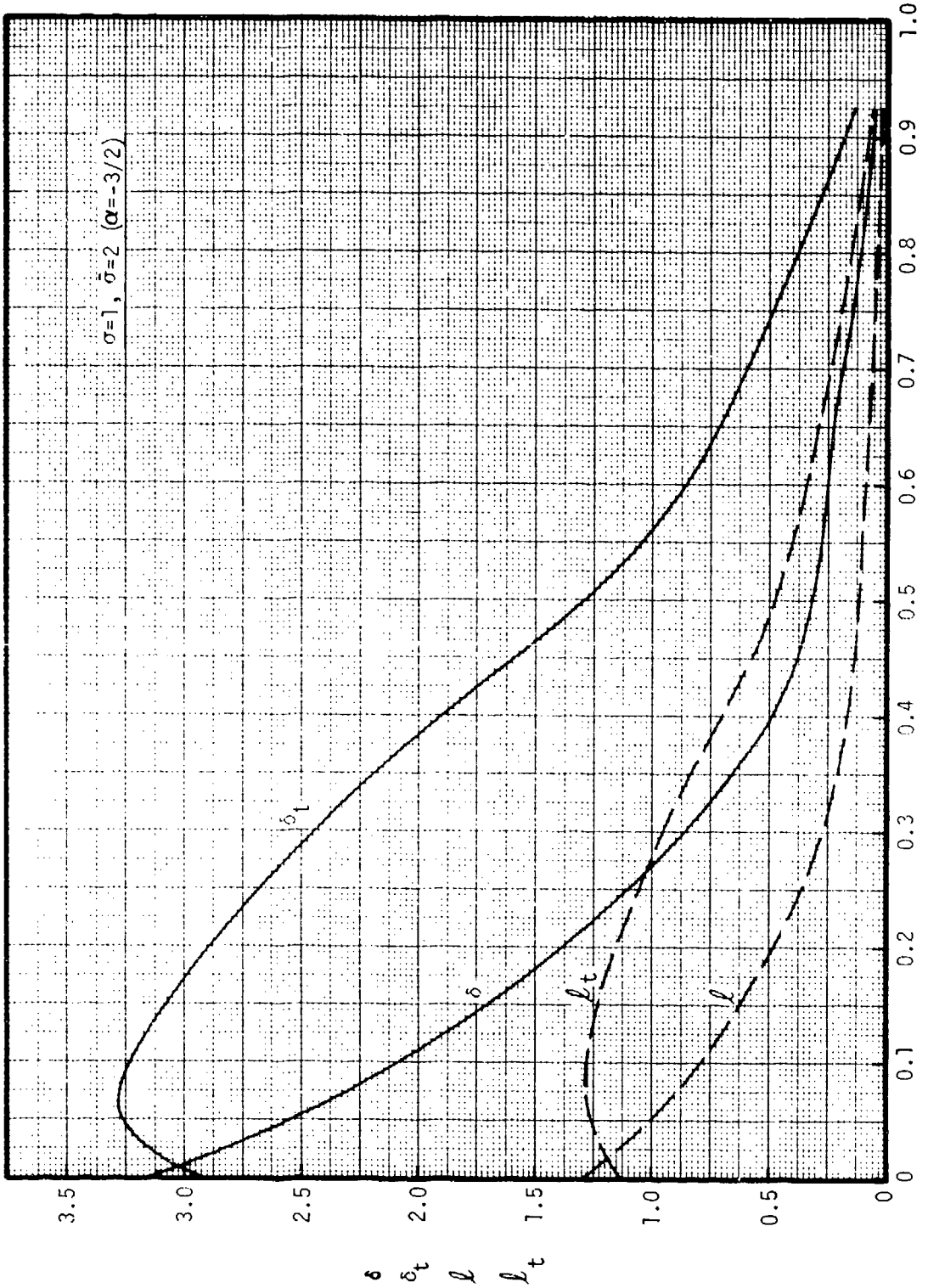

FIGURE 3-4 BOUNDARY LAYER PARAMETERS FOR AXISYMMETRIC FLOW BEHIND SPHERICAL SHOCK

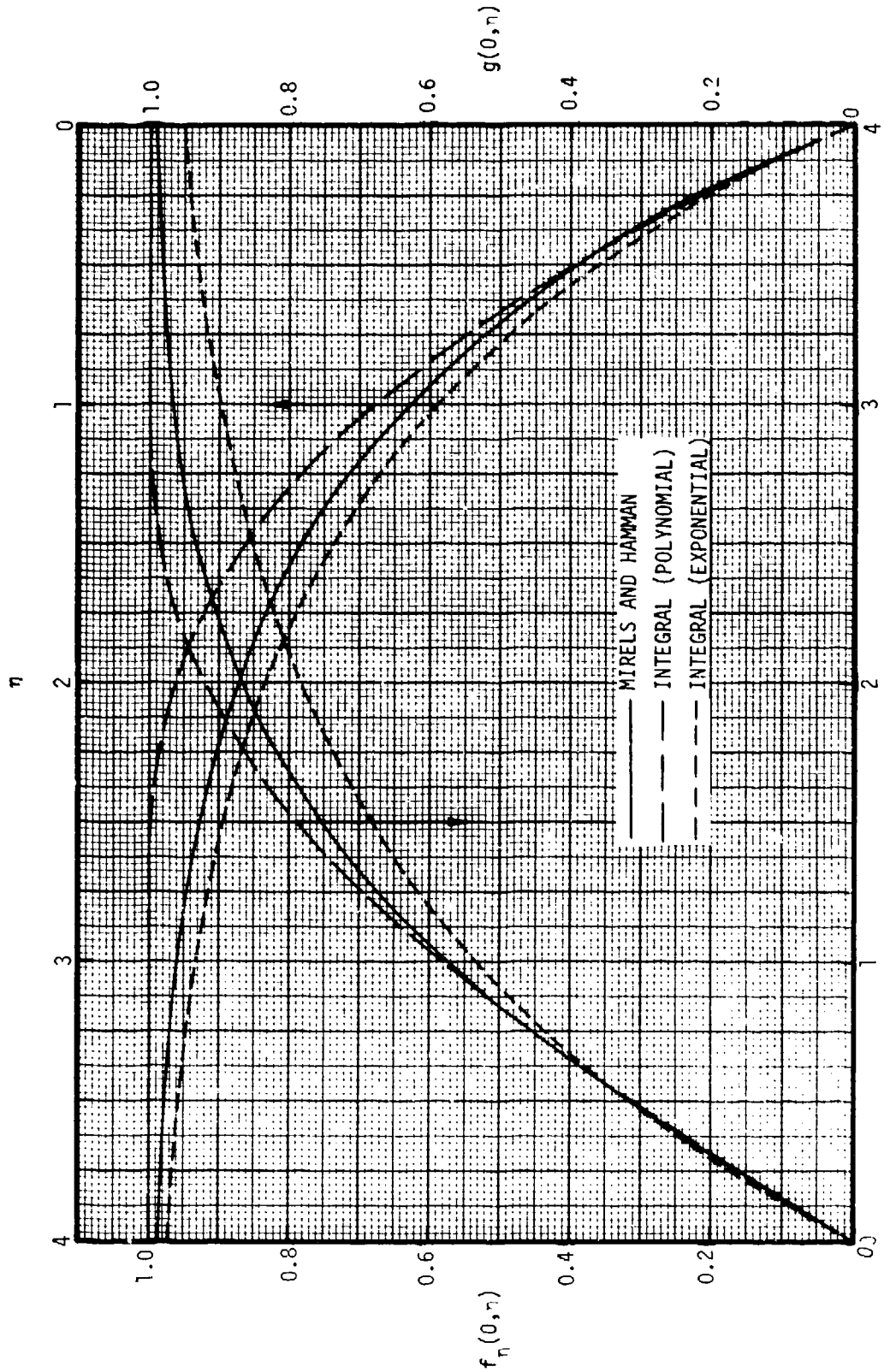

FIGURE 3-5 VELOCITY AND TEMPERATURE PROFILES AT SHOCK FRONT

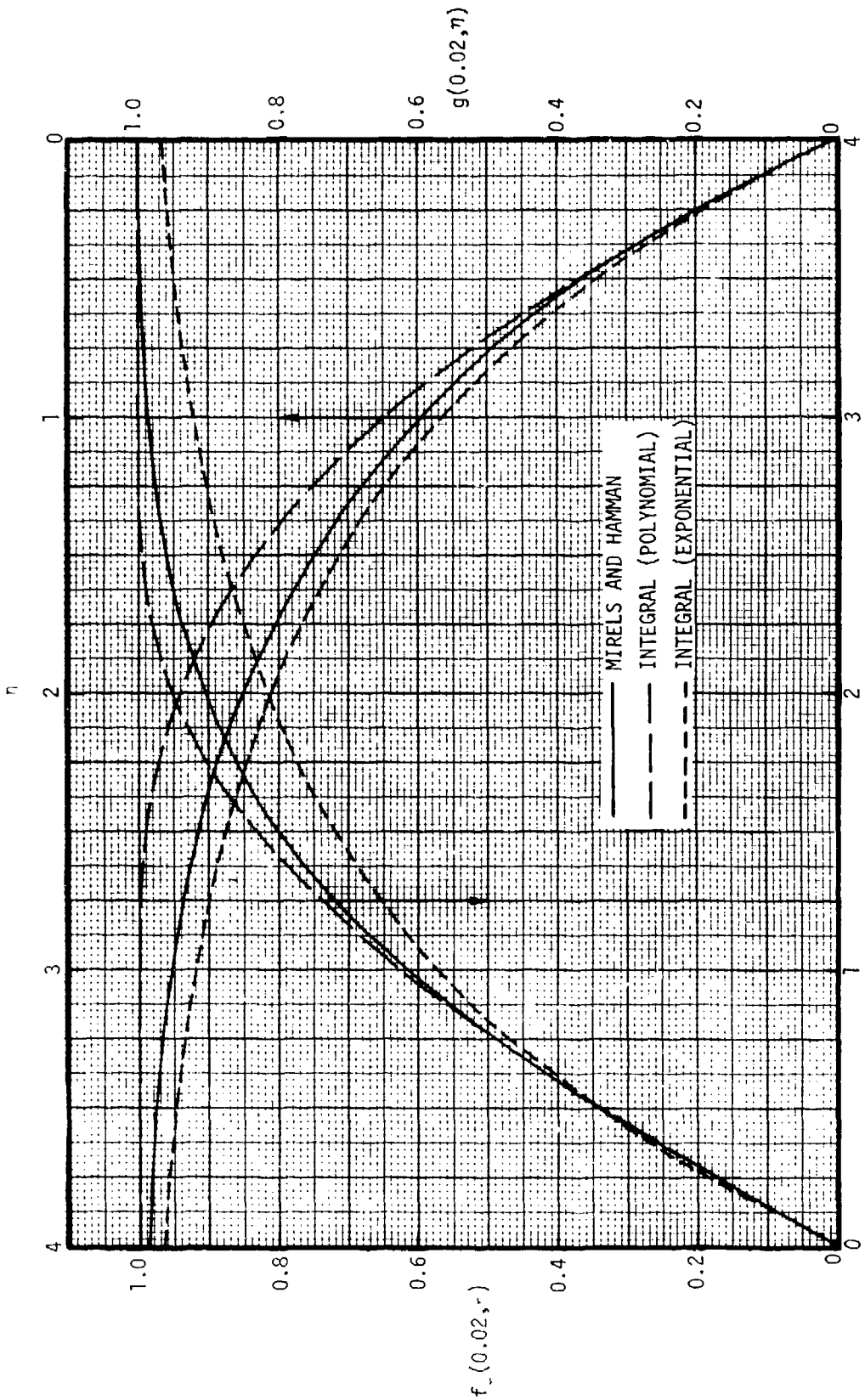

FIGURE 3-6 VELOCITY AND TEMPERATURE PROFILES AT ξ=0.02

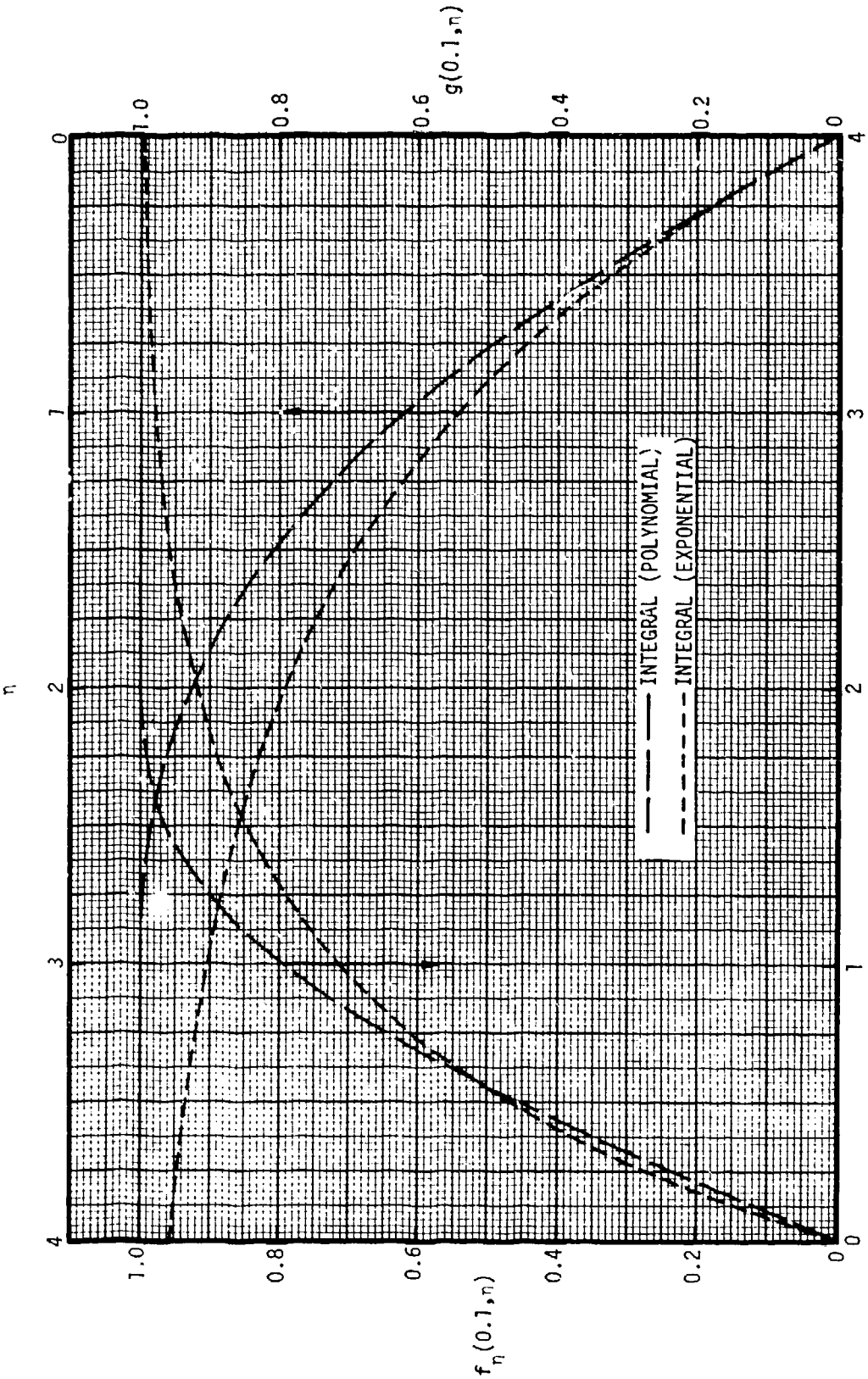

FIGURE 3-7 VELOCITY AND TEMPERATURE PROFILES AT ξ=0.1

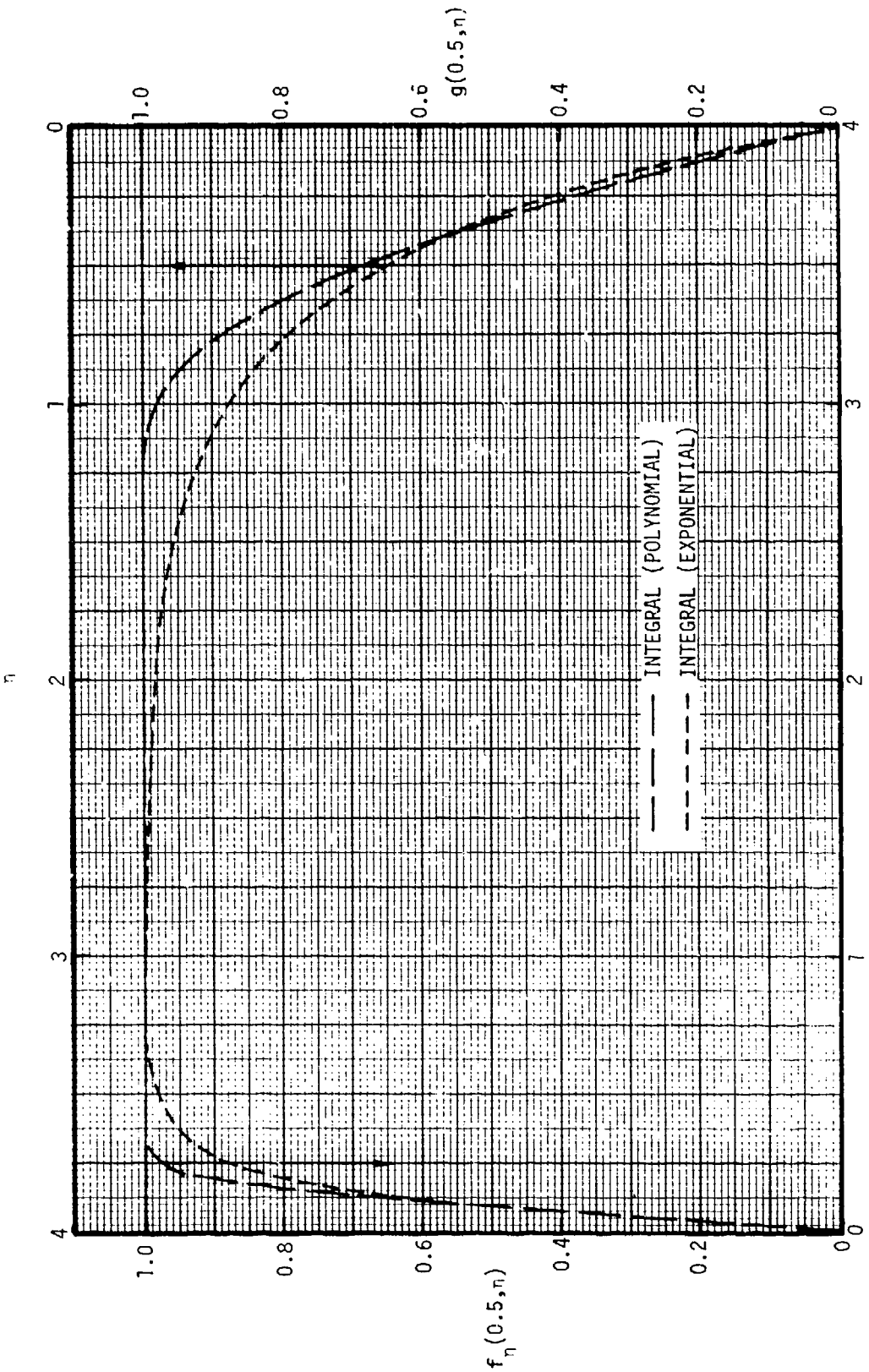

FIGURE 3-8 VELOCITY AND TEMPERATURE PROFILES AT ξ=0.5

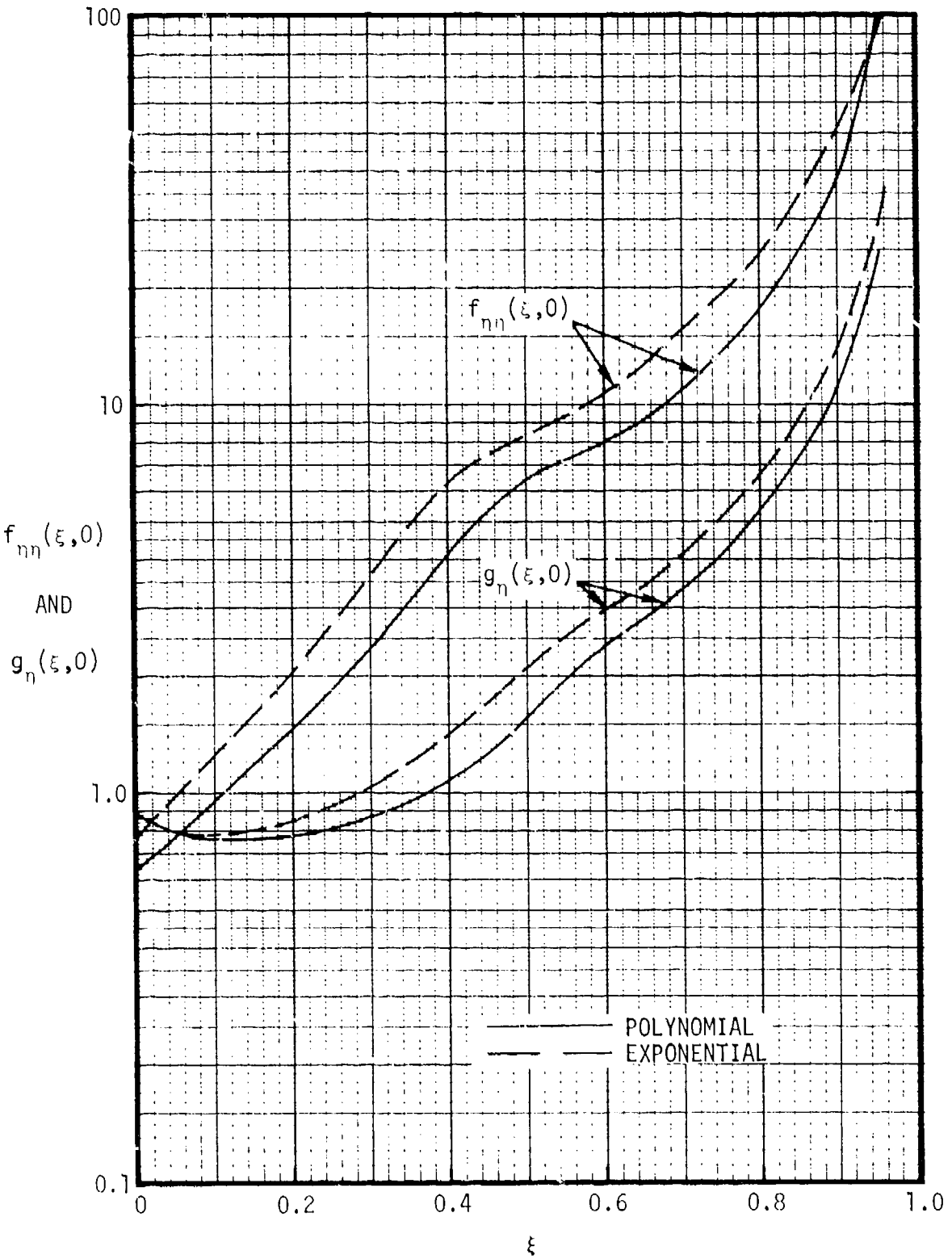

FIGURE 3-9 WALL SHEAR STRESS AND HEAT TRANSFER FACTORS

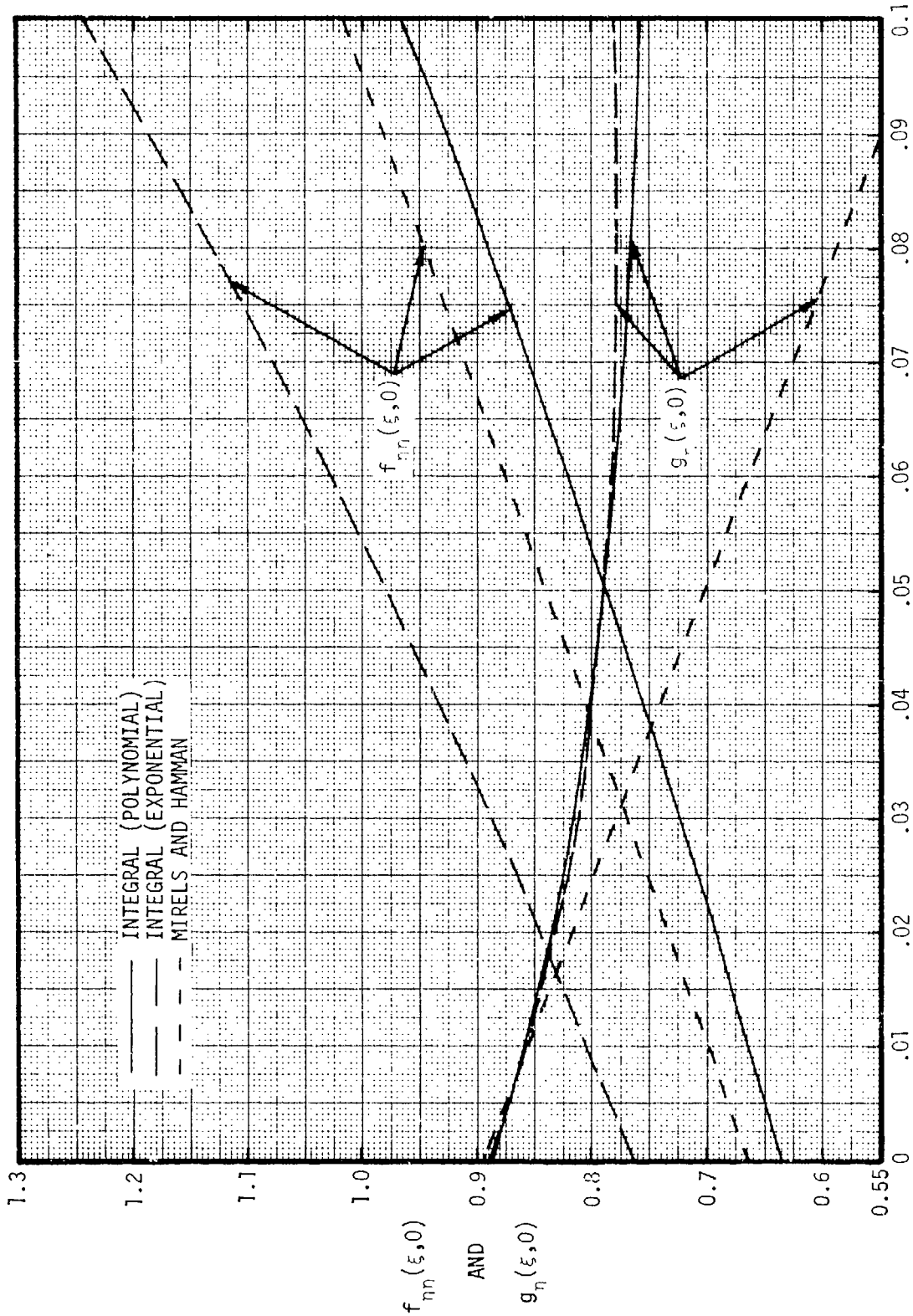

FIGURE 3-10 WALL SHEAR STRESS AND HEAT TRANSFER FACTORS NEAR SHOCK FRONT

(Reverse of Page is Blank)

4. QUASI-STEADY SOLUTION

The second method of solving the blast wave laminar boundary layer is referred to as the quasi-steady solution. Two solution procedures performed in a quasi-steady sense, along with rationale for attempting them are discussed in this section. The two procedures, though independent in method and application, are complementary in that they represent varying degrees of approximation to the actual physical problem. The first quasi-steady procedure, referred to herein as the "steady and locally square wave" procedure, is described in Section 4.1. This procedure uses available solutions[6,11] for the boundary layer behind a square wave shock and applies them in a locally similar sense to the decaying, spherically expanding blast wave. The "quasi-steady and locally similar" shock boundary layer solution is discussed in Section 4.2. This solution represents a more complete description of the local free-stream flow properties and therefore provides a more realistic test of the appropriateness of the local similarity assumption. Both solution schemes are developed for the Taylor-Sedov self-similar blast wave flow and are compared near the shock front to Mirels and Hamman's boundary layer solution (Appendix B). A discussion of the applicability of both solutions to the self-similar blast wave and possible extension to non-ideal blast waves is presented in Section 4.3.

4.1 STEADY AND LOCALLY SQUARE-WAVE PROCEDURE

The "steady and locally square wave" solution procedure was an obvious initial step in examining quasi-steady, locally similar type solutions to the blast wave boundary layer problem. It was originally performed with the intention of determining the accuracy of a very crude local similarity assumption, based on known shock boundary layer solutions. The comparison of the resulting solution to the other solutions presented in this document was such that it was deemed proper to briefly discuss the solution method and results. The solution is discussed in the following paragraphs with the intention of suggesting a simple procedure for getting rough estimates for the general blast wave boundary layer.

The complete solution for a square wave shock boundary layer is given by Mirels in References 6 and 11. The solution was obtained by solving the boundary layer equations in a steady, shock fixed coordinate system. The solution was effected by reducing the equations to non-linear ordinary differential equations with a similarity transformation based on the similarity parameter:

$$\eta_q = \sqrt{\frac{(u_s-u_e)\rho_w}{2(x_s-x)\mu_w}}\ \frac{\rho_\infty}{\rho_w}\int_o^y \frac{\rho}{\rho_\infty}\,dy \qquad (4\text{-}1)$$

The subscript q refers to the square wave boundary layer solution. A numerical solution of the resulting two point boundary value problem was then obtained for various strength shocks as defined by the ratio of the shock velocity to fluid velocity in the shock fixed coordinates or $u_s/(u_s-u_e)$. These solutions are tabulated in References 6 and 11. The procedure for applying these square-wave solutions to the boundary layer for a transient, spacially decaying blast wave is to use the tabulated solution for the local, instantaneous value of the velocity parameter $u_s/(u_s-u_e)$. This parameter is calculated from any blast wave solution (Taylor-Sedov or numerical) using the instantaneous shock velocity at the time of interest and using the free-stream velocity (u_e) at the position behind the shock of interest. In this simplified sense, then, the solution is both quasi-steady and locally similar; that is the boundary layer solution is assumed to depend only upon the instantaneous shock front and local free-stream properties (u_s, x_s, u_e, T_e, ρ_e).

The relevant boundary layer parameters from Mirels solution are written below in terms of the variables used in the present report. The boundary layer velocity and enthalpy are given by:

$$\frac{u_s-u}{u_s-u_e} = f'_q(\eta_q) \qquad (4\text{-}2)$$

where the prime denotes differentiation with respect to the independent variable η_q and:

$$\frac{h}{h_e} = 1 + \frac{\gamma-1}{2}\left[\frac{u_e}{u_s-u_e}\bar{M}_e\right]\left[r(\eta_q) - r(0)\,s(\eta_q)\right] + \left(\frac{T_w}{T_e} - 1\right)s(\eta_q)$$

$$\bar{M}_e^{\,2} = \frac{2(u_s-u_e)}{2u_s + (\gamma-1)u_e} \qquad (4\text{-}3)$$

The wall shear stress (τ_w) and heat transfer (q_w) are given by:

$$\tau_w = \mu_w(u_s-u_e)\sqrt{\frac{(u_s-u_e)}{2\nu_w(x_s-x)}}\; f_q''(0) \qquad (4\text{-}4)$$

and

$$q_w = k_w\sqrt{\frac{(u_s-u_e)}{2\nu_w(x_s-x)}}\; s'(0)\left\{T_e + \frac{\gamma-1}{2}\left[\frac{u_e}{(u_s-u_e)}\bar{M}_e\right]^2 r(0)T_e - T_w\right\} \qquad (4\text{-}5)$$

The boundary layer thickness is:

$$y_\delta\sqrt{\frac{u_s-u_e}{2\nu_w(x_s-x)}} = \frac{T_e}{T_w}\left\{\eta_\delta + \frac{3}{10}\left(\frac{T_w}{T_e} - 1\right)\eta_\delta + \frac{\gamma-1}{2}\bar{M}_e^{\,2}\left[\frac{3}{10}\frac{u_s\,u_e}{(u_s-u_e)^2}\,\eta_\delta + f_q''(0)\right]\right\}$$

where (4-6)

$$\eta_\delta = 2\sqrt{\frac{315(u_s - u_e)}{189u_s - 74u_e}}$$

and where y_δ is the physical momentum boundary layer thickness. The boundary layer thickness is derived in Reference 11 by using an approximate integral technique which compares with the exact numerical technique within 5%.

Curves for the wall shear stress parameter [$f_q'(0)$] and heat transfer parameter [$s'(0)$] and recovery factor [$r(0)$] are plotted as functions of the free-stream velocity parameter in Figure 4-1 below. Data presented in Reference 11 was used in these plots.

For purposes of comparison with Mirels and Hamman's solution, the solution procedure outlined above was completed for the Taylor-Sedov blast wave flow given in Appendix A. The assumptions made in the square wave boundary layer solution are consistent with the assumptions of Mirels and Hamman for the self similar blast wave boundary layer (i.e., constant Pr

and c_p and μ linearly proportioned to T) so that these assumptions will not affect the validity of the comparison. To compare the two solutions requires a transformation from the square wave similarity variable [Equation (4-1)] and the Mirels and Hamman similarity parameter. Equations relating the relevant parameters are given below. The similarity variables are related by:

$$\eta_q = \frac{1}{(1-\xi)^{\sigma}} \left[\frac{2}{(\gamma+1)} \frac{\left(1 - \frac{2}{\gamma+1}\phi(\xi)\right)}{F(\xi)} \right]^{1/2} \eta \qquad (4\text{-}7)$$

The non-dimensional velocity [f'(η)] and non-dimensional temperatures [g(η)] are related through Equations (4-8) and (4-9):

$$f'(\eta) = \frac{u_s}{u_e} - \frac{u_s - u_e}{u_e} f'(\eta_q) \qquad (4\text{-}8)$$

$$g(\eta) = 1 + \frac{\gamma-1}{2}\left(\frac{u_e}{u_s-u_e}\bar{M}_e\right)^2\left[r(\eta_q) - r(0)\, s(\eta_q)\right] + \left(\frac{T_w}{T_e} - 1\right)s(\eta_q) \qquad (4\text{-}9)$$

It is reiterated that the prime denotes differentiation with respect to the independent variable (η or η_q). The parameters which determine the shear and heat transfer are related through Equations (4-10) and (4-11).

$$f''(\eta) = -\frac{(u_s-u_e)}{u_e}\left(\frac{\partial \eta_q}{\partial \eta}\right) f_q''(\eta_q) \qquad (4\text{-}10)$$

$$g'(\eta) = \left[\frac{T_w}{T_e} - 1 - \frac{\gamma-1}{2}\left(\frac{u_e}{u_s-u_e}\bar{M}_e\right)^2 r(0)\right]\left(\frac{\partial \eta_q}{\partial \eta}\right) s'(\eta_q) \qquad (4\text{-}11)$$

where $\partial\eta_q/\partial\eta$ is derived from Equation (4-7).

A meaningful comparison of the two solutions can be made by comparing the values of f''(0) and g'(0) as calculated by Mirels and Hamman and as calculated from the steady and locally square wave procedures. This essentially compares the wall shear stress and heat transfer. The values of f''(0) and g'(0) are plotted as functions of the non-dimensional

distance behind the shock front in Figures 4-2 and 4-3. The results of the steady and locally similar procedure are compared to Mirels and Hamman's two term expansion (with respect to ξ) very near the shock front in Figure 4-2. As shown in that figure the solutions are identical at the shock front. This is not very surprising since a square wave is the "zeroth" order approximation to the decaying self similar blast wave flowfield which is changing very rapidly with ξ near the shock front. The reasons for this will become more apparent when the terms in the boundary layer formulation which are neglected in the local square wave procedure are examined in Section 4.2. As will be shown in Section 4.3, the accuracy of the solution improves with distance behind the shock as compared to the integral solution and the quasi-steady and locally similar solution. Some reasons for this will be discussed in that section.

4.2 QUASI-STEADY AND LOCALLY SIMILAR PROCEDURE

The "quasi-steady, locally similar" blast boundary layer solution is presented in this section. The spirit of the solution is to extend Mirels and Hamman's solution[5] to all regions of the blast wave and to allow for the use of non-ideal blast waves (weak shocks, precursors, heights of burst) in the boundary layer solution. This section includes a description of the solution method and presents results using the Taylor-Sedov self-similar inviscid blast flowfield. Comment on the accuracy of the assumptions is reserved for Section 4.3.

The basic boundary layer equations are given in Section 2. The first step in the solution is to transform the continuity, momentum and energy equations [Equations (2-1),(2-2), and (2-3), respectively] to a shock fixed coordinate system and to concurrently apply a similarity transformation for the y coordinate. The transformation equations used are identical with those of Mirels and Hamman and are given by Equation (3-2) of this report. The effect of the transformation is to reduce the effect of the time varying terms, thereby making the quasi-steady assumption valid, and to stretch the y coordinate to account for compressibility effects. As was pointed out by Mirels and Hamman, time is eliminated completely by their similarity transformation for the self-similar blast

wave flowfield. Thus for this "ideal" blast wave the quasi-steady assumption is superfluous. This, however, is not the case for a "non-ideal" blast wave.

The flow velocity components (u, v) are assumed to depend upon some scalar function $\psi(\xi,\eta,\tau)$ in such a way that continuity is identically satisfied as given by Equations (3-1) earlier. The non-dimensional boundary layer velocity and enthalpy are thus given by:

$$\frac{u}{u_e} = f(\xi,\eta) \quad , \quad \frac{h}{h_e} = g(\xi,\eta) \tag{4-12}$$

The momentum and energy equations [Equations (2-2) and (2-3)] are now transformed as described above into Equations (4-13) and (4-14) below:

$$\frac{x_s^{2\sigma}(1-\xi)^{2\sigma}(\rho\mu)}{A\rho_\infty^2\tau^{2m(\sigma+1)-1}} f_{\eta\eta\eta} = -\frac{x_s^{2\sigma}(1-\xi)^{2\sigma}(\rho\mu)_\eta}{A\rho_\infty^2\tau^{2m(\sigma+1)-1}} f_{\eta\eta}$$

$$- \frac{\xi}{\rho_e u_e x_s}\frac{\partial p_e}{\partial \xi} g - \left\{[m(\sigma+1)-1/2]\frac{\xi}{\tau} + \frac{u_s}{2x_s}(1-\xi)\right\}\eta f_{\eta\eta}$$

$$+ \frac{u_e}{x_s}\left(\frac{1}{2} + \frac{\xi}{u_e}\frac{\partial u_e}{\partial \xi}\right) f f_{\eta\eta}$$

$$+ \underline{\frac{u_e \xi}{x_s} f_\xi f_{\eta\eta}} - \underline{\frac{\xi}{x_s}\left[u_e f_\eta - u_s(1-\xi)\right] f_{\eta\xi}}$$

$$- \frac{\xi}{x_s}\frac{\partial u_e}{\partial \xi}(f_\eta)^2 + \frac{\xi}{u_e}\left[\frac{\partial u_e}{\partial \tau} + \frac{u_s}{x_s}(1-\xi)\frac{\partial u_e}{\partial \xi}\right] f_\eta \tag{4-13}$$

$$\frac{1}{Pr}\frac{x_s^{2\sigma}(1-\xi)^{2\sigma}(\rho\mu)}{A\,\rho_\infty^2\tau^{2m(\sigma+1)-1}}\,g_{\eta\eta} = -\frac{1}{Pr}\frac{x_s^{2\sigma}(1-\xi)^{2\sigma}(\rho\mu)_\eta}{A\,\rho_\infty^2\tau^{2m(\sigma+1)-1}}\,g_\eta$$

$$-\frac{x_s^{2\sigma}(1-\xi)^{2\sigma}}{\rho_\infty^2 A\tau^{2m(\sigma+1)-1}}\frac{u_e^2}{h_e}(\rho\mu)(f_{\eta\eta})^2$$

$$+\frac{\xi}{h_e}\left[\frac{\partial h_e}{\partial\tau}-\frac{1}{\rho_e}\frac{\partial p_e}{\partial\tau}+\frac{u_s}{x_s}(1-\xi)\left(\frac{\partial h_e}{\partial\xi}-\frac{1}{\rho_e}\frac{\partial p_e}{\partial\xi}\right)\right]g$$

$$+\frac{u_e}{x_s}\left(\frac{1}{2}+\frac{\xi}{u_e}\frac{\partial u_e}{\partial\xi}\right)fg_\eta$$

$$+\underline{\frac{u_e\xi}{x_s}f_\xi\,g_\eta}-\underline{\frac{u_s\xi}{x_s}\left[\frac{u_e}{u_s}f_\eta-(1-\xi)\right]g_\xi}$$

$$-\left\{[m(\sigma+1)-1/2]\frac{\xi}{\tau}+\frac{u_s}{2x_s}(1-\xi)\right\}\eta\,g_\eta$$

$$-\frac{u_e\xi}{h_e x_s}\left(\frac{\partial h_e}{\partial\xi}-\frac{1}{\rho_e}\frac{\partial p_e}{\partial\xi}\right)f_\eta\,g \qquad (4\text{-}14)$$

where the boundary conditions are taken as:

$$f(\xi,0) = f_\eta(\xi,0) = 0\,,\quad f_\eta(\xi,\infty) = 1$$

$$g(\xi,0) = \frac{h_w}{h_e}\,,\quad g(\xi,\infty) = 1 \qquad (4\text{-}15)$$

The constant A in the above equations is defined by Mirels and Hamman and given by Equation (3-3). For a general inviscid flowfield the constant C is defined as x_s/t^m so that A is represented in a slightly different form as:

$$A = \frac{2mF_o x_s^{2(\sigma+1)}}{t^{2m(\sigma+1)}}\frac{\mu_\infty}{p_\infty} \qquad (4\text{-}16)$$

It is important to note that the governing differential equations (4-13) and (4-14) reduce identically to Mirels and Hamman's equations (3-6a) and (3-6b) for the self-similar blast wave. For that ideal case, the coefficients in Equations (4-13) and (4-14) become independent of time. For a general blast wave flowfield these coefficients are functions of time so that the quasi-steady assumption is required. By this assumption then the solution (f, g) is a function of time but only in the sense that the coefficients in Equations (4-13) and (4-14) vary with time. The quasi-steady assumption, in essence, involves neglecting all terms which involve time derivatives of the functions f and g. As noted above this is justified apriori for the Taylor-Sedov blast wave by the elimination of time dependence from the differential equations. The assumption essentially freezes the boundary layer at a given instant of time and the solution is assumed to depend only upon the instantaneous flowfield. Physically the assumption is accurate if the rate of diffusion of momentum and heat through the transformed boundary layer is greater than the time rate of change of the external flow properties. Some consequences of this assumption are discussed in Section 4.3.

The problem, as it now stands, requires the quite formidable solution of a pair of simultaneous non-linear partial differential equations. To reduce these to a tractable form the assumption of local similarity is made. This assumption is put forth in the same cavalier spirit as the quasi-steady assumption. Whereas in the quasi-steady assumption time derivatives of f and g were neglected, local similarity dictates that space derivatives with respect to ξ of f and g are neglected. This assumption is advanced with somewhat weaker justification than the quasi-steady assumption. Mirels and Hamman have shown that for the ideal blast wave, the proper similarity transformation makes the quasi-steady assumption redundant. Local similarity, however, requires neglecting the underlined terms in Equations (4-13) and (4-14). The feeling is that away from the shock front the terms neglected by local similarity become smaller relative to the other terms in Equations (4-13) and (4-14). The fair agreement with the integral solution as seen in Section 4.3 is advanced as justification for the local similarity assumption.

In essence the assumption of local similarity requires that all boundary layer flow parameters (u/u_e, h/h_e, $\rho\mu$) be a function only of the similarity variable η at any given time (τ) or distance behind the shock (ξ). This assumption reduces Equations (4-13) and (4-14) to two simultaneous non-linear ordinary differential equations with split boundary conditions. The resulting two-point boundary value problem can be solved by standard numerical methods. The method used is known as a shooting technique whereby guesses are made for the higher order derivatives at the wall [$f_{\eta\eta}(\xi,0)$, $g_\eta(\xi,0)$]. Equations (4-13) and (4-14) are then integrated numerically to some large value of η. Guesses are then made for $f_{\eta\eta}(\xi,0)$, $g_\eta(\xi,0)$ until the resulting solution gives values of $f_\eta(\xi,\infty)$ and $g(\xi,\infty)$ which are equal to 1 within some arbitrary small error. This can be carried out by an iteration scheme which is found to converge quite rapidly and efficiently to the proper solution This process is repeated for the values of $\xi=1-x/x_s$ of interest. This can be performed for the blast wave flowfield at any instant of time thereby determining the blast boundary layer as a function of position (x,y) and time t.

Once the functions f and g (and their derivatives) are determined for the values of ξ and τ of interest the problem is essentially solved. It remains to calculate the physical parameters of interest and re-transform the independent variables ξ, η back into physical coordinates (x,y). This is done using the following equations:

$$x = x_s(1-\xi) \quad , \quad y = \frac{\left[A\tau^{2m(\sigma+1)-1}\left(1-\frac{x}{x_s}\right)\right]^{1/2}}{x^\sigma} \frac{\rho_\infty}{\rho_e}\int_o^\eta g(\xi,\eta)d\eta \qquad (4\text{-}17)$$

The velocity and enthalpy become:

$$u = u_e(x,y,t)f_\eta[\xi(x,t) \ , \ \eta(x,y,t)]$$

$$h = h_e(x,y,t)g[\xi(x,t) \ , \ \eta(x,y,t)] \qquad (4\text{-}18)$$

Parameters of particular interest are the wall shear stress and heat transfer. These are given by Equations (4-19) and (4-20), respectively.

$$\tau_w = \left[\frac{p_\infty}{2mF_o\mu_\infty\rho_\infty^2 t^{m-1}(x_s-x)}\right]^{1/2}\left(\frac{x}{x_s}\right)^\sigma u_e(\rho\mu)_w f_{\eta\eta}(\xi,0) \qquad (4\text{-}19)$$

$$q_w = \frac{1}{Pr}\left[\frac{p_\infty}{2mF_o\mu_\infty\rho_\infty^2 t^{m-1}(x_s-x)}\right]^{1/2}\left(\frac{x}{x_s}\right)^\sigma h_e(\rho\mu)_w g_\eta(\xi,0) \qquad (4\text{-}20)$$

Equations (4-13) and (4-14) were solved using the procedure outlined above for the Taylor-Sedov blast wave flowfield and by assuming Pr, c_p, and μ/T to be constant. The results for the shear stress and heat transfer parameters are given near the shock front in Figure 4-4 and for the complete flowfield in Figure 4-5. As expected these parameters compare more favorably with Mirels and Hamman's solution near the shock front than the steady and locally square-wave solution. It is noted that the solution is identical with Mirels at the shock front and that very near shock front the trend in both $f_{\eta\eta}$ and g_η compare favorably. Boundary layer velocity and enthalpy profiles at the shock front and at ξ=0.5 are given in Figures 4-6 and 4-7. Of note in these figures is the indicated decrease in transformed boundary layer thickness with distance behind the shock front.

4.3 DISCUSSION OF QUASI-STEADY SOLUTIONS

Figures 4-8 through 4-11 provide a comparison of the wall shear stress and heat transfer parameters as calculated by each of the flow calculational schemes discussed in this report. Figures 4-8 and 4-9 compare the solutions very near the shock front in which region Mirels and Hamman's original boundary layer solution is applicable, and Figures 4-10 and 4-11 compare the solutions presented in this report over the entire blast wave. Figures 4-8 and 4-9 show that all the solutions compare well near the shock front with the integral solution showing the best agreement with Mirels and Hamman's solution with respect to variation of $f_{\eta\eta}$ and g_η with distance from the shock front (ξ). This trend with ξ is indicative of the inadequacy of the assumptions of local

similarity of both quasi-steady solutions. This point is further verified by the fact that the quasi-steady and locally similar solution shows a slightly better trend with respect to ξ than the steady square wave solution. This is attributed to the better approximation of variations with ξ in the quasi-steady and locally similar formulation. The rather good comparison of both quasi-steady solutions with the integral solution away from the shock front is indication that the assumption of local similarity improves with distance from the shock front. This is to be expected since the blast wave flowfield (and boundary layer flow) varies less rapidly with respect to ξ as ξ increases away from the shock front. It is thus expected that the terms neglected by local similarity (f_{ξ} and $f_{\eta\xi}$) will decrease in significance (relative to the other terms in the boundary layer equation) as ξ increases.

It is difficult to justify or to speculate on the accuracy of the steady and locally square wave solution. Suffice it to point out that the above figures show that the solution compares surprisingly well with the more rigorous integral solution for the Taylor-Sedov blast wave. The good agreement is fortuitous. The solution's utility rests on the fact that it provides a relatively simple procedure for estimating the important boundary layer flow parameter (shear stress, heat transfer and boundary layer thickness). It can also be used to estimate such parameters for the boundary layer of a general non-ideal blast wave. The relatively good comparison shown here with the more rigorous boundary layer solutions should add some credibility to the numbers calculated in such a manner.

The results of the quasi-steady and locally similar solution for the Taylor-Sedov blast wave are quite satisfying. The primary advantage of the solution, and the reason for performing it, is that it is not dependent upon a self-similar inviscid flowfield, i.e., the assumption of a strong shock is not required. This opens the possibility of extending the solution to include non-ideal effects in the free-stream. In particular, a numerical solution valid in the weak shock regime or one which includes radiation effects (which cause a shock precusor) could be used for the boundary layer analysis. The accuracy of the quasi-steady

and local similarity assumptions for such a flowfield can only be conjectured upon. The quasi-steady assumption could be quite good. As pointed out earlier, the similarity transformation used eliminates time from the boundary layer equations [Equations (4-13) and (4-14)] for any power law shock ($x_s=Ct^m$) for which the trailing blast wave flow properties have a similar spatial distribution for different times. This condition at least partially holds for a high explosive or nuclear blast wave for even late time. That is, even for weak shocks, the spatial distribution of blast wave flow properties varies little in general shape. Thus it is conceivable that even for such a case the quasi-steady and locally similar procedure could give good results. As far as the applicability of the local similarity assumption is concerned, it can only be pointed out that the assumption provides quite good results in comparison to the integral solution for the Taylor-Sedov flowfield. It is expected that this would carry over to the more general blast wave.

The quasi-steady and locally similar solution also presents the possibility of being extended to include turbulence by using a phenomenological theory of turbulence, or the solution could be numerically coupled to a semi-empirical theory for wall turbulence. The solutions presented in this report assume viscosity is a linear function of temperature. This restriction is not required in the quasi-steady and locally similar solution. In any practical calculation viscosity would be made a function of temperature using an empirical equation like the Sutherland viscosity relation. This would be consistent with local similarity and $\rho\mu$ would be some function of the temperature ratio g. In summary, this solution method is attractive because of the straightforward manner in which it may be extended to include effects which are difficult to handle theoretically but which add considerably to the accuracy of the physical model.

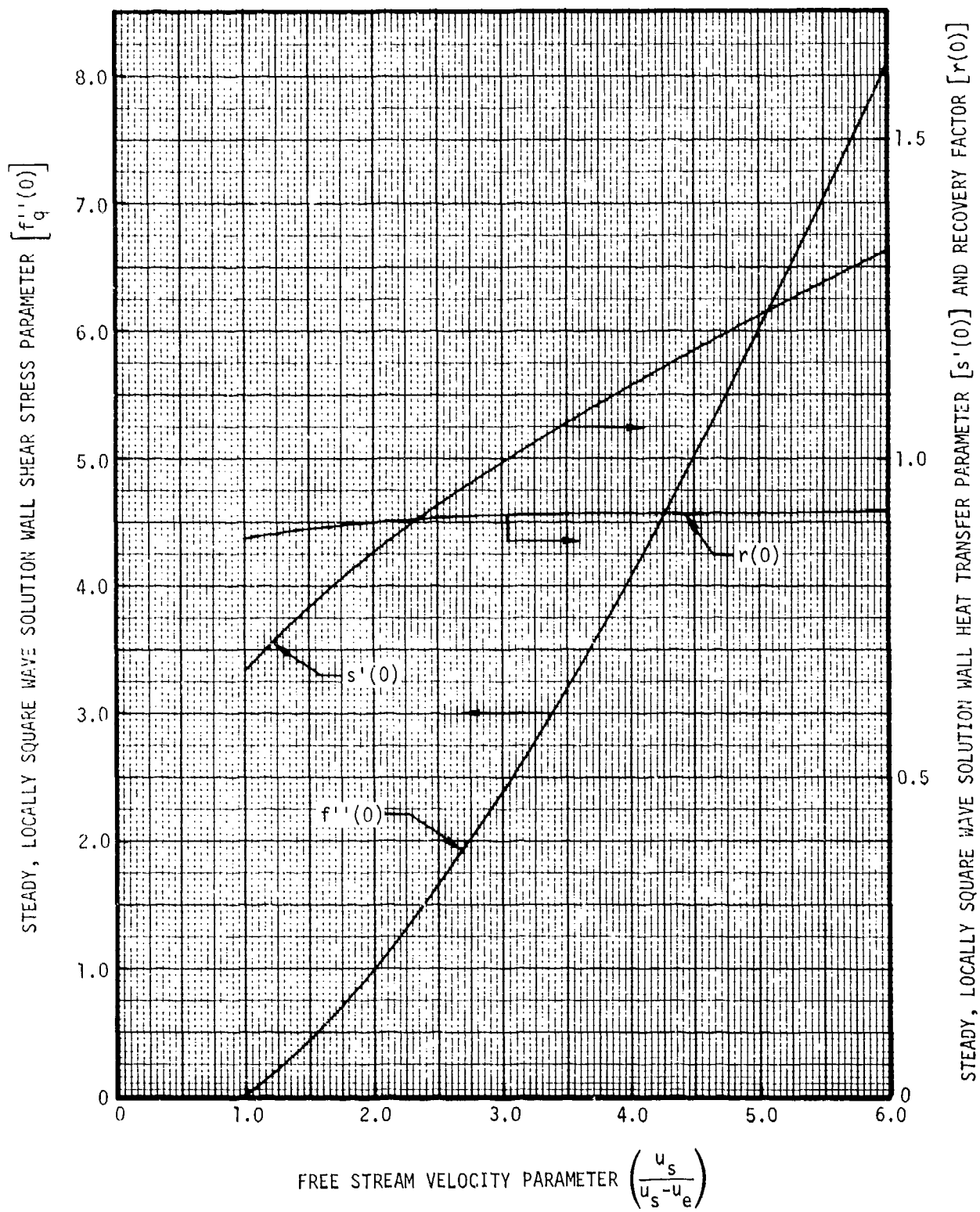

FIGURE 4-1 WALL SHEAR STRESS AND HEAT TRANSFER PARAMETERS VS NON-DIMENSIONAL FREE-STREAM VELOCITY PARAMETER

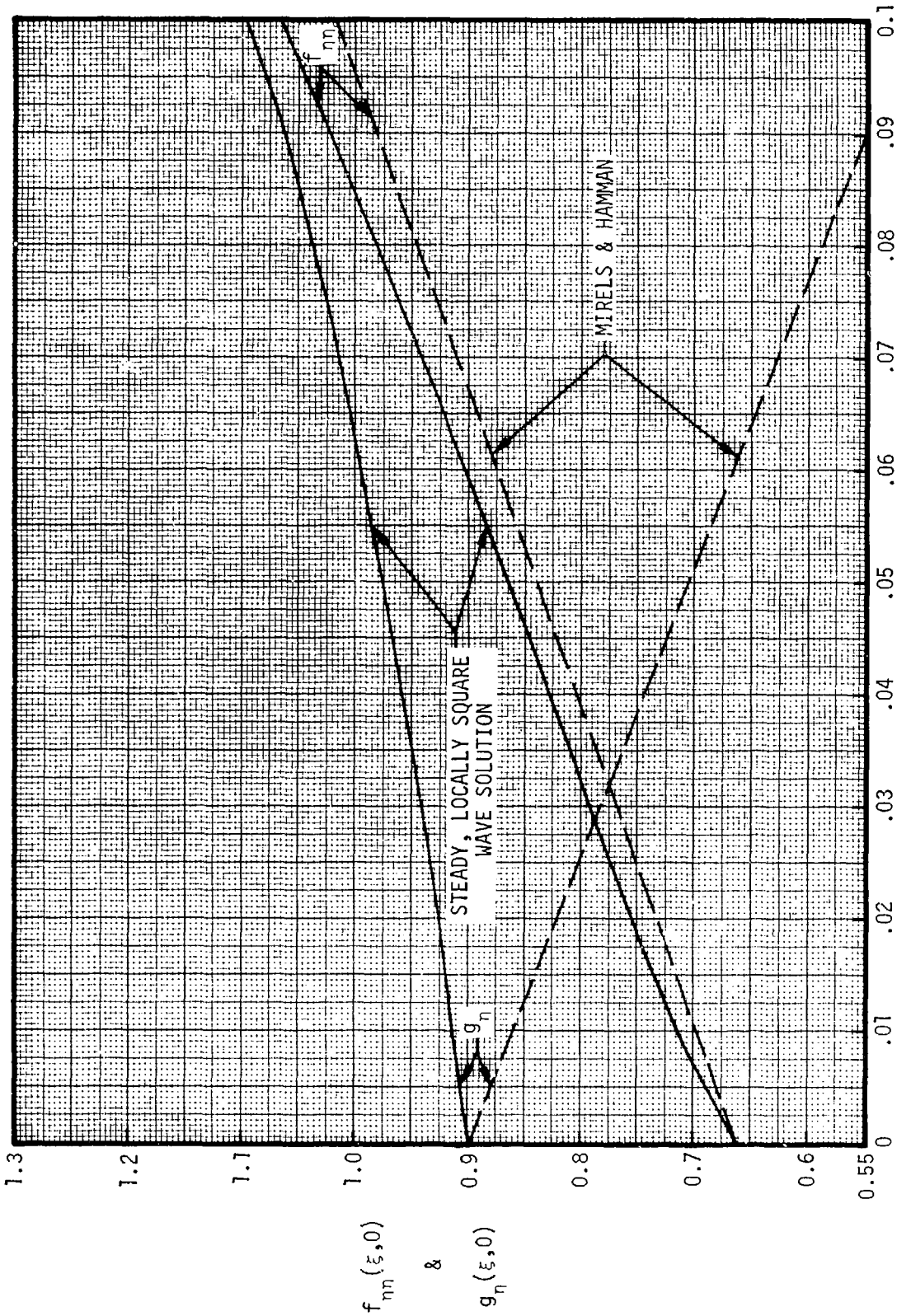

FIGURE 4-2 WALL SHEAR AND HEAT TRANSFER PARAMETERS FOR STRONG SPHERICALLY EXPANDING SHOCK NEAR SHOCK FRONT USING STEADY, LOCALLY SQUARE WAVE PROCEDURE

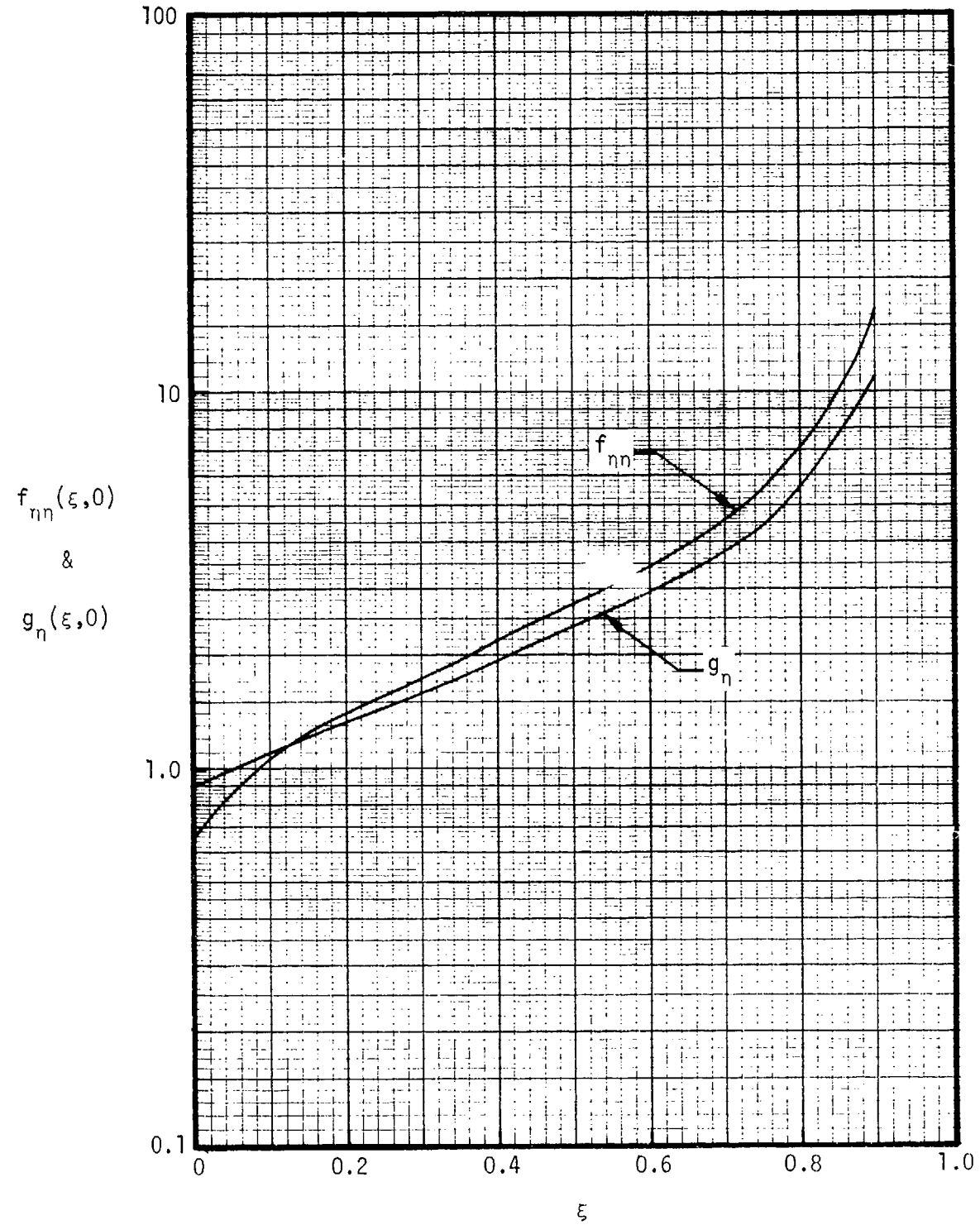

FIGURE 4-3 WALL SHEAR AND HEAT TRANSFER PARAMETERS FOR STRONG, SPHERICALLY EXPANDING SHOCK USING STEADY, LOCALLY SQUARE WAVE PROCEDURE

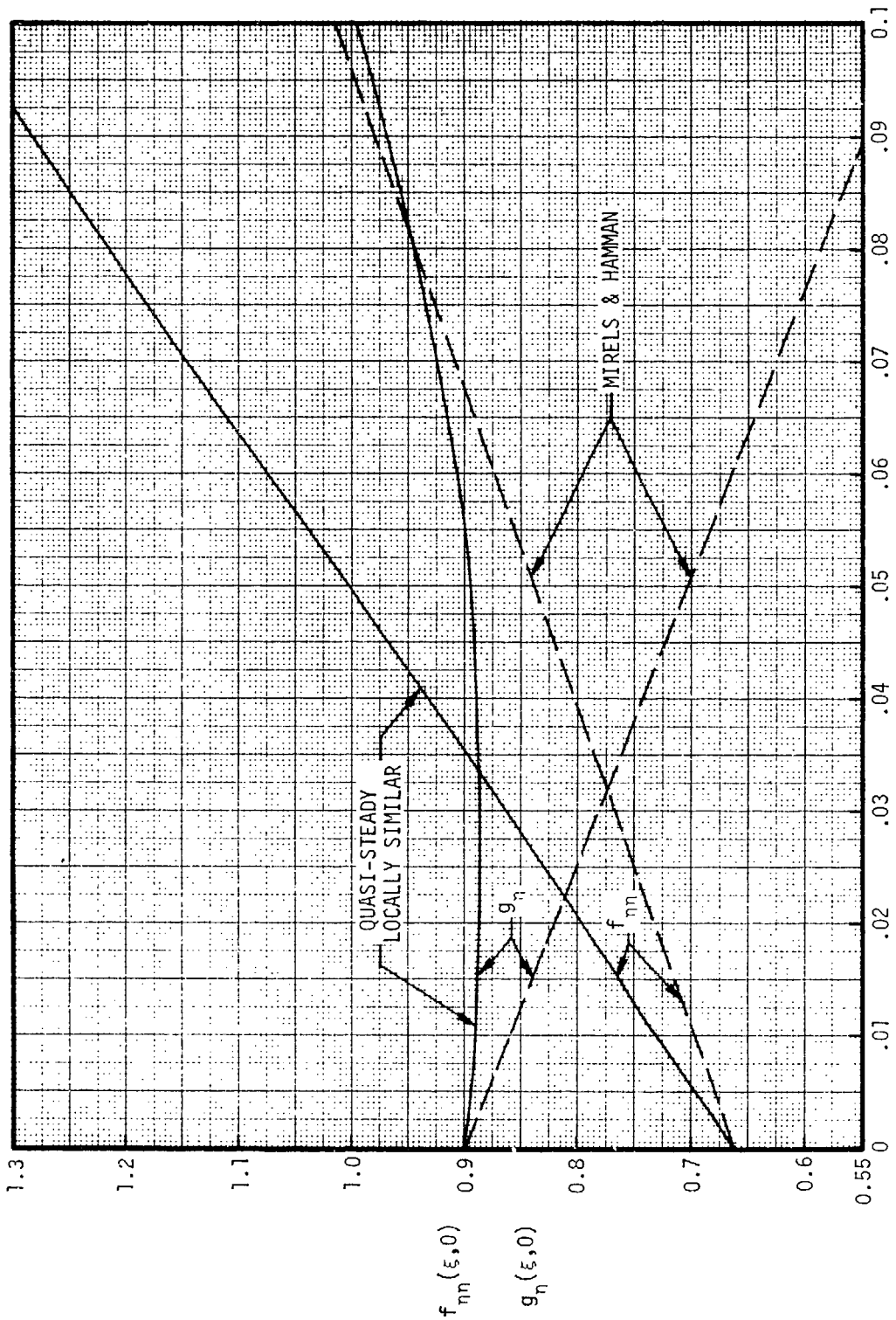

FIGURE 4-4 WALL SHEAR AND HEAT TRANSFER PARAMETERS FOR STRONG SPHERICALLY EXPANDING SHOCK NEAR SHOCK FRONT USING QUASI-STEADY, LOCALLY SIMILAR SOLUTION

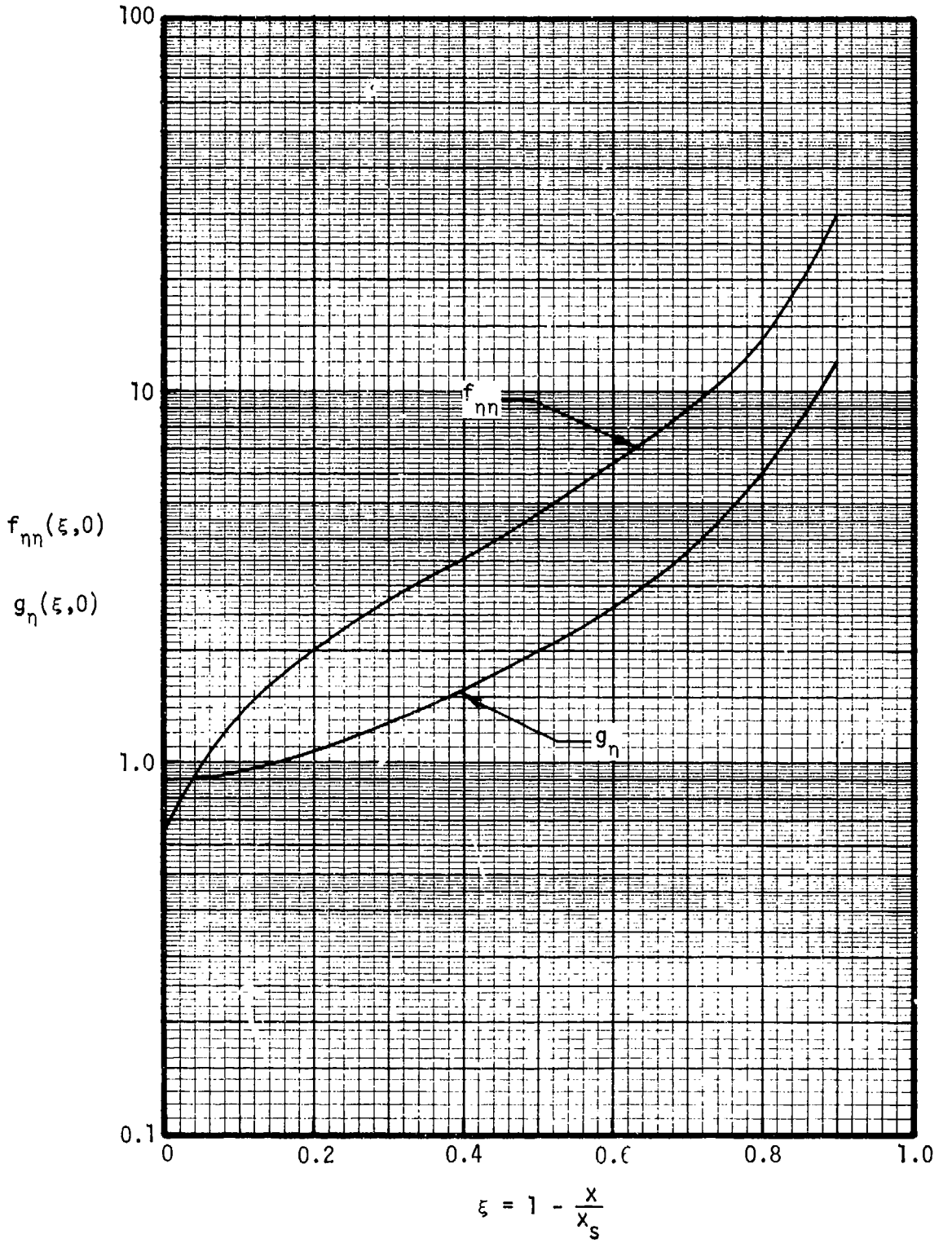

FIGURE 4-5 WALL SHEAR AND HEAT TRANSFER PARAMETER FOR STRONG SPHERICALLY EXPANDING SHOCK USING QUASI-STEADY, LOCALLY SIMILAR SOLUTION

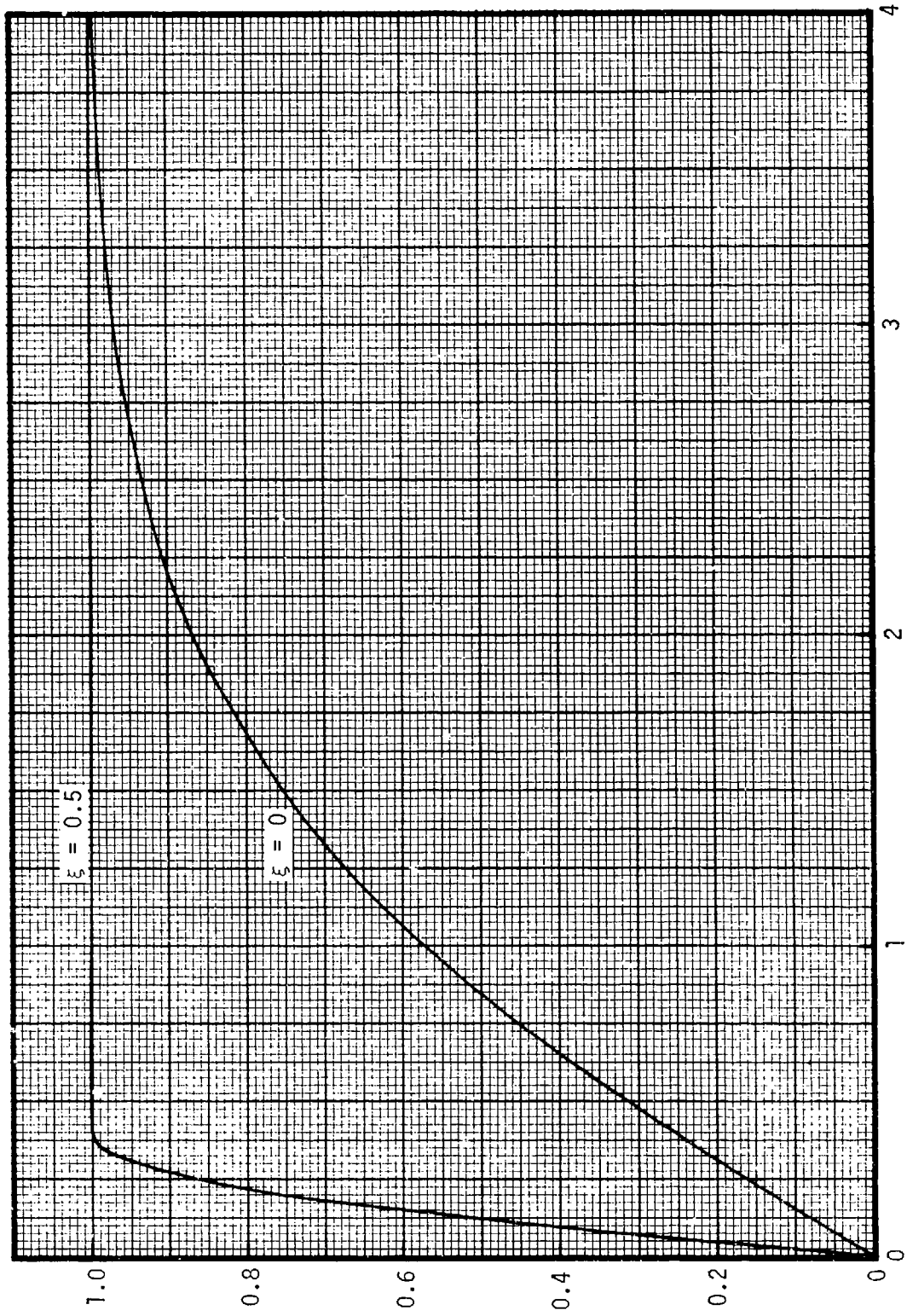

FIGURE 4-6 BOUNDARY LAYER VELOCITY PROFILES

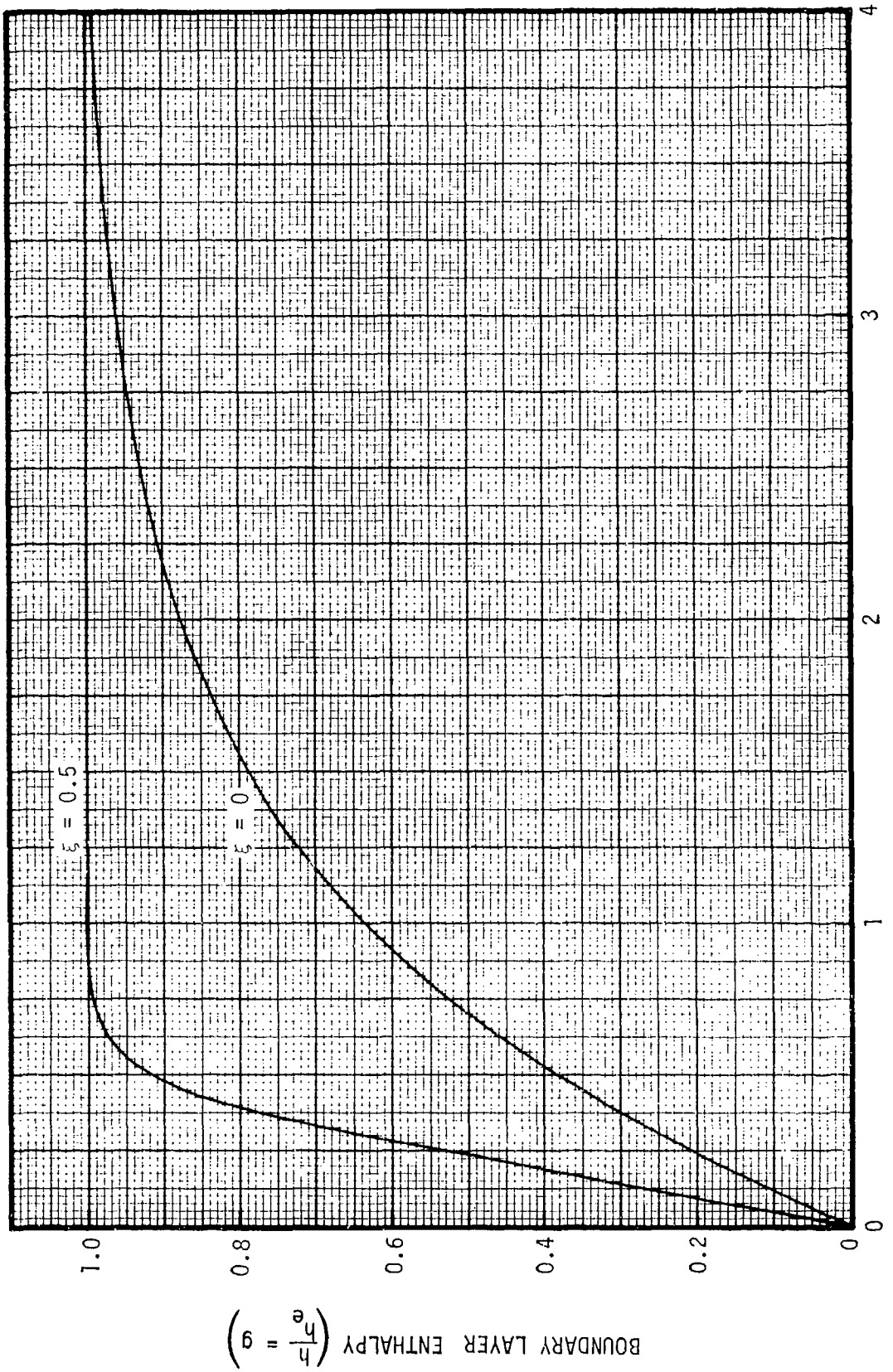

FIGURE 4-7 BOUNDARY LAYER ENTHALPY PROFILES

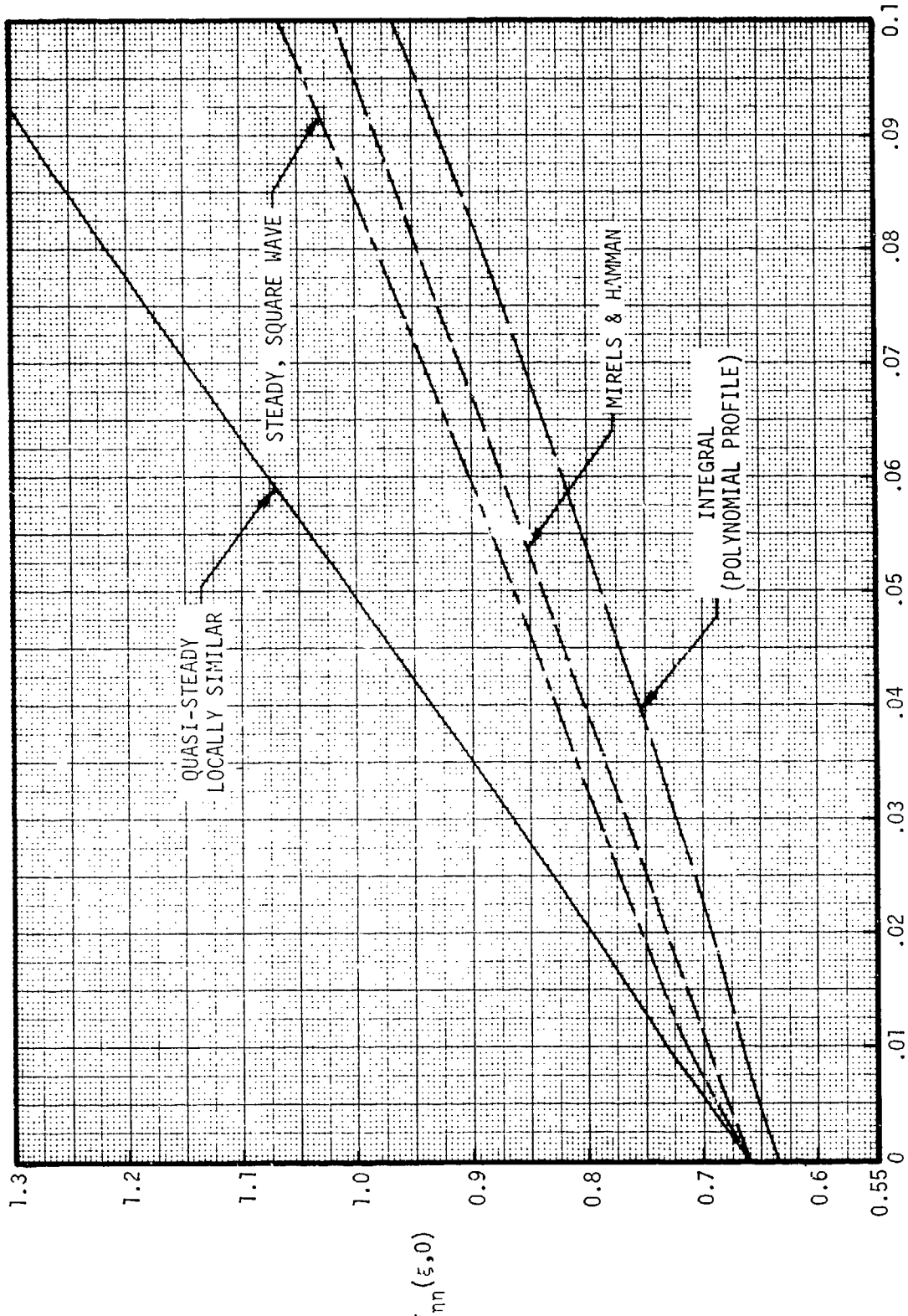

FIGURE 4-8 WALL SHEAR STRESS PARAMETER FOR STRONG, SPHERICALLY EXPANDING SHOCK NEAR SHOCK FRONT

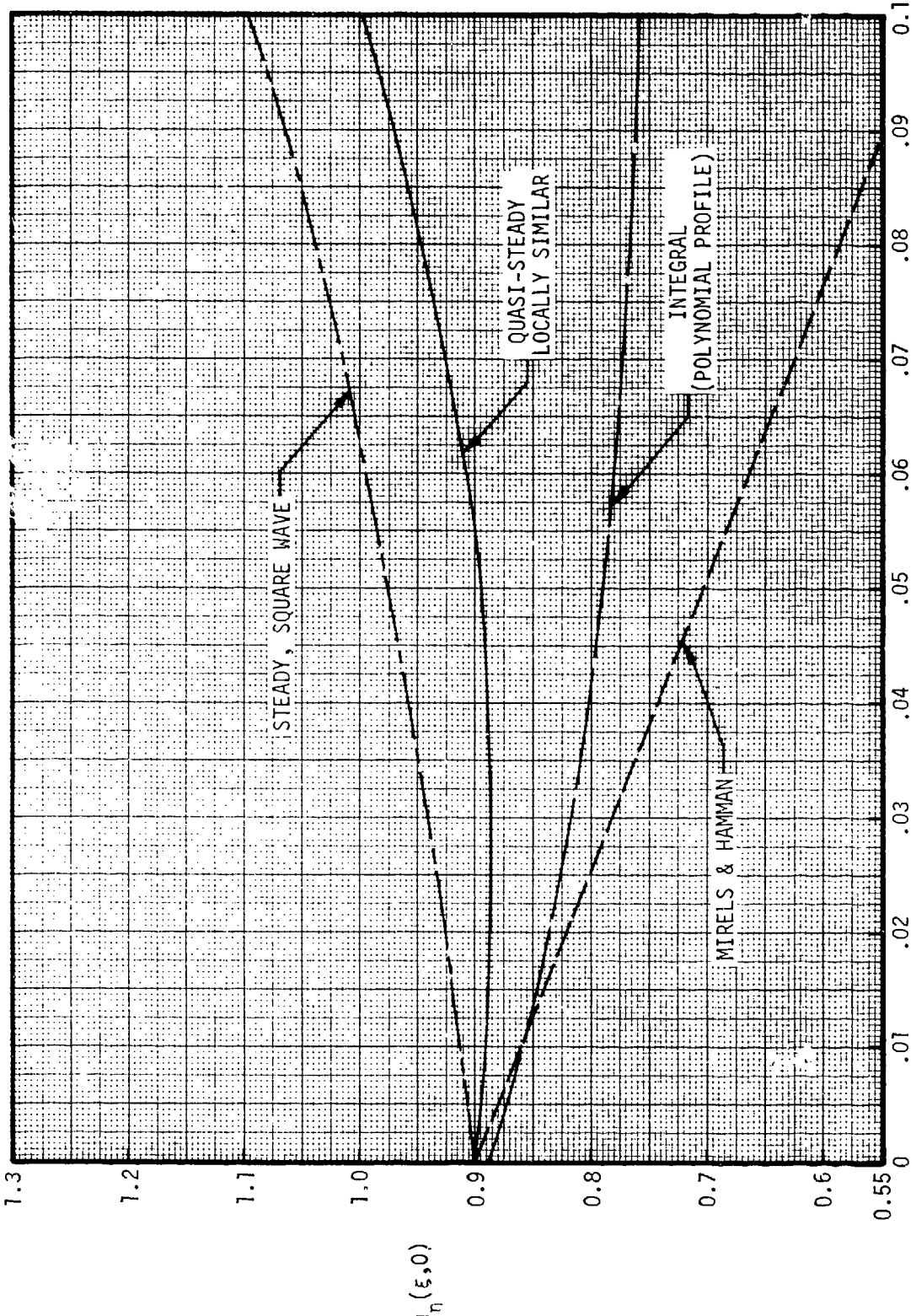

FIGURE 4-9 WALL HEAT TRANSFER PARAMETER FOR STRONG, SPHERICALLY EXPANDING SHOCK NEAR SHOCK FRONT

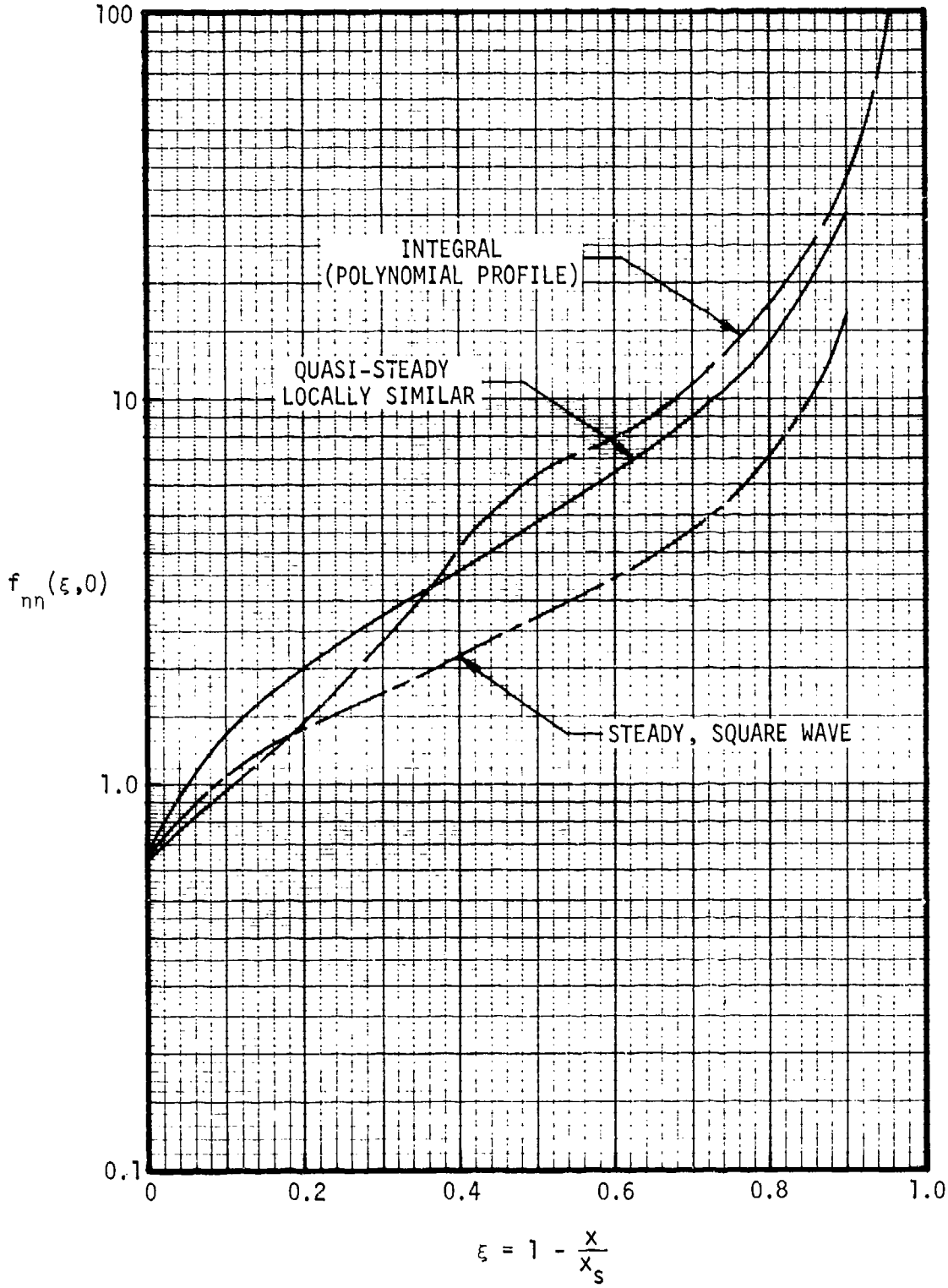

FIGURE 4-10 WALL SHEAR STRESS PARAMETER FOR STRONG, SPHERICALLY EXPANDING SHOCK

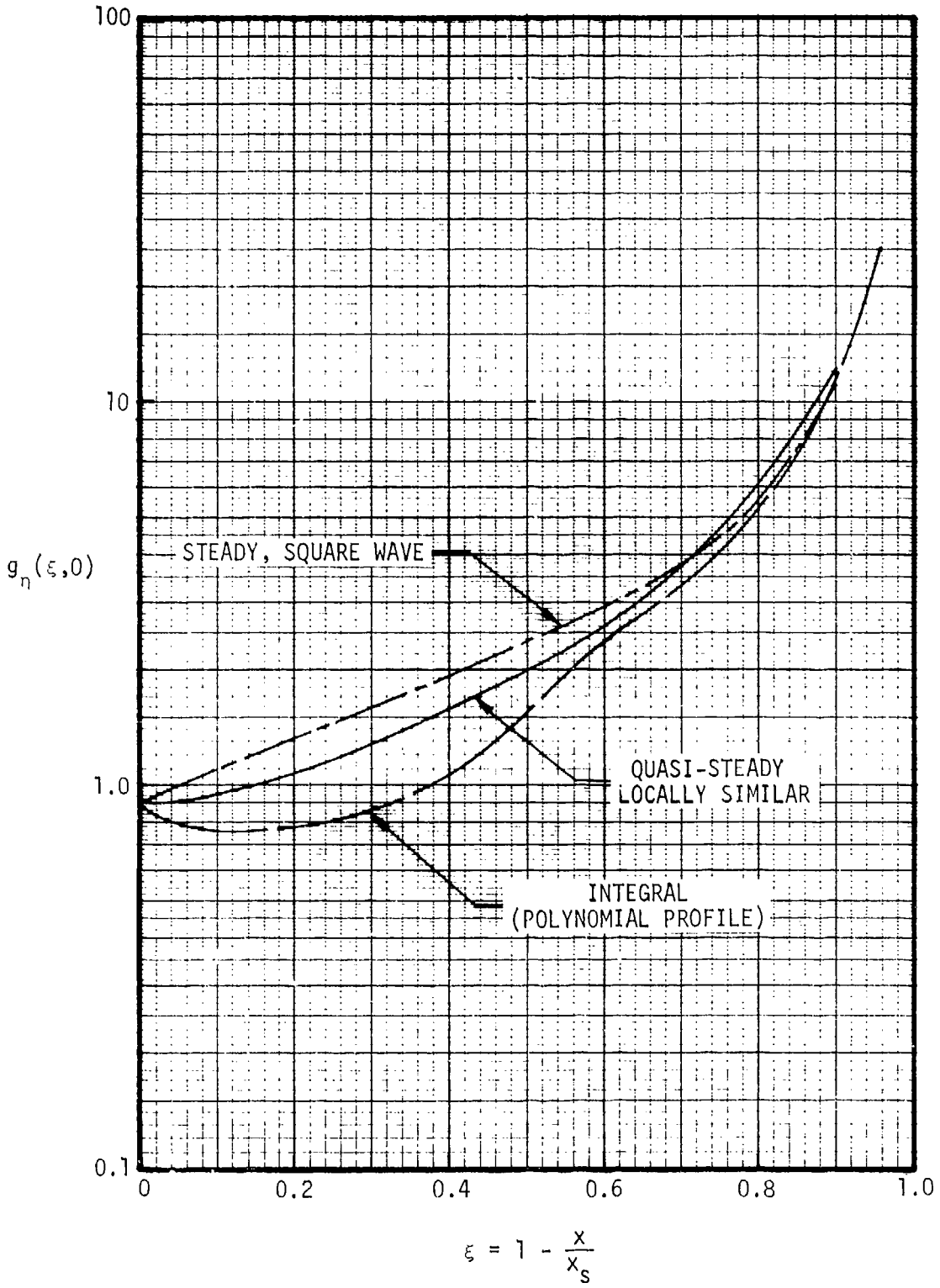

FIGURE 4-11 WALL HEAT TRANSFER PARAMETER FOR STRONG, SPHERICALLY EXPANDING SHOCK

(Reverse of Page is Blank)

5. ILLUSTRATION OF RESULTS

The solutions to the blast wave laminar boundary layer equations have been given in Sections 3 and 4. Of the several solutions presented, the most rigorous one is the integral solution with the polynomial representation for velocity and temperature profiles. This solution is employed to illustrate some physical properties of interest in this section.

The velocity thickness y_δ and the temperature thickness y_{δ_t} can be obtained by setting $\eta=\delta$ and $\eta=\delta_t$, respectively, in Equation (3-2b). The result is

$$y_{\delta_t} = \left(\frac{At^{2m-1}}{C^{2\sigma}}\right)^{1/2} \frac{\xi^{1/2}}{(1-\xi)^{\sigma}} \frac{\delta_t}{R} \left(\frac{7}{10} - \frac{1}{60} b_2\right) \tag{5-1}$$

and

$$y_\delta = y_{\delta_t} \zeta \Big/ \left(\frac{7}{10} - \frac{1}{60} b_2\right) \tag{5-2}$$

where

$$\zeta = \frac{1}{\Delta} - \frac{3}{10} - \frac{1}{60} b_2 \qquad \text{for } \Delta \leq 1$$

$$\zeta = \frac{1}{\Delta^2} - \frac{1}{2\Delta^4} + \frac{1}{5\Delta^5} - \frac{1}{3} b_2 \left(\frac{1}{2\Delta^2} - \frac{1}{\Delta^3} + \frac{3}{4\Delta^4} - \frac{1}{5\Delta^5}\right) \qquad \text{for } \Delta \geq 1 \tag{5-3}$$

Thus, both y_δ and y_{δ_t} can be given as products of a function of t and a function of ξ. By letting

$$Q(t) = \left(\frac{At^{2m-1}}{C^{2\sigma}}\right)^{1/2} \tag{5-4}$$

the results for $y_\delta/Q(t)$ and $y_{\delta_t}/Q(t)$ are plotted in Figures 5-1 and 5-2 for spherical shock. Since A is proportional to $C^{2(\sigma+1)}$, the scaling is that y_δ and y_{δ_t} are proportional to C which varies with the explosion energy E as $C \sim E^{m/2}$. Also, at given ξ, y_δ and y_{δ_t} are proportional to $t^{m-0.5}$. For C=3800 ft/sec$^{0.4}$ (corresponding roughly to a 1.0 megaton yield*) and t=0.1 and 1.0 sec, y_δ and y_{δ_t} are shown as functions of x in Figure 5-3. It is seen that the boundary layer thicknesses are quite thin for a long distance behind the shock, after which the thicknesses increase rapidly. The velocity thickness for the blast wave at 0.1 second is compared to the velocity thickness for a square wave (using peak uniform free-stream properties) in Figure 5-4. It is seen that large differences exist.

The shear stress τ_w and heat transfer rate q_w can be written as

$$\tau_w = W(t)\left[\frac{(1-\xi)^\sigma}{\xi^{1/2}} F\phi\left(\frac{2}{\delta}\right)\right] \tag{5-5}$$

and

$$q_w = W(t)(Cmt^{m-1})\left[\frac{1}{Pr}\frac{\gamma-1}{\gamma}\frac{(1-\xi)^\sigma}{\xi^{1/2}}\frac{F^2}{R}\frac{(2-b_2/\xi)}{\delta_t}\right] \tag{5-6}$$

where

$$W(t) = \frac{\mu_\infty \rho_\infty}{p_\infty}\left(\frac{C^{2\sigma}}{At^{2m-1}}\right)^{1/2}\left(Cmt^{m-1}\right)^3 \tag{5-7}$$

Thus τ_w can be scaled with W(t), and q_w with $W(t)Cmt^{m-1}$ or $W(t)u_s(t)$. From the expression for W(t), it is seen that τ_w and q_w decrease rapidly as time is increased. The functions $\tau_w/W(t)$ and $q_w/W(t)u_s(t)$ are plotted in Figure 5-5 for the spherical shock. It is seen that near the shock, both shear stress and heat transfer rate decrease with distance from the shock. Some distance away, however, the heat transfer rate increases rapidly. The reason for this is that the free-stream temperature increases more rapidly than the heat transfer coefficient decreases in this regime. For C=3800 ft/sec$^{0.4}$ and t=0.1 and 1.0 sec, τ_w and q_w are shown as functions of x in Figure 5-6.

*This is calculated based on 1.0 megaton free air burst which corresponds roughly to 1/2 megaton surface burst.

The velocity and temperature distributions shown in Section 3 are given in terms of η. These distributions can be given in terms of y through Equation (3-2b) which relates η to y. For the polynomial solution, the relation becomes

$$y = Q(t) \frac{\xi^{1/2}}{(1-\xi)^{1/2}} \frac{1}{R} \left[\frac{\eta^2}{\delta_t} - \frac{\eta^4}{2\delta_t^3} + \frac{\eta^5}{5\delta_t^4} - \frac{1}{3} b_2 \left(\frac{\eta^2}{2\delta_t} - \frac{\eta^3}{\delta_t^2} + \frac{3\eta^4}{4\delta_t^3} - \frac{\eta^5}{5\delta_t^4} \right) \right] \quad \text{for } \eta \leq \delta_t \tag{5-8}$$

$$y = Q(t) \frac{\xi^{1/2}}{(1-\xi)^{1/2}} \frac{1}{R} \left[\delta_t \left(\frac{7}{10} - \frac{1}{60} b_2 \right) + \eta - \delta_t \right] \quad \text{for } \eta \geq \delta_t$$

The results of the velocity and temperature profiles as functions of $y/Q(t)$ and ξ are shown in Figures 5-7 and 5-8 for the spherical shock.

The following and last illustration does not require the results of the boundary layer study but may be of interest. It is difficult to assess the transition point from laminar flow to turbulent flow. However, one may wish to estimate the Reynolds number variation. For this purpose, one may define a Reynolds number Re as

$$Re = \frac{u_e(x_s - x)}{\mu_e} = \frac{p_\infty t}{\mu_\infty m} \frac{\phi R^2 \xi}{F} = \frac{p_\infty t}{\mu_\infty m} Z(\xi) \tag{5-9}$$

The value of $Re/(p_\infty t/\mu_\infty m)$ is plotted in Figure 5-9 for the spherical shock. It is seen that Re first increases and then decreases as ξ is increased.

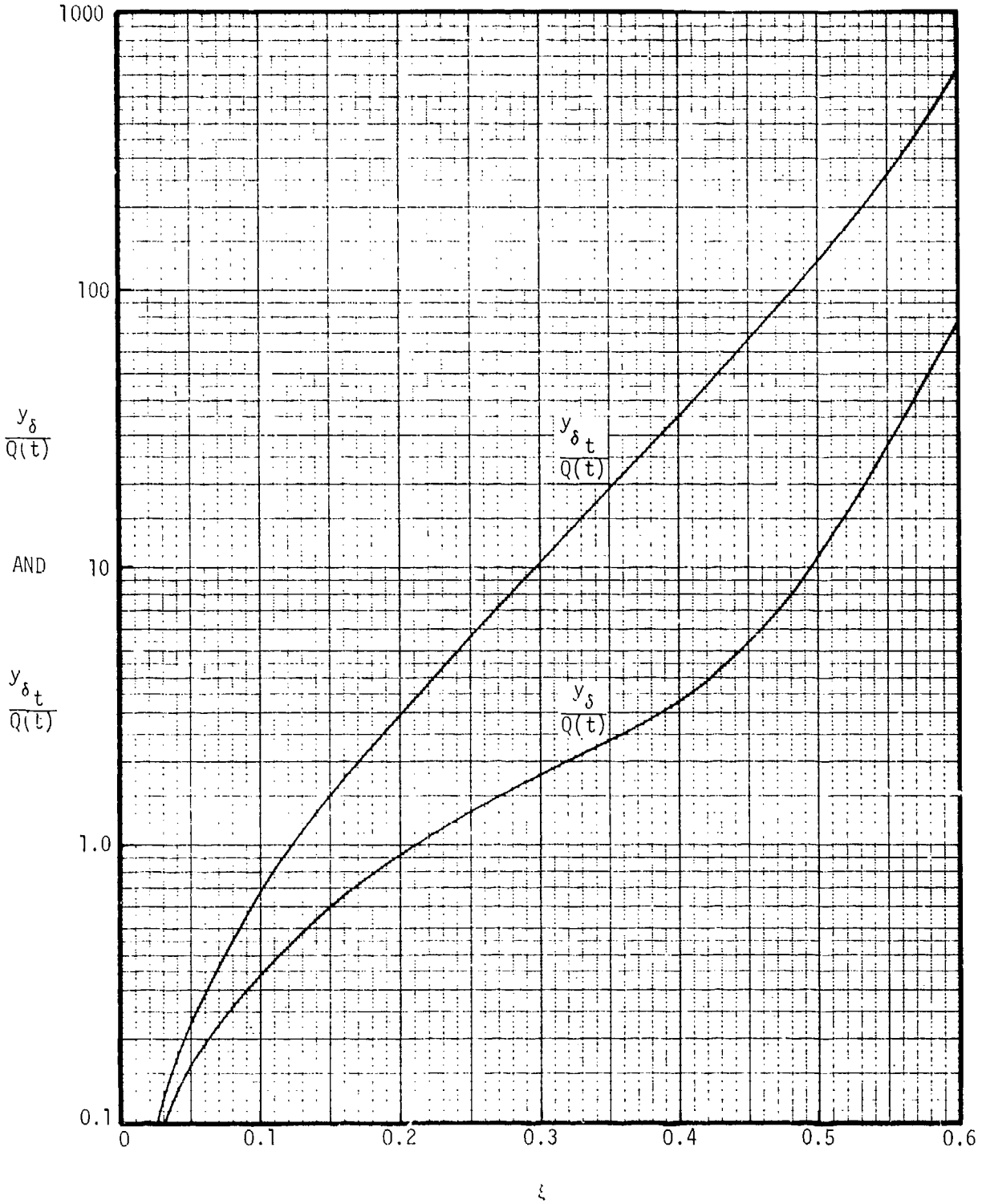

FIGURE 5-1 SCALED BOUNDARY LAYER VELOCITY AND TEMPERATURE THICKNESSES

CONFIDENTIAL

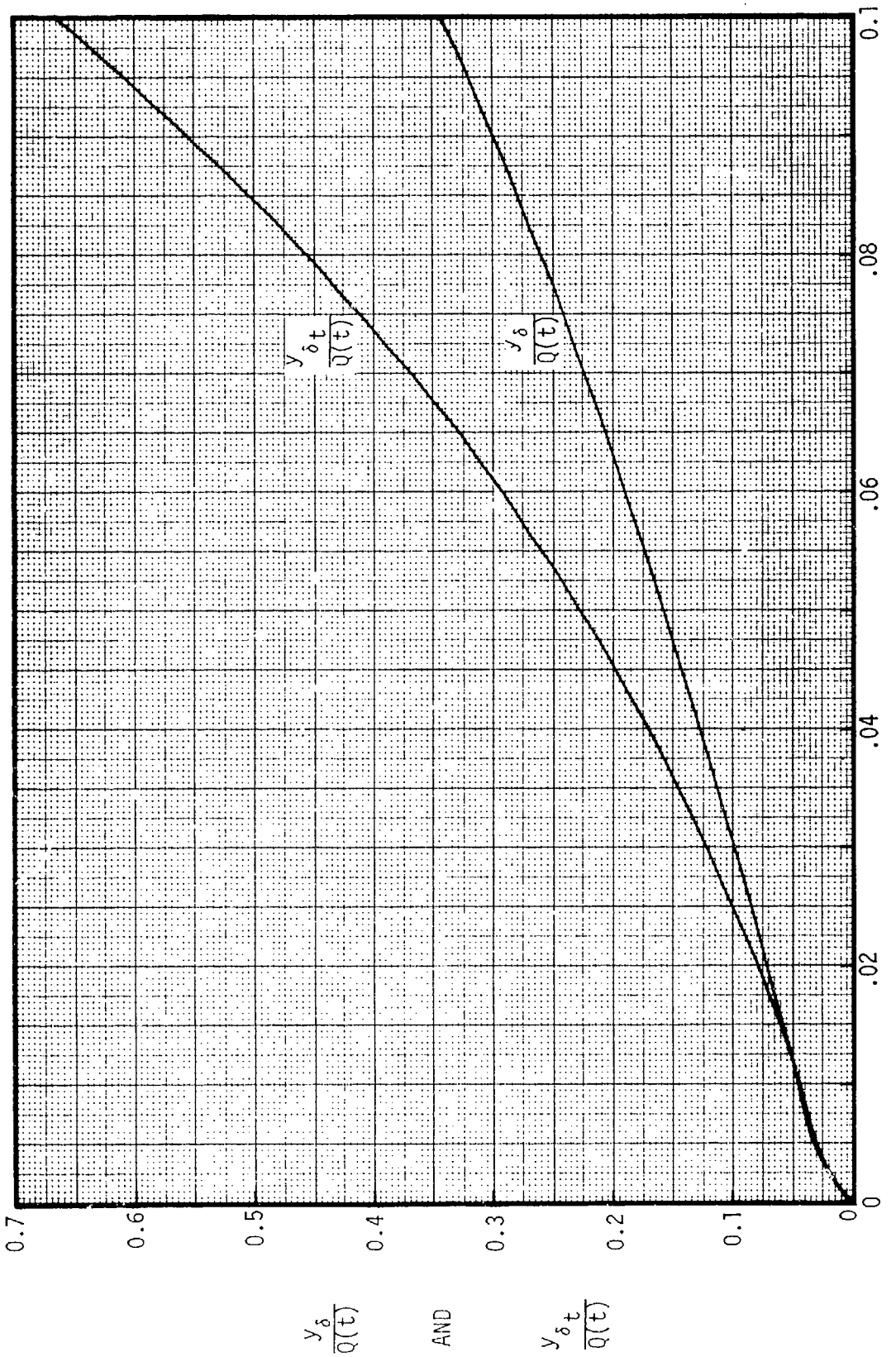

FIGURE 5-2 SCALED BOUNDARY LAYER VELOCITY AND TEMPERATURE THICKNESSES NEAR SHOCK FRONT

CONFIDENTIAL

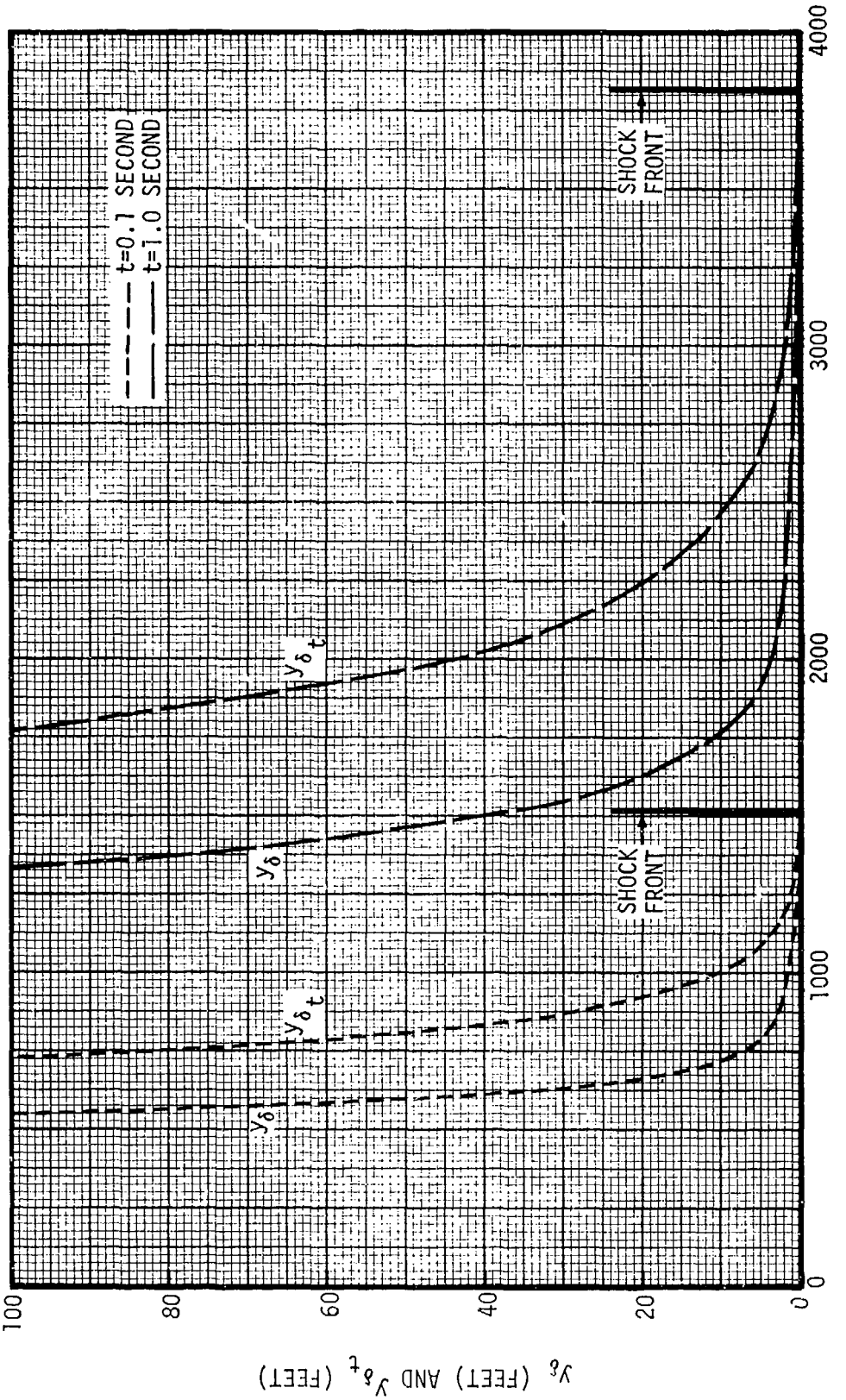

FIGURE 5-3 BOUNDARY LAYER VELOCITY AND TEMPERATURE THICKNESSES FOR 1.0 MEGATON YIELD AT 0.1 AND 1.0 SECOND AFTER BURST

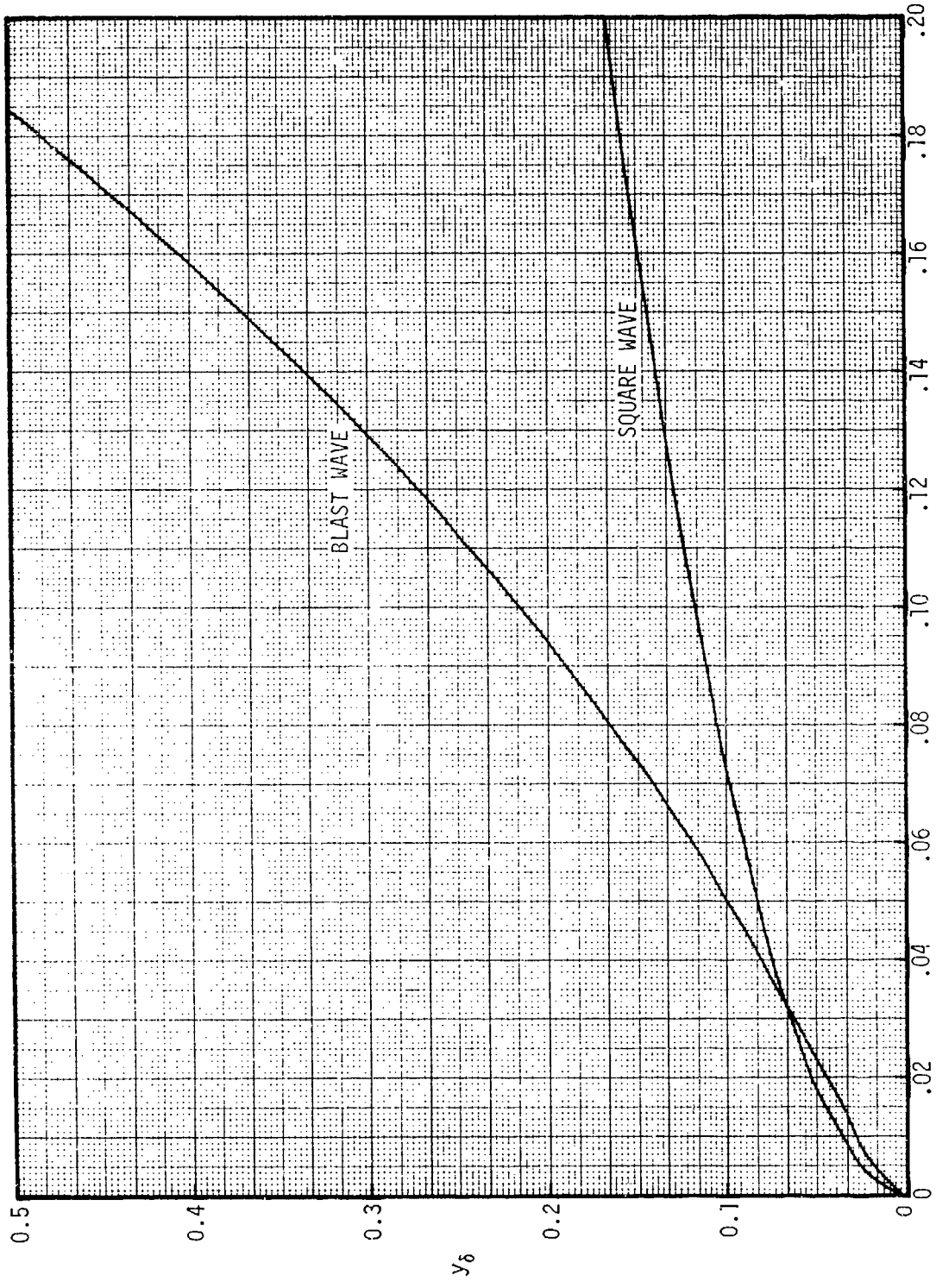

FIGURE 5-4 BLAST WAVE VELOCITY THICKNESS COMPARED TO SQUARE WAVE (FLAT PLATE) VELOCITY THICKNESS, FOR 1.0 MEGATON YIELD AT 0.1 SECOND AFTER BURST

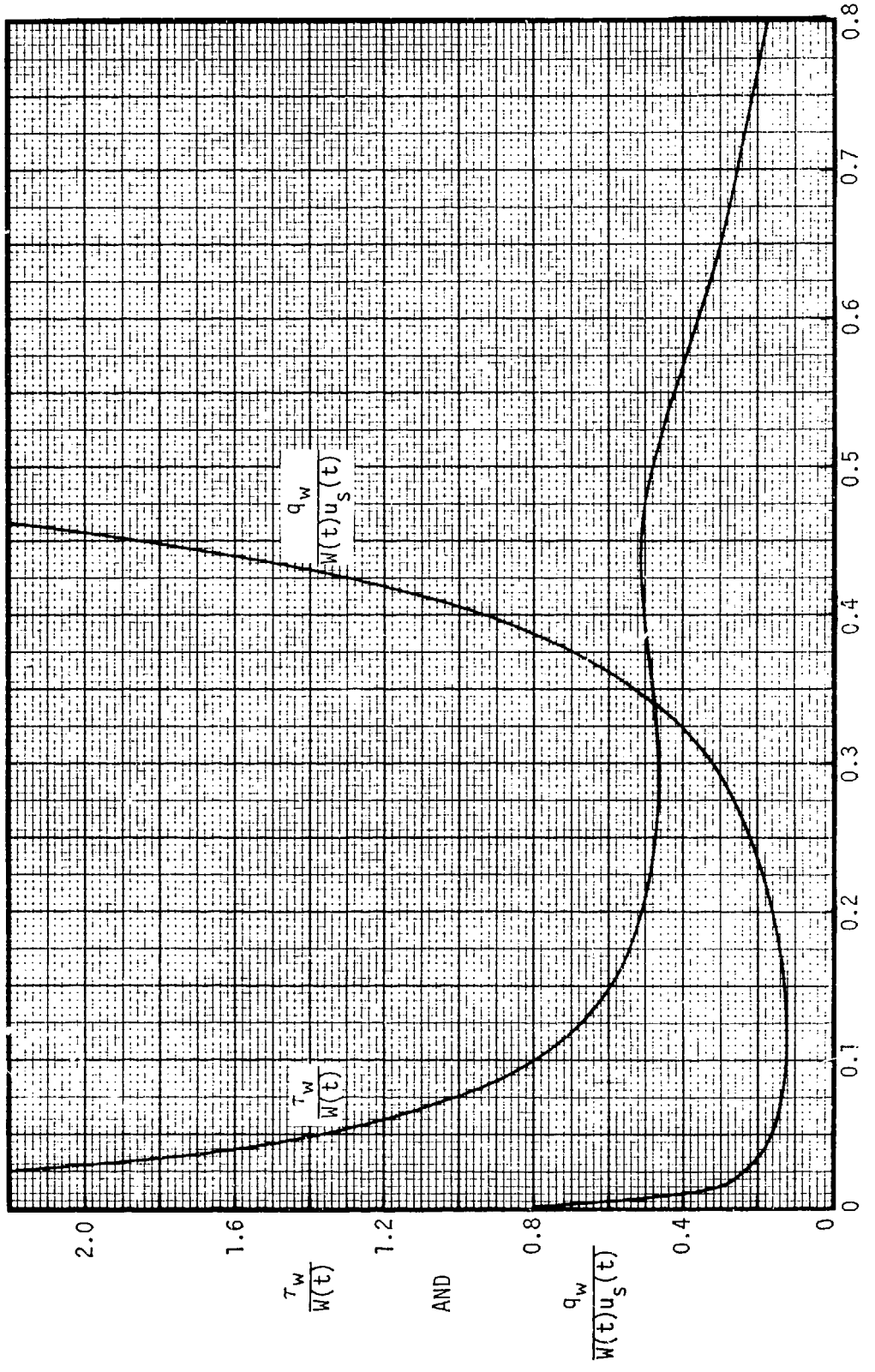

FIGURE 5-5 SCALED WALL SHEAR STRESS AND HEAT TRANSFER

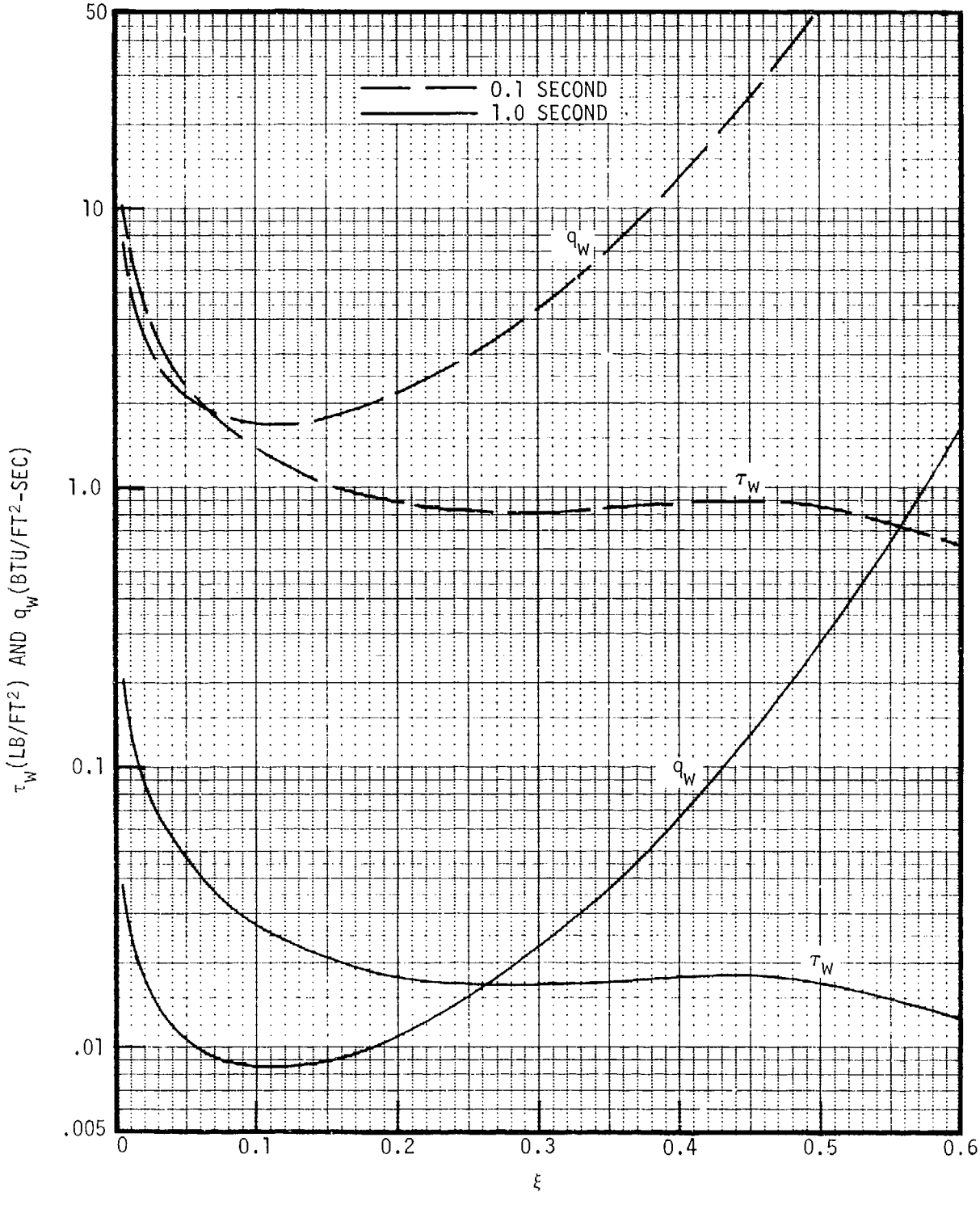

FIGURE 5-6 WALL SHEAR STRESS AND HEAT TRANSFER FOR 1.0 MEGATON YIELD AT 0.1 AND 1.0 SECOND AFTER BURST

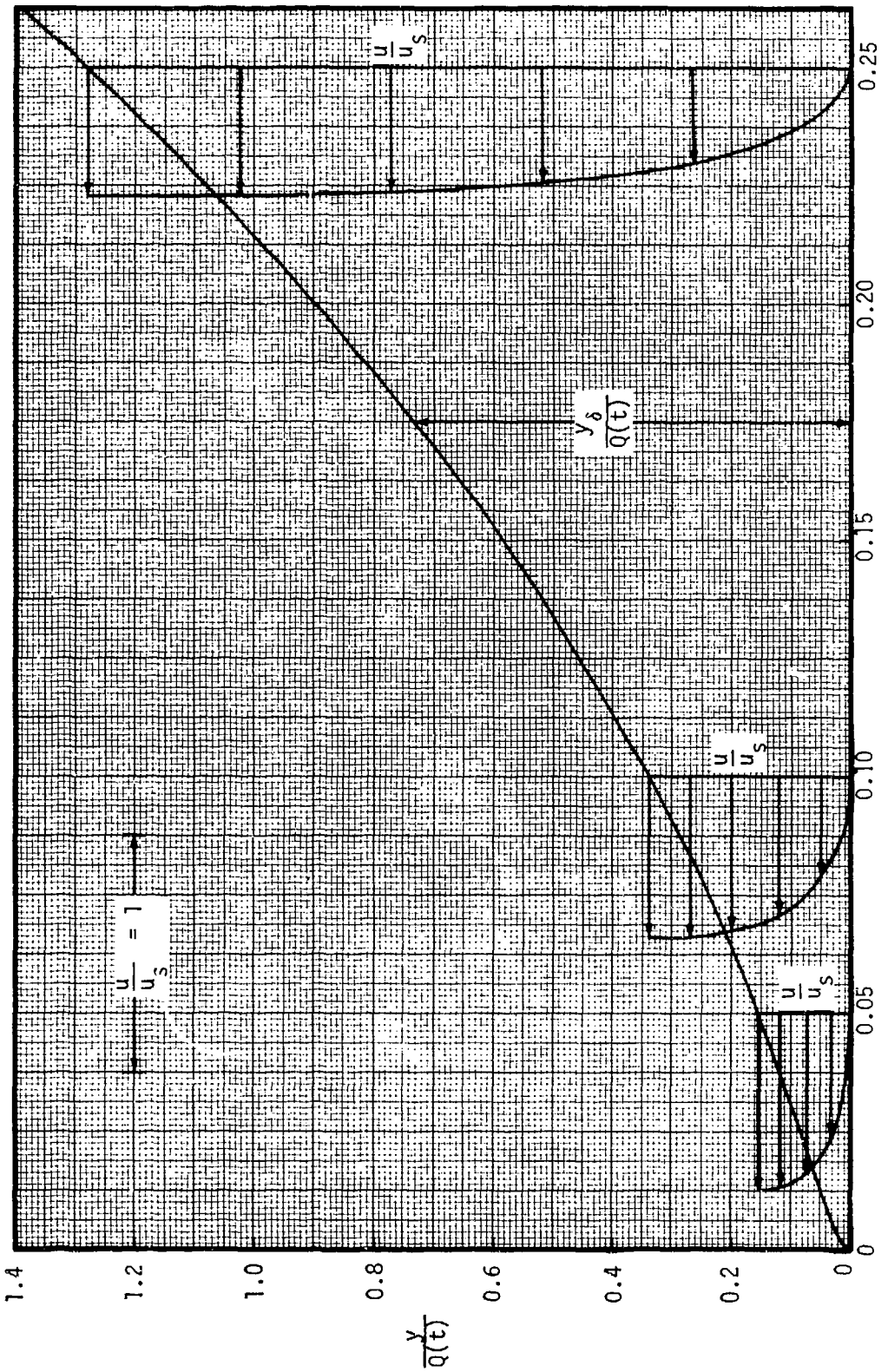

FIGURE 5-7 SCALED VELOCITY PROFILES

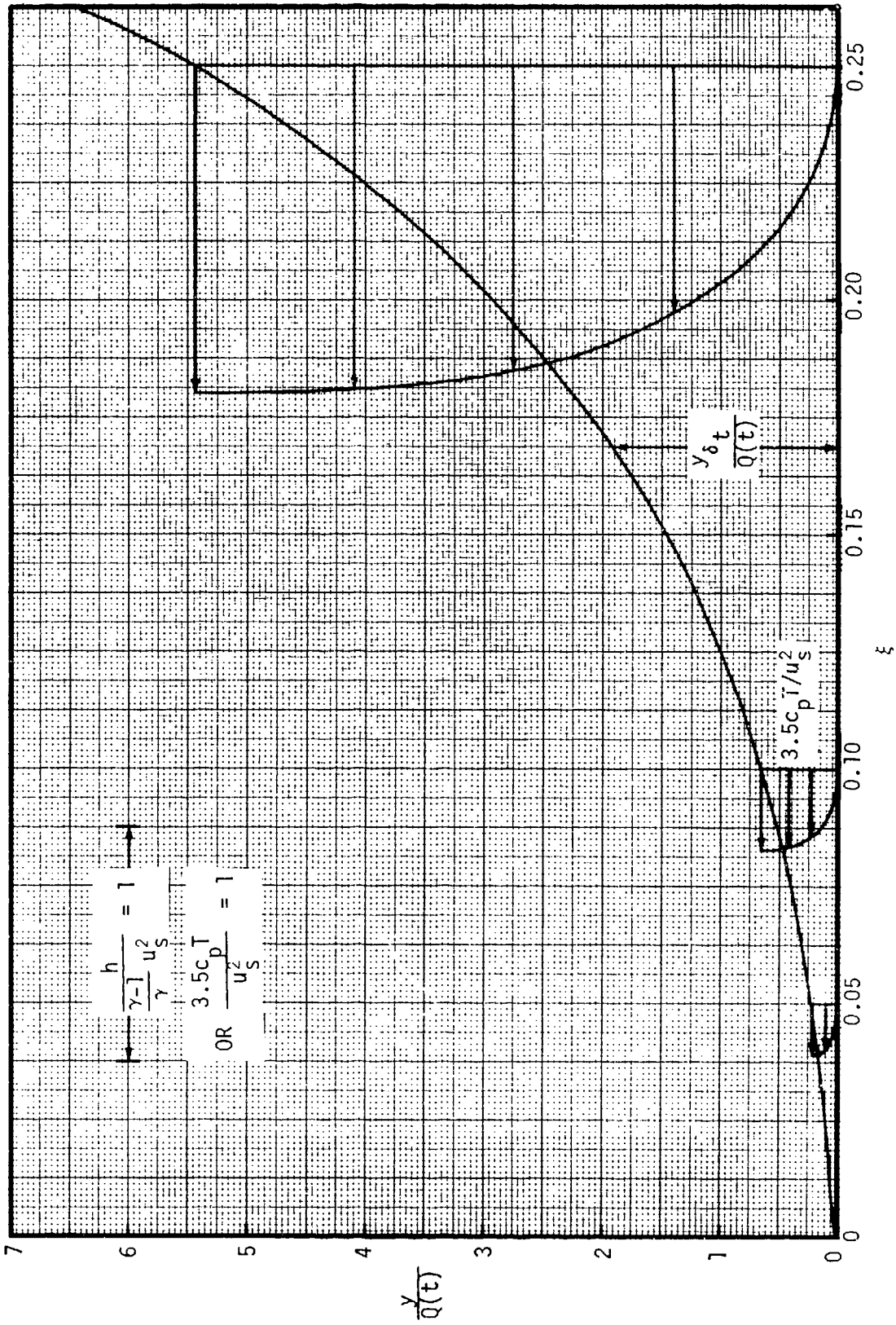

FIGURE 5-8 SCALED TEMPERATURE PROFILES

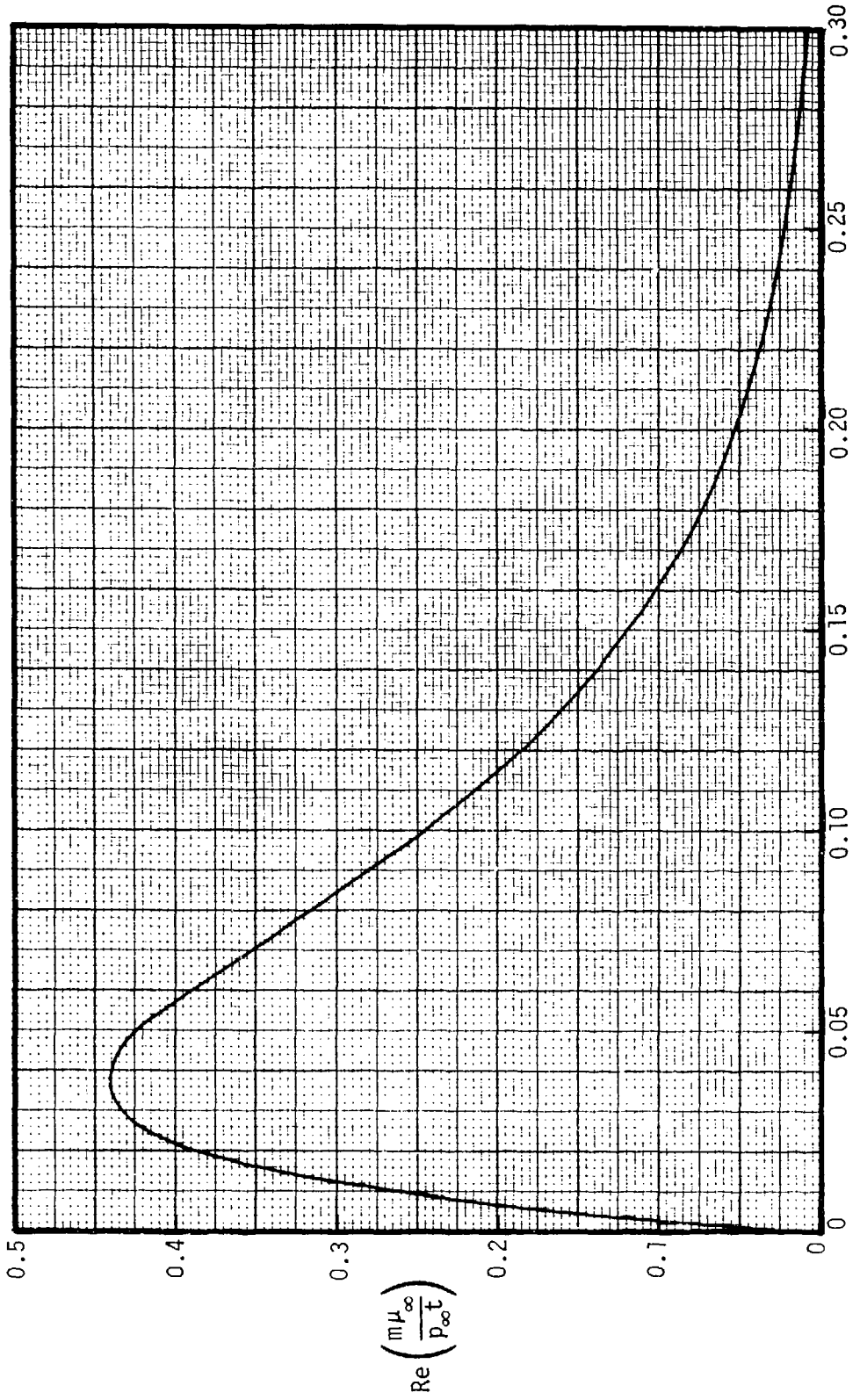

FIGURE 5-9 SCALED REYNOLDS NUMBER

6. DISCUSSION AND CONCLUSIONS

The blast wave laminar boundary layer equations have been solved by four procedures. The most rigorous solution is the one obtained using the integral technique with the polynomial representation for velocity and temperature. The integral solution with the exponential representation is simpler to derive and it agrees quite will with the integral solution with the polynomial representation. The steady and locally square wave method allows for rapid estimation of the flow properties; however, although it yields fair agreement with the more rigorous solutions, it lacks theoretical justification. The quasi-steady and locally similar method is a more reasonable approach than the steady and locally square wave method and the results are generally more accurate, but it requires more extensive computation.

In the region near the shock front, only the integral solution yields close agreement with a previously established solution.[5] Since the integral solution is obtained using a rigorous method, this solution is recommended for general use. However, if weak-shock and non-ideal gas effects must be considered, then the quasi-steady method can be used to obtain rough estimates of the flow properties.

The integral solution shows that the boundary layer thicknesses remain quite thin for a long distance behind the shock, then they increase very rapidly with the distance. This is in contrast to a flat plate or square-wave solution for which the boundary layer thickness increases with distance behind the shock to 0.5 power. The integral solution also shows the temperature thickness to be much greater than the velocity thickness except for a short distance from the shock. Near the shock front, both shear stress and heat transfer decrease as the distance behind the shock is increased. However, at a distance behind the shock of about one-third of the length between the shock and the explosion point, the heat transfer increases very rapidly. This is due to the fact that the free-stream temperature increases at a much higher rate than the heat transfer coefficient decreases as the distance behind the shock is increased.

The results presented in Section 3 for the integral solution allow one to compute any physical properties for laminar flow such as shear stress, heat transfer, velocity and temperature profiles, etc., by using the appropriate equations. The results can also be used for strong shocks of various explosion energies by using proper scaling. Some illustrations of the results are shown in Section 5 where the method of scaling is also indicated.

The flow is expected to be laminar only for a short distance from the shock. It then becomes turbulent for a predominant portion of the flowfield. At less than half the distance between the shock and the explosion point, the density becomes extremely low and the continuum boundary layer equations may become invalid. However, the boundary layer properties near the explosion point are not of primary interest. Hence the next flow regime that should be investigated is that of turbulent flow. For turbulent boundary layers, a method of solution has been formulated by Quan[8] and is shown in Appendix C. It is recommended that calculations be carried out to obtain numerical results.

APPENDIX A

BLAST WAVE INVISCID FLOWFIELD

The inviscid flowfield generated by an intense explosion in a uniform atmosphere has been studied by a number of investigators. In a classic paper, Taylor[3] presented a self-similar solution for a point explosion. He presented an exact solution in numerical form and an approximate solution in closed-form. Sedov[4] independently arrived at an exact solution and generalized it to a line explosion (cylindrical shock) and a plane explosion (plane shock). Sedov's solution is given in analytical form and is the one used in this report.

A strong shock moves according to a power law in time t of the form

$$x_s = Ct^m, \qquad u_s = Cmt^{m-1} \tag{A-1}$$

where x_s is the shock position and u_s is the shock velocity. The constant m is determined by shock geometry and is given by $m=2/(3+\bar{\sigma})$ where $\bar{\sigma}=0$, 1, and 2 for plane, cylindrical, and spherical shocks, respectively. The constant C is determined by the explosion strength and is given by $C=(E/\rho_\infty)^{m/2}$ where ρ_∞ is the ambient density and E is a certain constant which has the dimensions of and is proportional to the energy E_o (kinetic energy and heat energy) liberated during the explosion, i.e., $E=\bar{\alpha}E_o$. The constant $\bar{\alpha}$, which depends on γ and $\bar{\sigma}$, has been shown in graphical form by Sedov.[4] For air and spherical shock, $\bar{\alpha}=1.175$. It should be pointed out that E_o is not the total energy liberated in an explosion since a large part of the energy is expended in radiation.

The inviscid flow properties behind the shock are given by

$$p_e = \rho_\infty u_s^2 F(\xi), \qquad \rho_e = \rho_\infty R(\xi)$$
$$u_e = u_s \phi(\xi), \qquad h_e = \frac{\gamma}{\gamma-1}\frac{p_e}{\rho_e} \tag{A-2}$$

where p, ρ, a, and h are the pressure, density, velocity, and enthalpy, respectively. The subscript e refers to conditions behind the shock, and ∞ refers to the undisturbed atmosphere; F, R, and ϕ are the solution parameters given as functions of the non-dimensional blast wave coordinate $\xi=1-x/x_s$. From Sedov's results, one may write

$$\phi = \left(\frac{\nu+2}{2}\right) V(1-\xi) \tag{A-3}$$

$$R = \left(\frac{\gamma+1}{\gamma-1}\right)\left[\frac{\gamma+1}{\gamma-1}\left(\frac{(\nu+2)\gamma}{2} V - 1\right)\right]^{\alpha_3}\left[\frac{\gamma+1}{\gamma-1}\left(1 - \frac{\nu+2}{2} V\right)\right]^{\alpha_5} \cdot \left[\frac{(\nu+2)(\gamma+1)}{(\nu+2)(\gamma+1)-2[2+\nu(\gamma-1)]}\left(1 - \frac{2+\nu(\gamma-1)}{2} V\right)\right]^{\alpha_4} \tag{A-4}$$

$$F = \left(\frac{2}{\gamma+1}\right)\left[\frac{(\nu+2)(\gamma+1)}{4} V\right]^{\frac{2\nu}{2+\nu}}\left[\frac{\gamma+1}{\gamma-1}\left(1 - \frac{\nu+2}{2} V\right)\right]^{\alpha_5+1} \cdot \left[\frac{(\nu+2)(\gamma+1)}{(\nu+2)(\gamma-1)-2[2+\nu(\gamma-1)]}\left(1 - \frac{2+\nu(\gamma-1)}{2} V\right)\right]^{\alpha_4-2\alpha_1} \tag{A-5}$$

where V is an implicit function of ξ given by

$$\xi = 1 - \left[\frac{(\nu+2)(\gamma+1)}{4} V\right]^{-\frac{2}{2+\nu}}\left[\frac{\gamma+1}{\gamma-1}\left(\frac{(\nu+2)\gamma}{2} V - 1\right)\right]^{-\alpha_2} \cdot \left[\frac{(\nu+2)(\gamma+1)}{(\nu+2)(\gamma+1)-2[2+\nu(\gamma-1)]}\left(1 - \frac{2+\nu(\gamma-1)}{2} V\right)\right]^{-\alpha_1} \tag{A-6}$$

and

$$
\begin{aligned}
\nu &= 1 + \bar{\sigma} \\
\alpha_1 &= \frac{(\nu+2)\gamma}{2+\nu(\gamma-1)} \left[\frac{2\nu(2-\gamma)}{\gamma(\nu+2)^2} - \alpha_2 \right] \\
\alpha_2 &= \frac{1-\gamma}{2(\gamma-1)+\nu} \\
\alpha_3 &= \frac{\nu}{2(\gamma-1)+\nu} \\
\alpha_4 &= \frac{\alpha_1(\nu+2)}{2-\gamma} \\
\alpha_5 &= \frac{2}{\gamma-2}
\end{aligned}
\qquad \text{(A-7)}
$$

The functions ϕ, R, and F for $\bar{\sigma}=2$ (spherical shock) and $\gamma=1.4$ are shown in Figure A-1 which illustrates the severe nonuniformities near the shock front.

Only the similar solution as given in this appendix is used in this report, since the integral boundary layer solution requires the similarity transformation. It should be mentioned, however, that non-similar solutions to the inviscid flowfield are available and they can be used in the quasi-steady method of boundary layer solution. The non-similar inviscid solutions involve the numerical solution of the continuity, momentum, and energy equations which take into account the real gas effects, ambient pressure, and radiation heat transport. In the strong shock phase, these numerical solutions agree closely with the similar solution.

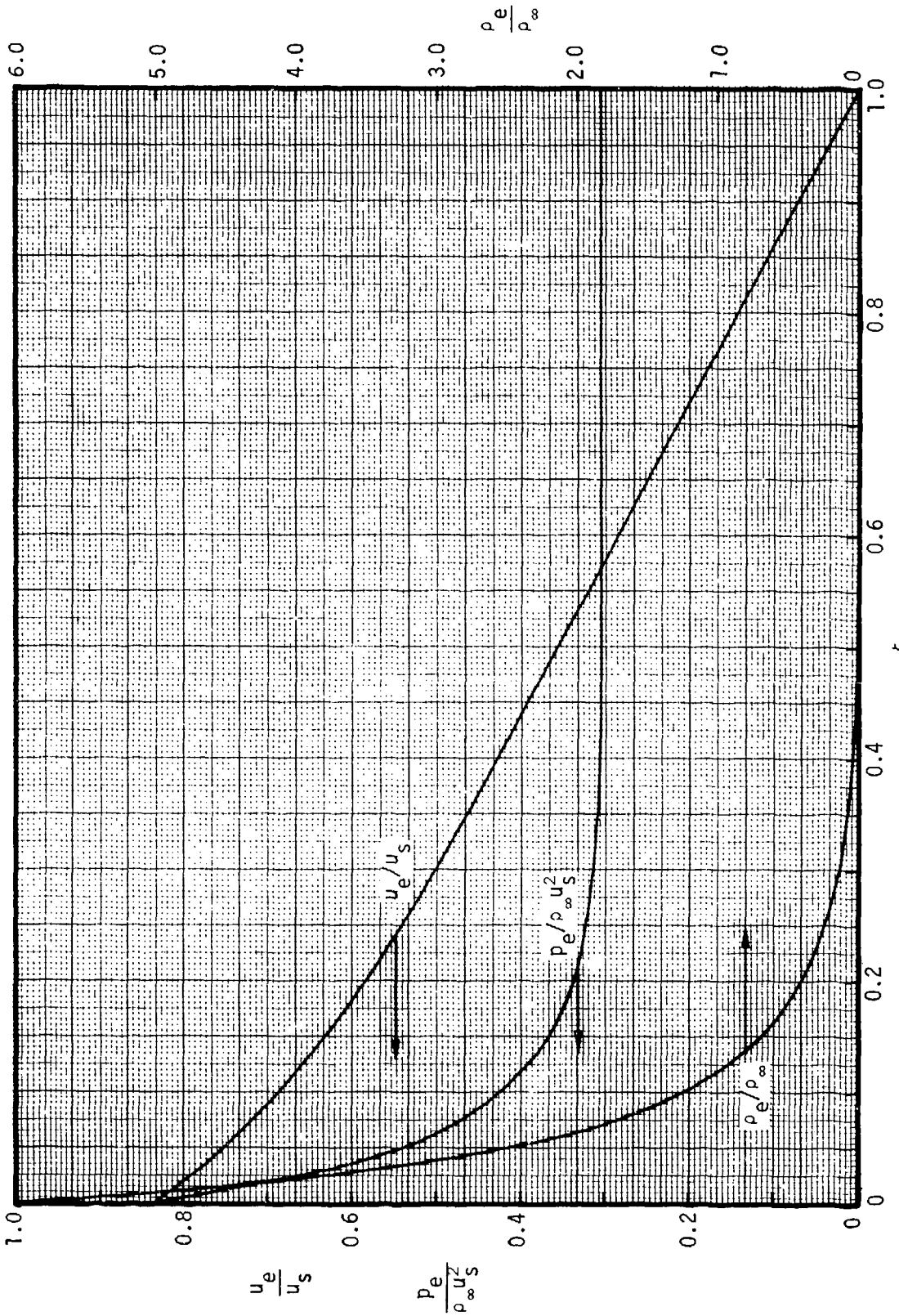

FIGURE A-1 FREE-STREAM VELOCITY, PRESSURE, AND DENSITY DISTRIBUTIONS

APPENDIX B

MIRELS AND HAMMAN'S BOUNDARY LAYER SOLUTION

As noted in Section 1, Mirels and Hamman performed a solution to the blast wave boundary layer which is valid near the shock front.[5] For reference purposes, the method and results of that solution are outlined in this appendix.

The basic transformed equations and boundary conditions used by Mirels and Hamman are given in Section 3. These equations are partial differential equations with two independent variables ξ and η. Mirels and Hamman's solution method is to expand the dependent variables f and g as power series in ξ. Substituting f and g into the differential equations and equating coefficients of like powers of ξ reduces the equations to a series of non-linear ordinary differential equations which can be integrated using a shooting technique as discussed in Section 4.2. The solution can thus be continued to any desired order of approximation although each successive approximation becomes increasingly more complicated.

The functions f and g are expanded in the form

$$f(\xi,\eta) = f_o(\eta) + (\alpha\xi)f_1(\eta) + (\alpha\xi)^2 f_2(\eta) + \ldots$$

$$g(\xi,\eta) = g_o(\eta) + (\alpha\xi)g_1(\eta) + (\alpha\xi)^2 g_2(\eta) + \ldots \qquad \text{(B-1)}$$

Sedov's solution to the freestream flowfield parameters is expanded in a similar power series to the same degree of accuracy as follows:

$$F(\xi) = F_o + (\alpha\xi)F_1 + (\alpha\xi)^2 F_2 + \ldots$$

$$\phi(\xi) = \phi_o + (\alpha\xi)\phi_1 + (\alpha\xi)^2 \phi_2 + \ldots \qquad \text{(B-2)}$$

$$R(\xi) = R_o + (\alpha\xi)R_1 + (\alpha\xi)^2 R_2 + \ldots$$

The constant α is dependent upon the exponent in the power law shock relation (Appendix A) with the form $\alpha=(m-1)/m$. Substituting these expansions into the transformed differential equations and equating terms of like order of ξ results in a sequence of ordinary differential equations. In Reference 5 the solution is carried to first order (linear in ξ) and the resulting equations are given here. The zero-order equations are:

$$f_o''' + (\eta - \phi_o f_o) f_o'' = 0$$

$$\frac{1}{Pr} g_o'' + (\eta - \phi_o f_o) g_o' = -\frac{2}{\gamma} (f_o'')^2 \tag{B-3}$$

with boundary conditions:

$$f_o(0) = f_o'(0) = 0, \qquad g_o(0) = 0$$

$$f_o(\infty) = 1, \qquad g_o(\infty) = 1 \tag{B-4}$$

The prime denotes differentiation with respect to η. All other variables are defined in other sections of the report. The first-order equations, which are coupled with the zero-order equations, are:

$$\begin{aligned} &f_1''' + (\eta - \phi_o f_o) f_1'' + 2(\phi_o f_o) f_1'' + 2(\phi_o f_o' - 1) f_1' - 3\phi_o f_o f_1 \\ &\quad = \left(\frac{2\sigma}{\alpha} - \frac{F_1}{F_o}\right) f_o''' + \left[3\phi_o f_o - \left(\frac{2\sigma}{\alpha} + 1\right)\eta\right] f_o'' \\ &\qquad + 2\left(1 + \frac{\phi_1}{\phi_o}\right) f_o' - 2\phi_1 (f_o')^2 - \frac{2F_1}{R_o \phi_o} g_o \end{aligned}$$

$$\begin{aligned} &\frac{1}{Pr} g_1'' + (\eta - \phi_o f_o) g_1' + 2(\phi_o f_o' - 1) g_1 \\ &\quad = \frac{1}{Pr}\left(\frac{2\sigma}{\alpha} - \frac{F_1}{F_o}\right) g_o'' + \left[3(f_o \phi_o + \phi_o f_1) - \left(\frac{2\sigma}{\alpha} + 1\right)\eta\right] g_o' \\ &\qquad + 2\left[\frac{2}{\gamma} + (\phi_o f_o' - 1)\left(\frac{R_1}{R_o} - \frac{F_1}{\gamma F_o}\right)\right] g_o + \frac{4}{\gamma}\left(\frac{\sigma}{\alpha} - \frac{\phi_1}{\phi_o} - \frac{R_1}{2R_o} - \frac{f_1'''}{f_o''}\right)(f_o'')^2 \end{aligned} \tag{B-5}$$

with boundary conditions:

$$f_1(0) = f_1'(0) = f_1'(\infty) = 0$$

$$g_1(0) = g_1(\infty) = 0 \qquad \text{(B-6)}$$

Equations (B-3) to (B-6) have been solved for γ=1.4 and Pr=0.72 and for various values of σ and α. The resulting solutions for f_o' and f_1' are presented in Figure B-1 and the solutions for g_o and g_1 are given in Figure B-2.

Because of the nature of the solution technique, this first-order solution can be strictly applicable only very near the shock. The actual region in which it is accurate is questionable although some measure can be obtained by examining the accuracy of the two term expansion of the external flow properties. The results of Appendix A indicate that the flow properties, in particular density, change very rapidly near the shock. The two term expansion of the density function $R(\xi)$ is given by extending a straight line from the shock front (ξ=0) with a slope equal to the slope of R at ξ=0. By this straight line approximation, R=0 for $\xi=(\gamma^2-1)/[3(\gamma+1) + \bar{\sigma}(\gamma+5)]$. This yields ξ=0.048 for γ=1.4 and $\bar{\sigma}$=2. The inviscid flow density is obviously in serious error for ξ less than that and the boundary layer solution cannot be expected to be any more accurate. Thus the boundary layer solution presented in this appendix is probably accurate for ξ<0.02 at best.

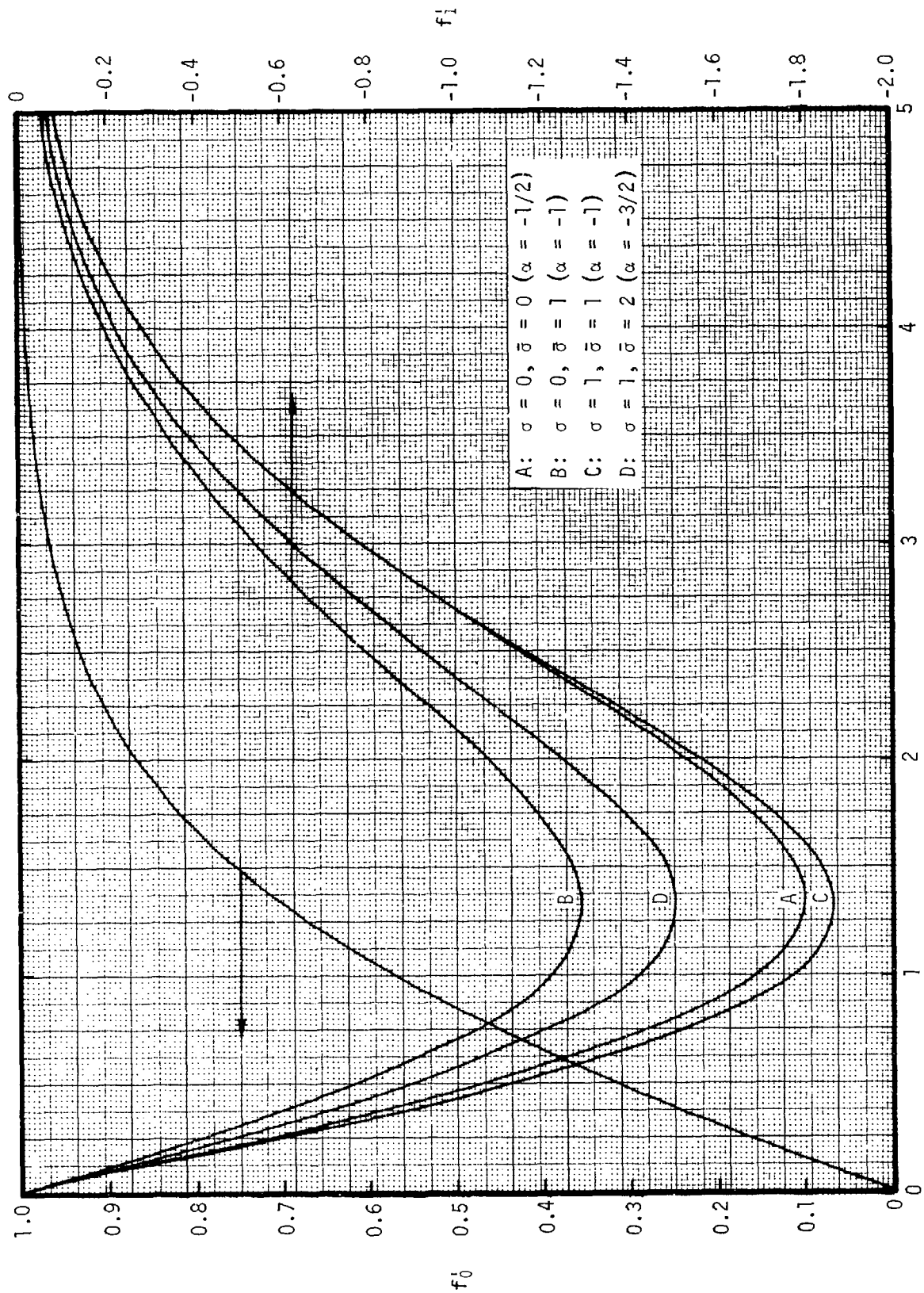

FIGURE B-1 VARIATION OF f_0' AND f_1' WITH η

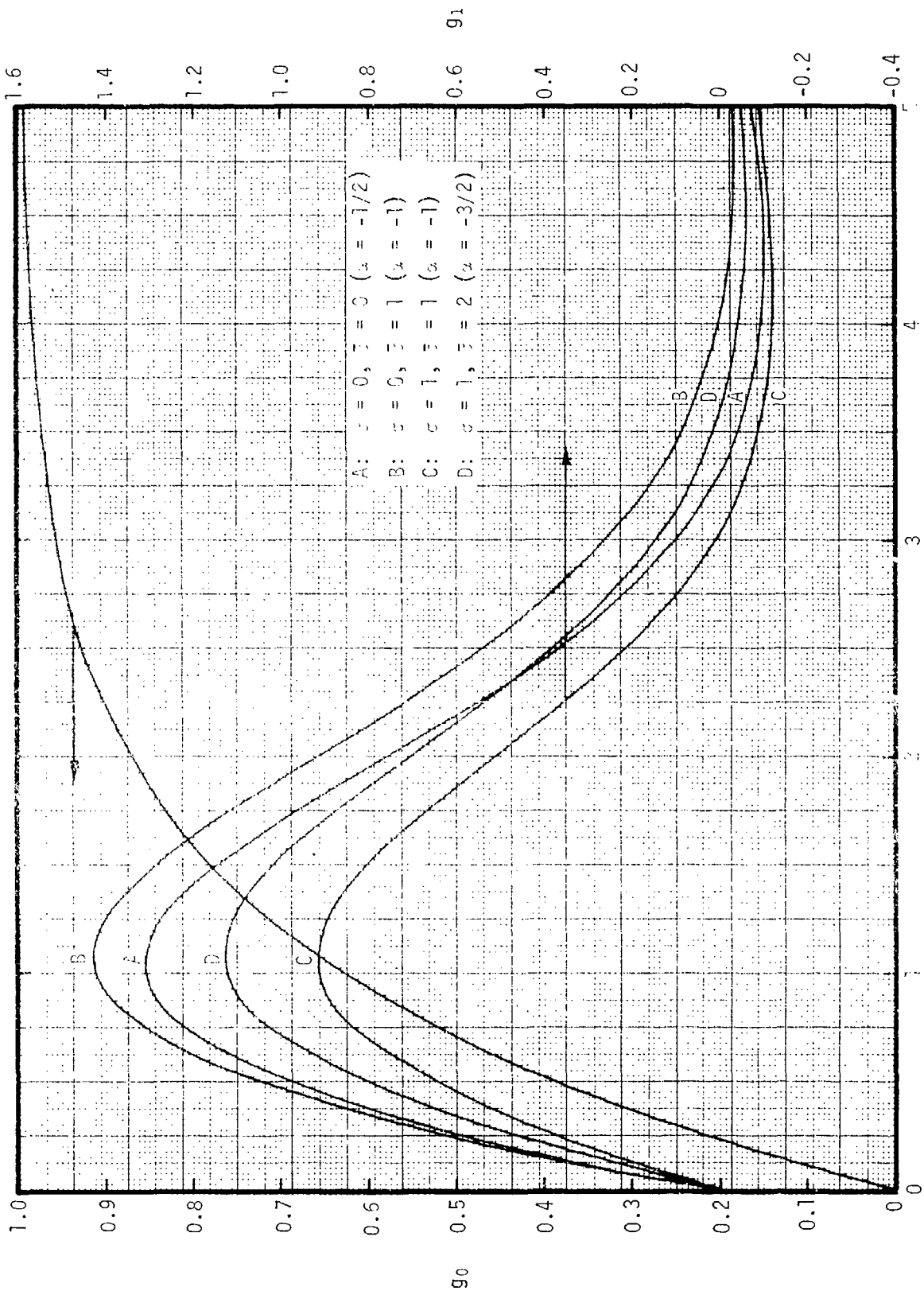

FIGURE B-2 VARIATION OF g_o AND g_1 WITH η

(Reverse of Page is Blank)

APPENDIX C

METHOD FOR TURBULENT BOUNDARY LAYER SOLUTION

A method of solving the transient two-dimensional equations that govern the turbulent boundary layer flows generated by plane, cylindrical, and spherical strong blast waves has been formulated by Quan.[8] Since a predominant portion of the blast wave boundary layer is turbulent, this analysis constitutes a logical complement to the laminar boundary layer study. In the turbulent flow study, the integral momentum and integral energy equations are utilized to reduce the number of independent variables from three to two (time and distance along the surface). A similarity condition further reduces the two independent variables to one. The resulting ordinary differential equations can then be solved by standard numerical procedure. Quan's formulation of the solution is outlined in this appendix. The nomenclature here is at places different from that of the main text of this report.

The transient two-dimensional compressible turbulent boundary layer equations have been given by Van Driest.[12] It can be shown that the equations have the following form for the blast wave problem where the free-stream flow is nonuniform and time-dependent:

$$\frac{\partial \bar{\rho}}{\partial t} + \frac{1}{x^{\sigma}} \frac{\partial (\overline{\rho u} x^{\sigma})}{\partial x} + \frac{\partial (\overline{\rho v})}{\partial y} = 0 \qquad \text{(C-1)}$$

$$\bar{\rho} \frac{\partial \bar{u}}{\partial t} + \overline{\rho u} \frac{\partial \bar{u}}{\partial x} + \overline{\rho v} \frac{\partial \bar{u}}{\partial y} = - \frac{\partial p_e}{\partial x} + \frac{\partial}{\partial y} \left(\bar{\mu} \frac{\partial \bar{u}}{\partial y} \right) + \frac{\partial}{\partial y} \left[-\overline{(\rho v)' u'} \right] \qquad \text{(C-2)}$$

$$\bar{\rho} \frac{\partial \bar{h}}{\partial t} + \overline{\rho u} \frac{\partial \bar{h}}{\partial x} + \overline{\rho v} \frac{\partial \bar{h}}{\partial y} = \frac{\partial p_e}{\partial t} + \bar{u} \frac{\partial p_e}{\partial x} + \frac{1}{Pr} \frac{\partial}{\partial y} \left(\bar{\mu} \frac{\partial \bar{h}}{\partial y} \right) + \bar{\mu} \left(\frac{\partial \bar{u}}{\partial y} \right)^2$$

$$+ \frac{\partial}{\partial y} \left[-\overline{(\rho v)' h'} \right] - \overline{(\rho v)' u'} \frac{\partial \bar{u}}{\partial y} \qquad \text{(C-3)}$$

where the bars indicate temporal mean values and the primes indicate instantaneous fluctuations from the mean. The symbols ρ, u, v, h, and μ refer to the density, x velocity component, y velocity component, enthalpy, and viscosity, respectively; p_e is the pressure at the edge of the boundary layer; Pr is the Prandtl number which is assumed to be constant; and t, x, and y refer to time, distance along the surface, and distance normal to the surface, respectively. The temperature is given by $T=h/c_p$ where c_p is a constant specific heat. The value for σ is 0 for two-dimensional boundary layer and 1 for axisymmetric boundary layer.

There are two common methods of solving turbulent boundary layer equations. The first is to employ semi-empirical expressions relating the fluctuation, or eddy diffusivity, terms to local mean properties, and the partial differential equations governing the mean values are then solved by finite-difference procedure. This method, at least in the mathematical sense, is quite accurate. However, the accuracy and reliability of the semi-empirical expressions have not been established at present. Moreover, this finite-difference procedure is very tedious even for steady-state problems. For the transient problem at hand, this method is unappealing, to say the least.

The second method, which is simpler both in treating the physics of turbulence and in obtaining numerical results, is the explicit integral method. Here, the differential equations are integrated across the boundary layer and the dependency on the y-direction is eliminated. With this method, one is mainly interested in the gross effect of turbulence on the boundary layer growth and not in the detail mechanics of turbulence. Instead of evaluating the local diffusivity terms for momentum and energy as is done in the first method, one prescribes the velocity and temperature profiles, a skin-friction law explicitly relating shear stress to momentum thickness and an explicit relation between heat and momentum transfer. The resulting partial differential equations are first-order and they describe the momentum and energy thicknesses as functions of x and t. Two questions naturally arise with the integral method here. First, are the boundary layer growth results sensitive to the velocity and temperature shapes that are assumed? Second, can a transformation be found such that x and t are related by a single variable?

Evidence[13] shows that the answer to the first question is negative. In fact, the integral procedure is currently the standard method used in computing turbulent boundary layers in nozzles[14,15] where finite pressure gradients exist. It is also used in shock tube turbulent boundary layer studies[6,16] in which pressure gradients are absent. It should be noted, however, that, especially for the present problem, the skin-friction law and the heat and momentum correlation, like the eddy diffusivity expressions, are of uncertain validity.

The answer to the second question is, fortunately, yes. It is shown below that, indeed, under certain restrictions on the skin-friction law, a similarity transformation can be found. Thus, the present problem starting with second-order differential equations with three independent variables (t, x, and y) is reduced to the relatively simple task of solving first-order ordinary differential equations. To our knowledge, a rigorous transient solution to two-dimensional turbulent flow has not been obtained previously (of course, one can always construct what may be called a locally-similar and temporally-steady solution of unassessed accuracy). The method of combining an integral technique and a similarity transformation appears quite attractive. The governing equations will be derived below and numerical results will be obtained at a later time.

Equation (C-1) can be used to eliminate $\overline{\rho v}$; Equation (C-2) can be integrated across the boundary layer to yield:

$$\tau_w = \frac{\partial}{\partial t}\left(\rho_e u_e \omega\right) + \rho_e \frac{\partial u_e}{\partial t}\lambda^* + \frac{1}{x^\sigma}\frac{\partial}{\partial x}\left(x^\sigma \rho_e u_e^2 \theta\right) + \rho_e u_e \frac{\partial u_e}{\partial x}\delta^* \qquad \text{(C-4)}$$

and Equation (C-3) can be integrated to yield:

$$q_w = \frac{\partial}{\partial t}\left(\rho_e H_e \Omega\right) + \rho_e \frac{\partial H_e}{\partial t}\lambda^* + \frac{1}{x^\sigma}\frac{\partial}{\partial x}\left(x^\sigma \rho_e u_e H_e \phi\right) + \rho_e u_e \frac{\partial H_e}{\partial x}\delta^* \qquad \text{(C-5)}$$

where τ_w is the shear stress at the wall and q_w is the convective heat flux to the wall. The subscript e denotes conditions at the edge of the boundary layer; H is the stagnation enthalpy ($H=h+u^2/2$) and

$$\delta^* = \int_0^\infty \left(1 - \frac{\overline{\rho}\,\overline{u}}{\rho_e u_e}\right) dy \qquad \text{(C-6a)}$$

$$\theta = \int_0^\infty \frac{\overline{\rho}\,\overline{u}}{\rho_e u_e}\left(1 - \frac{\overline{u}}{u_e}\right) dy \qquad \text{(C-6b)}$$

$$\phi = \int_0^\infty \frac{\overline{\rho}\,\overline{u}}{\rho_e u_e}\left(1 - \frac{\overline{H}}{H_e}\right) dy \qquad \text{(C-6c)}$$

$$\lambda^* = \int_0^\infty \left(1 - \frac{\overline{\rho}}{\rho_e}\right) dy \qquad \text{(C-6d)}$$

$$\omega = \int_0^\infty \frac{\overline{\rho}}{\rho_e}\left(1 - \frac{\overline{u}}{u_e}\right) dy \qquad \text{(C-6e)}$$

$$\Omega = \int_0^\infty \frac{\overline{\rho}}{\rho_e}\left(1 - \frac{\overline{H}}{H_e}\right) dy \qquad \text{(C-6f)}$$

The dispalcement thickness δ^*, momentum thickness θ, and energy thickness ϕ are those commonly encountered in steady-state problems. It is seen that three other th'ckness parameters are introduced in the transient problem. We shall temporarily call λ^* the density thickness, ω the acceleration thickness, and Ω the enthalpy thickness.

In deriving Equations (C-4) and (C-5), it has been assumed that

$$\int_0^\infty \overline{\rho u}\, dy \simeq \int_0^\infty \overline{\rho}\,\overline{u}\, dy \qquad \text{(C-7a)}$$

$$\int_0^\infty \overline{\rho u}\,\overline{u}\, dy \simeq \int_0^\infty \overline{\rho}\,\overline{u}^2\, dy \qquad \text{(C-7b)}$$

$$\int_0^\infty \overline{\rho u}\,\overline{H}\, dy \simeq \int_0^\infty \overline{\rho}\,\overline{u}\,\overline{H}\, dy \qquad \text{(C-7c)}$$

This assumption is generally employed in integral methods for turbulent flow.[17] Also, the following boundary conditions have been employed:

$$u = 0, \quad v = 0, \quad h = 0 \qquad \text{at} \quad y = 0 \qquad \text{(C-8a)}$$

$$u = u_e, \; h = h_e \qquad \text{at} \quad y \to \infty \qquad \text{(C-8b)}$$

It is now assumed that the velocity and stagnation enthalpy can be represented by power law profiles of the form

$$\frac{\bar{u}}{u_e} = \left(\frac{y}{\delta}\right)^n \qquad y \leq \delta \qquad \text{(C-9a)}$$

$$\frac{\bar{u}}{u_e} = 1 \qquad y > \delta \qquad \text{(C-9b)}$$

$$\frac{\bar{H}}{H_e} = \left(\frac{y}{\Delta}\right)^n \qquad y \leq \Delta \qquad \text{(C-10a)}$$

$$\frac{\bar{H}}{H_e} = 1 \qquad y > \Delta \qquad \text{(C-10b)}$$

where δ is the velocity thickness, Δ is the temperature thickness, and n is an empirical number usually given the value of 1/7.

From Equations (C-9) and (C-10) and the definition of H, one can obtain $\bar{\rho}/\rho_e$ as a function of $(y/\delta)^n$ and $(y/\Delta)^n$. Its explicit expression depends on whether $y \leq \Delta$ or $y > \Delta$ and whether $\delta \leq \Delta$ or $\delta > \Delta$. Integration of Equation (C-6) yields

$$\delta^*/\delta = f_1(\zeta) \qquad \text{(C-11a)}$$

$$\theta/\delta = f_2(\zeta) \qquad \text{(C-11b)}$$

$$\phi/\delta = f_3(\zeta) \qquad \text{(C-11c)}$$

$$\lambda^*/\delta = f_4(\zeta) \qquad \text{(C-11d)}$$

$$\omega/\delta = f_5(\zeta) \qquad \text{(C-11e)}$$

$$\Omega/\delta = f_6(\zeta) \qquad \text{(C-11f)}$$

where $\zeta \equiv \Delta/\delta$. Using Equation (C-11), one may write Equations (C-4) and (C-5) in the form

$$\tau_w = \frac{\partial}{\partial t}\left[\rho_e u_e g_3(\zeta)\theta\right] + \rho_e \frac{\partial u_e}{\partial t} g_2(\zeta)\theta + \frac{1}{x^\sigma}\frac{\partial}{\partial x}\left(x^\sigma \rho_e u_e^2 \theta\right) + \rho_e u_e \frac{\partial u_e}{\partial x} g_1(\zeta)\theta \tag{C-12}$$

$$q_w = \frac{\partial}{\partial t}\left[\rho_e H_e g_6(\zeta)\phi\right] + \rho_e \frac{\partial H_e}{\partial t} g_5(\zeta)\phi + \frac{1}{x^\sigma}\frac{\partial}{\partial x}\left(x^\sigma \rho_e u_e H_e \phi\right) + \rho_e u_e \frac{\partial H_e}{\partial x} g_4(\zeta)\phi \tag{C-13}$$

where

$$g_1(\zeta) = f_1(\zeta)/f_2(\zeta) \tag{C-14a}$$

$$g_2(\zeta) = f_4(\zeta)/f_2(\zeta) \tag{C-14b}$$

$$g_3(\zeta) = f_5(\zeta)/f_2(\zeta) \tag{C-14c}$$

$$g_4(\zeta) = f_1(\zeta)/f_3(\zeta) \tag{C-14d}$$

$$g_5(\zeta) = f_4(\zeta)/f_3(\zeta) \tag{C-14e}$$

$$g_6(\zeta) = f_6(\zeta)/f_3(\zeta) \tag{C-14f}$$

It is noted that ζ can be written as a function of ϕ/θ through Equations (C-11b) and (C-11c). Equations (C-12) and (C-13) can then be solved for θ and ϕ simultaneously provided that relations for τ_w and q_w as functions of θ and ϕ are given. We are, however, interested in a more ambitious step, namely, in reducing Equations (C-12) and (C-13) to ordinary differential equations. In this regard, we note that similarity exists in the free-stream conditions for strong shocks for which

$$\rho_e = \rho_\infty R(\xi) \tag{C-15a}$$

$$u_e = u_s(\tau)\psi(\xi) \tag{C-15b}$$

$$H_e = u_s^2(\tau)\left[\frac{\gamma-1}{\gamma}\frac{F(\xi)}{R(\xi)} + \frac{1}{2}\psi^2(\xi)\right] \equiv u_s^2(\tau)\beta(\xi) \tag{C-15c}$$

where

$$\xi = 1 - \frac{x}{Ct^m} \tag{C-16a}$$

$$\tau = t \tag{C-16b}$$

and ρ_∞, γ, C, and m are constants, and

$$u_s(\tau) = Cm\tau^{m-1} \tag{C-17}$$

Equation (C-12) can be written as

$$\tau_w x^\sigma = \frac{m}{\tau}(1-\xi)\rho_\infty u_s \frac{\partial}{\partial \xi}\left(R\psi g_3 x^\sigma \theta\right) + \rho_\infty R\psi \frac{\partial}{\partial t}\left(u_s g_3 x^\sigma \vartheta\right)$$

$$+ \rho_\infty R g_2 x^\sigma \theta \left[\frac{m}{\tau}(1-\xi)u_s \frac{d\psi}{d\xi} + \psi \frac{du_s}{d\tau}\right]$$

$$- \frac{1}{C\tau^m}\rho_\infty u_x{}^2 \frac{\partial}{\partial \xi}\left(R\psi^2 x^\sigma \theta\right) - \frac{1}{C\tau^m}\rho_\infty R u_s{}^2 \psi g_1 x^\sigma \theta \frac{d\psi}{d\xi} \tag{C-18}$$

We now assume that ζ or the ratio ϕ/θ depends only on ξ and that θ can be written in the form

$$\theta(x,t) = \frac{Bt^a \theta_1\left(1 - \frac{x}{Ct^m}\right)}{x^\sigma} \tag{C-19a}$$

or

$$x^\sigma \theta(x,t) = B\tau^a \theta_1(\xi) \tag{C-19b}$$

where the constant a is to be determined and the constant B can be arbitrarily selected for convenience. Equation (C-18) becomes

$$\frac{1}{\rho_\infty \beta}\tau_w x^\sigma = \frac{m}{\tau}(1-\xi)u_s \tau^a \frac{d}{d\xi}\left(R\psi g_3 \theta_1\right) + R\psi g_3 \theta_1 \frac{d}{d\tau}\left(u_s \tau^a\right)$$

$$+ R g_2 \tau^a \theta_1 \left[\frac{m}{\tau}(1-\xi)u_s \frac{d\psi}{d\xi} + \psi \frac{du_s}{d\tau}\right]$$

$$- \frac{1}{C\tau^m} u_s{}^2 \tau^a \frac{d}{d\xi}\left(R\psi^2 \theta_1\right) - \frac{1}{C\tau^m} R u_s{}^2 \psi g_1 \tau^a \theta_1 \frac{d\psi}{d\xi} \tag{C-20}$$

Equation (C-20) can be written in the form

$$\tau_w = \tau^{m+a-2-m\sigma} G(\xi) \tag{C-21}$$

where

$$G(\xi) = \frac{\rho_\infty B C^{1-\sigma_m}}{(1-\xi)^\sigma} \left\{ m(1-\xi) \frac{d}{d\xi}\left(R\psi g_3 \theta_1\right) + (m-1+a) R\psi g_3 \theta_1 \right.$$

$$+ R g_2 \theta_1 \left[m(1-\xi) \frac{d\psi}{d\xi} + (m-1)\psi \right]$$

$$\left. - m \frac{d}{d\xi}\left(R\psi^2 \theta_1\right) - mR\psi g_1 \theta_1 \frac{d\psi}{d\xi} \right\} \tag{C-22}$$

The question now is can one find an expression for τ_w that is a function of ξ and varies with t to some power. Fortunately, a physically acceptable expression for such purpose does exist. For turbulent flow in nozzles[16] and in shock tubes,[6,16] a relation between skin-friction and boundary layer thickness can be taken as

$$\tau_w = 0.0225\, j\, \rho_e u_e^2 \left(\frac{\mu_e}{\rho_e u_e \delta} \right)^{1/4} \tag{C-23}$$

where

$$j = \left(\frac{\mu_m}{\mu_e} \right)^{1/4} \left(\frac{T_e}{T_m} \right)^{3/4} \tag{C-24}$$

and

$$T_m = 0.5\,(T_w + T_e) + 0.22\,(T_r - T_e) \tag{C-25}$$

Assuming μ to vary directly with T, considering $T_w << T_e$, taking the recovery temperature to be $T_r = T_e + (Pr)^{1/3} u_e^2/2c_p$, and using $h = c_p T$, one obtains

$$j = \left[\frac{1}{0.5 + \frac{0.11\gamma Pr^{1/3}\psi^2 R}{(\gamma-1)F}}\right]^{1/2} = j(\xi) \qquad \text{(C-26)}$$

and

$$\tau_w = \tau^{2m-2+(m-1+m\sigma-a)/4} K(\xi) \qquad \text{(C-27)}$$

where

$$K(\xi) = 0.0225\, j\, \rho_\infty R\psi^2 (Cm)^{9/4} \left[\frac{\gamma F C^\sigma (1-\xi)^\sigma \mu_\infty f_2}{(\gamma-1)B\psi\rho_\infty R h_\infty \theta_1}\right]^{1/4} \qquad \text{(C-28)}$$

Equating the powers of τ in Equations (C-21) and (C-27), one obtains

$$m+a-2-m\sigma = 2m-2+(m-1+m\sigma-a)/4 \qquad \text{(C-29)}$$

which yields

$$a = m(\sigma+1) - 1/5 \qquad \text{(C-30)}$$

Thus, a similarity solution can be achieved for θ. It may be pointed out here that, while other power-law expressions for τ_w still allow for similarity transformation, certain nonpower-law expressions, which may be more accurate, do not yield similarity conditions. The sacrifice of such possible gain in accuracy is of r. concern here since turbulent flow is subject to a great many other inaccuracies and one is interested in obtaining a reasonable solution.

For convective heat transfer, Equation (C-13) can be written as

$$q_w x^\sigma = \frac{m}{\tau}(1-\xi)\rho_\infty u_s^2 \frac{\partial}{\partial\xi}\left(R\beta g_6 x^\sigma \phi\right) + \rho_\infty R\beta \frac{\partial}{\partial\tau}\left(u_s^2 g_6 x^\sigma \phi\right)$$

$$+ \rho_\infty R g_5 x^\sigma \phi\left[\frac{m}{\tau}(1-\xi)u_s^2 \frac{d\beta}{d\xi} + 2\beta u_s \frac{du_s}{d\tau}\right]$$

$$- \frac{1}{C\tau^m}\rho_\infty u_s^3 \frac{\partial}{\partial\xi}\left(R\psi\beta x^\sigma \phi\right) - \frac{1}{C\tau^m}\rho_\infty R u_s^3 \psi g_4 x^\sigma \phi \frac{d\beta}{d\xi} \qquad \text{(C-31)}$$

Let $\phi(x,t)$ be given by

$$x^{\sigma}\phi(x,t) = B\tau^{b}\phi_1(\xi) \tag{C-32}$$

Then Equation (C-31) can be written in the form

$$q_w = \tau^{2m+b-3-m\sigma}L(\xi) \tag{C-33}$$

where

$$L(\xi) = \frac{\rho_\infty BC^{2-\sigma}m^2}{(1-\xi)^{\sigma}} \left\{ m(1-\xi)\frac{d}{d\xi}\left(R\beta g_6\phi_1\right) + (2m-2+a)R\beta g_6\phi_1 \right.$$

$$+ Rg_5\phi_1\left[m(1-\xi)\frac{d\beta}{d\xi} + 2(m-1)\beta\right]$$

$$\left. - m\frac{d}{d\xi}\left(R\psi\beta\phi_1\right) - mR\psi g_4\phi_1\frac{d\beta}{d\xi}\right\} \tag{C-34}$$

It is now needed to find an expression for q_w that varies with τ to some power. In addition, this expression must yield a value of b that is equal to a in order for the assumption of ϕ/θ as a function of only ξ to hold. For this purpose, one may employ an expression that has been used in shock tube studies:[6,16]

$$q_w = \frac{c_p T_r}{u_e} Pr^{-2/3}\ \tau_w \tag{C-35}$$

which yields

$$q_w = \tau^{3m-3+(m-1+m\sigma-a)/4}Q(\xi) \tag{C-36}$$

where

$$Q(\xi) = CmPr^{-2/3}\left(\frac{\gamma-1}{\gamma}\frac{F}{R\psi} + \frac{1}{2}Pr^{1/3}\psi\right)K(\xi) \tag{C-37}$$

Equating the powers of τ in Equations (C-33) and (C-36) and using Equation (C-30), it is found that indeed

$$b = a = m(\sigma+1) - 1/5 \qquad \text{(C-38)}$$

Thus, a similarity solution can also be obtained for ϕ. Equating $G(\xi)$ to $K(\xi)$ and equating $L(\xi)$ to $Q(\xi)$ results in two ordinary differential equations to solve for θ_1 and ϕ_1. The calculations will be carried out in detail at a later date.

In summary, the equations that govern blast wave turbulent boundary layer flows are second-order partial differential equations with three independent variables. In the present report, the integral method is used to reduce the equations to first-order and the number of independent variables to two. Similarity transformation is shown to be achievable and is used to reduce the problem to the relatively simple task of solving two coupled ordinary differential equations. These equations are derived in the present report and are to be programmed for numerical results.

REFERENCES

1. Brode, H. L., "Review of Nuclear Weapons Effects," Annual Review of Nuclear Science, Vol. 18, 1968, pp. 153-202.

2. Trulio, J. G., McKay, M. W., and Carr, W. E., "Lofting of Solid Material by Vaporization, Thermal Expansion and Crater Splash in a Near-Surface Burst," DASA 2270, Washington, D.C., February 1969.

3. Taylor, G. I., "The Formation of a Blast Wave by a Very Intense Explosion, I. Theoretical Discussion," Proc. Roy. Soc., London, Ser. A., Vol. 201, No. 1065, March 22, 1950, pp. 159-174.

4. Sedov, L. I., Similarity and Dimensional Methods in Mechanics, Academic Press, New York, 1959.

5. Mirels, H., and Hamman, J., "Laminar Boundary Layer Behind Strong Shock Moving with Nonuniform Velocity," Physics of Fluids, Vol. 5, January 1962, pp. 91-96.

6. Mirels, H., "Boundary Layer Behind Shock on Thin Expansion Wave Moving Into Stationary Fluid," NACA TN 3712, May 1956.

7. Murdock, J. W., "A Solution of Shock-Induced Boundary Layer Problems by an Integral Method," Air Force Report No. SAMSO-TR-68-435, August 1968.

8. Quan, V., "Blast Wave Turbulent Boundary Layers," IOC 70.4333.2-104, TRW Systems, 31 August 1970.

9. Stewartson, K., The Theory of Laminar Boundary Layers in Compressible Fluids, Oxford, 1964.

10. Schlichting, H., Boundary Layer Theory, translated by J. Kestin, fourth ed., McGraw-Hill, 1960, Chapter XII.

11. Mirels, H., "Laminar Boundary Layer Behind Shock Advancing Into Stationary Fluid," NACA TN 3401, March 1955.

12. Van Driest, E. R., "Turbulent Boundary Layer in Compressible Fluids," Journal of the Aeronautical Sciences, Vol. 18, 1951, pp. 145-160 and 216.

13. Tucker, M., "Approximate Calculation of Turbulent Boundary-Layer Development in Compressible Flow," NACA TN 2337, 1951.

14. Elliott, D. G., Bartz, D. R., and Silver, S., "Calculation of Turbulent Boundary-Layer Growth and Heat Transfer in Axi-Symmetric Nozzles," JPL TR 32-387, 1963.

REFERENCES (Continued)

15. Weingold, H. D., "ICRPG Turbulent Boundary Layer Nozzle Analysis Computer Program," developed by Pratt and Whitney Aircraft for the Interagency Chemical Rocket Propulsion Group, 1968.

16. H. Mirels, "The Wall Boundary Layer Behind a Moving Shock Wave," in Boundary Layer Research, Proceedings of the International Union of Theoretical Applied Mechanics," ed. by H. Gortler, 1958, pp. 283-284.

17. Shapiro, A. H., The Dynamics and Thermodynamics of Compressible Fluid Flow, Vol. II, Ronald Press, New York, 1954, p. 1090.

18. Bartz, D. R., "An Approximate Solution of Compressible Turbulent Boundary-Layer Development and Convective Heat Transfer in Convergent-Divergent Nozzles," ASME Trans. Vol. 77, 1955, pp. 1235-1245.

(Reverse of Page is Blank)

PART II

BOUNDARY LAYER PARTICLE ENTRAINMENT

(Reverse of Page is Blank)

ABSTRACT

This second part of the report is on particle entrainment. Using a lift force generated by the boundary layer velocity gradient, the particle velocity is estimated. Sample particle trajectories in strong blast wave flowfields are illustrated, and the amount of soil erosion due to aerodynamic entrainment is assessed.

CONTENTS OF PART II

ILLUSTRATIONS

NOMENCLATURE

a = particle radius

A = particle cross-sectional area; soil surface area

c_p = specific heat of gas at constant pressure

c_{ps} = specific heat of particle

C = constant related to explosion strength

C_D = drag coefficient

C_L = lift coefficient

d = particle diameter

D = particle diameter; pipe diameter

f = dimensionless average momentum of entrained particles

F = function given by Equation (3-9)

F_L = lift force

F_x = horizontal drag force

g = gravitational acceleration

G = function given by Equation (3-10)

k = gas conductivity

K = $3\rho/8\rho_s$

ℓ = boundary layer parameter

ℓ_t = boundary layer parameter

L = heat of vaporization for particle

m = mass of a particle; mass of soil per unit surface area

M = total mass of erosion

Nu = Nusselt number based on particle diameter

p = pressure in gas

p_s = pressure in soil

NOMENCLATURE (Continued)

$r = ag/Ku_e^2$

Re = Reynolds number based on particle diameter

$s = K^{1/2} C_D \delta/a$

t = time

T = gas temperature

T_p = particle temperature

T_{pv} = vaporization or ablation temperature

u = gas velocity in x-direction

u_p = particle velocity in x-direction

v = gas velocity in y-direction

v_p = particle velocity in y-direction

V = relative velocity between gas and particle

x = distance along soil surface

y = distance normal to soil surface

y_e = boundary layer thickness

y_m = height reached by a particle due to direct lift

$\alpha = a/\delta$

β = coefficient for soil erosion

γ = gas specific heat ratio

δ = boundary layer parameter, $= y_e/4.6$

η = boundary layer parameter

μ = gas viscosity

ν = gas dynamic viscosity

ρ = gas density

ρ_s = density of a particle

NOMENCLATURE (Continued)

τ_o = shear stress on soil surface

τ^* = restraining stress of soil

Subscripts

e = at edge of boundary layer during ascent

f = at edge of boundary layer during descent

g = at ground position

i = initial condition

m = at maximum height of a particle

p = particle

s = particle

w = wall condition

∞ = ambient condition

I. INTRODUCTION

In a nuclear explosion, soil can be lifted from the ground by several mechanisms such as crater splash, vaporization, elastic rebound, etc. These processes are inter-dependent and a complete study of the simultaneous processes has not been performed. Not only is the physics of the lofting mechanisms not yet well understood, but the rigorous mathematical models that can be proposed are very difficult to solve. The present study is only concerned with the aerodynamic effects on particle entrainment, and the interaction effects of other mechanisms are not considered.

On the soil erosion problem, one is mainly interested in answers to two questions: what is the initial velocity of a particle as it leaves the ground (or as it leaves the boundary layer) and how much dust of various particle sizes is entrained? Answers to these questions would allow one to predict the dust density distribution as a function of space and time for a given gas flowfield.

The aerodynamic ertrainment of surface particles into free streams has been investigated analytically and experimentally by workers of various disciplines. Early studies, [1,2] as well as some recent ones,[3] were concerned with wind erosion of soil. About a decade ago, the aerodynamic forces on surface particles were investigated in connection with the VTOL aircraft and helicopters downwash problem.[4] About the same time, studies were made to assess the dust entrainment caused by the rocket exhaust of a spacecraft during lunar landing.[5]

The investigations indicated above represent the pioneering efforts in their respective fields, and as such they constitute significant contributions. However, their results do not appear to be directly applicable to or sufficient for the problem of predicting the dust entrainment caused by a blast wave. The wind erosion studies are primarily one-dimensional, i.e., the wind variation along the surface and with time is neglected while a blast wave flowfield is strongly position- and time-dependent. The downwash impingement results of Vidal[4] provide an estimate of the lift and drag forces of a particle when it is on the ground, but the subsequent motion of the particle is not considered. For dust entrainment due to lunar landing, Roberts[5] assumed that the aerodynamic shear stress on the surface,

minus some value which represents a restraining stress, is proportional to the rate of transfer of momentum, per unit area, to the particles. The proportionality factor is related to the particle size and rocket exhaust conditions and is not directly applicable to blast wave conditions. Some of the results and ideas of Vidal and Roberts will be employed, however, in the present study.

For the problem of aerodynamic entrainment of soil by a blast wave, several studies have been performed recently. Swatosh and Wiedermann[6] assumed both the mass erosion rate and the vertical velocity (considered to be due to turbulence in the flow) to be proportional to the free-steam air velocity; and they performed experiments to determine the proportionality factors. Their results are important contributions to the present knowledge. However, since these results are not directly related to boundary layer properties, their applications are probably limited if shear stress is an important factor in determining erosion. For example, consider uniform flow over a flat plate. Since the shear stress on the surface decreases rapidly with distance from the leading edge, it is reasonable to expect a higher erosion rate near the leading edge. However, the relation given by Swatosh and Wiedermann would show a uniform erosion rate. The fact that boundary layer properties probably play an important role in determining soil erosion may partially account for the variations in the experimental data. For example, the erosion constant for variable air velocity is generally much higher (sometimes by two orders of magnitude) than that for steady air velocity; this may be due to effects related to boundary layer build-up.

Trulio and others[7] employed a simple model by assuming that the horizontal impulse delivered to the ground (due to shear stress) is entirely converted into vertical momentum of particles. The particles are considered to rotate, slide, or bounce along the surface until they accelerate by the horizontal aerodynamic drag force to a sufficient speed to bounce, or dislodge other particles, off the surface and into the free stream. The particles are considered to leave the ground vertically with a speed inversely proportional to the particle diameter; the maximum speed is taken to be half the free-stream gas speed. Due to the lack of a rigorous boundary layer solution, a local one-dimensional steady turbulent boundary

layer profile, which has been verified to be approximately correct for sandstorms, is employed to evaluate the shear stress. Again, the blast wave flowfield is actually highly transient and contains severe spacial gradients in properties. The validity of using any steady and one-dimensional model is questionable. It is the desire of obtaining a rigorous boundary layer solution that led to the current boundary layer studies by TRW Systems.

In the present study, the particle motion near the surface due to aerodynamic forces is estimated. Sample particle trajectory calculations are made. The amount of soil entrained is assessed using the laminar boundary layer solution developed. Since the blast wave boundary layer is expected to be predominantly turbulent, a turbulent flow solution is being pursued.[8] When this solution is completed, the amount of soil entrained can be similarly assessed.

(Reverse of Page is Blank)

2. PARTICLE LIFT IN BOUNDARY LAYER

The existence of a velocity difference between a particle and a fluid results in an aerodynamic force between them. The force component in the direction of the relative velocity is known as the drag and the component normal to it as the lift. The drag for a spherical particle in uniform, steady incompressible flow is a function of only the Reynolds number and is well known up to a Reynolds number of about a million.[9] The effects of particle shape, flow unsteadiness, and compressibility, etc. on drag have been investigated (e.g., References 10, 11, and 12), and some semi-empirical correlations are available. However, the lift on a sphere produced by a nonuniform flowfield such as a boundary layer is still not well understood, although it has been postulated to be the responsible cause for particle migration from a lower to a higher velocity region. An indication of the complexity of the lift mechanisms is the fact that the force on a rotating sphere in a uniform fluid, which is due to what is known as the Magnus effect and which accounts for the irregular flight of a tennis ball or baseball, has been studied for about three centuries and the magnitude of this force is still undetermined.

Recently, there appeared several analyses dealing with the lift exerted on a spherical particle by a shear flow. Eichhorn and Small[13] performed experiments for spheres suspended in Poiseuille flow and obtained the following relation

$$C_L = 7 \times 10^4 \left[\left(\frac{d}{u}\frac{du}{dy}\right)\frac{d}{D}\frac{1}{Re}\right]^2 \qquad (2\text{-}1)$$

where C_L is the lift coefficient (the ratio of the lift force to the product of the sphere's cross-sectional area and the fluid dynamic pressure), and d, u, y, D, and Re refer to particle diameter, fluid velocity at center of particle, distance from pipe wall, pipe diameter, and particle Reynolds number respectively. The experiments were performed using a 0.419 in. diameter tube and for d ranging from 0.061 in to 0.126 in., Re from 80 to 250, and (d/u)(du/dy) from 0 to 1.1. The value of C_L obtained range from 0 to about 1.0.

While Equation (2-1) showed C_L to vary with the velocity gradient (du/dy) to the 2.0 power, Saffman[14] found that at low particle Reynolds number C_L varies with the gradient to 0.5 power:

$$C_L = \frac{2}{\pi} \bar{K} \nu^{1/2} \frac{1}{u} \left(\frac{du}{dy}\right)^{1/2} \tag{2-2}$$

where $\bar{K} = 6.46$, ν is the fluid kinematic viscosity, and the distance y is measured normal to the flow direction. Saffman's analysis is for uniform shear flow and restricted to particle Reynolds numbers less than 1.0.

Vidal[4], by using Hall's results[15] for the tangential velocity variation on a sphere in uniform shear flow, found that

$$C_L = 0.998\ k \tag{2-3}$$

where

$$k = \frac{a}{u} \frac{du}{dy} \tag{2-4}$$

and a is the particle radius. Thus, Vidal's relation shows C_L to vary linearly with (du/dy). Equation (2-3) becomes invalid for $k \geq 1$.

A purpose of the present study is to illustrate the effects of lift on dust entrainment. Since there does not exist an established general formula to predict lift, it is advantageous to choose a least restrictive relation for the purpose of illustration. For a particle in a high speed boundary layer, the Reynolds number is very large (compared to 1.0) except for small particles at or near the ground. Small particles, however, have large values of drag coefficient; even if they are lifted off the surface, they soon approach and follow the fluid streamlines and will not reach a significant vertical distance above the ground. Therefore, Saffman's results will not be utilized in the present study. The pipe flow experiment, though it can conceivably be applied to external flows by relating the pipe diameter to boundary layer thickness, is also limited in particle Reynolds number range and in the ratio of particle size to boundary layer thickness. Therefore, the relation for lift coefficient given by Eichhorn and Small will also not be employed. Vidal's relation, Equation (2-3), is used in the present study. This relation is simple to apply, and its

restriction of $k < 1$, as will be shown later in this section, is not a severe limitation. It should be noted, however, that Vidal's relation is based on uniform shear flow over a particle at rest. In the present study of particle motion in a boundary layer, this relation is applied by using a local velocity gradient and a local relative velocity.

The particle trajectories inside and outside the boundary layer in the transient nonuniform blast flowfields will be shown in the next section. In the present section, it is desired to acquire some physical insight and some qualitative measure of the effects of various parameters on the potential motion of a particle as it is lifted off a surface. For this purpose, a steady one-dimensional boundary layer (i.e., a boundary layer of constant thickness along a surface) with constant properties is considered. The velocity distribution is represented by

$$u = u_e \left(1 - e^{-y/\delta}\right) \tag{2-5}$$

$$v = 0 \tag{2-6}$$

where u_e, u, v, and y denote the gas free-stream velocity, velocity parallel to the ground, velocity normal to the ground, and distance from the surface, respectively. The parameter δ is a measure of the boundary layer thickness; at $y = 4.6$, the velocity becomes $u = 0.99\ u_e$.

The particle is considered to be spherical, and u and y are measured at the particle center. It is assumed that the particle is initially at rest and tangent to the ground, i.e., $y = a$ initially. The equations governing the particle motion are taken as

$$m\, v_p \frac{dv_p}{dy} = \frac{1}{2}\, \rho\, A \left[C_L\, (u - u_p)^2 + C_D\, V\, (v - v_p)\right] - mg \tag{2-7}$$

$$m\, v_p \frac{du_p}{dy} = \frac{1}{2}\, \rho\, A\, C_D\, V\, (u - u_p) \tag{2-8}$$

where m, A, ρ, C_D, g, u_p, v_p, and V denote, respectively, the particle mass, particle cross-sectional area, fluid density, drag coefficient, gravitational acceleration, particle velocity parallel to the ground, partical velocity

normal to the ground, and relative velocity between particle and fluid. In deriving Equations (2-7) and (2-8), it has been assumed that lift is important only in the vertical direction and that the lift coefficient is based on relative horizontal fluid and particle velocities. Considering Equations (2-3) and (2-4), one may take

$$C_L = \frac{a}{u - u_p} \frac{du}{dy} \tag{2-9}$$

where the coefficient 0.998 has been replaced by 1.0 for simplicity and where u^{-1} du/dy has been interpreted as $(u-u_p)^{-1}$du/dy for a particle in motion. Equations (2-7) and (2-8) with v = 0 can be written as

$$v_p \frac{dv_p}{dy} = K \left[(u - u_p) \frac{du}{dy} - \frac{C_D}{a} V v_p\right] - g \tag{2-10}$$

$$v_p \frac{du_p}{dy} = K \frac{C_D}{a} V (u - u_p) \tag{2-11}$$

where

$$K = \frac{3\rho}{8\rho_s} \tag{2-12}$$

$$V = \left[(u - u_p)^2 + v_p^2\right]^{1/2} \tag{2-13}$$

and where ρ_s denotes the particle material density.

At this point, it appears advantageous to examine the variation of the lift force F_L. From Equation (2-10) it is seen that F_L is proportional to $(u-u_p)$du/dy. Within a short distance from the surface, u_p is negligible compared to u, and the lift force is proportional to u(du/dy) which varies with y according to Equation (2-5) so that

$$\frac{F_L}{m} = \frac{Ku_e^2}{\delta} (1 - e^{-y/\delta}) e^{-y/\delta} \tag{2-14}$$

Thus, the lift force per unit mass has a maximum value of $Ku_e^2/4\delta$ and occurs at y = 0.693δ. The variation of $F_L\delta/mKu_e^2$ with y/δ is shown in Figure 2-1.

From Equation (2-10), it is seen that K(udu/dy) at y = a must be greater than g in order for a particle that is initially resting on a flat surface to be lifted. Using Equation (2-5), this requirement can be written as

$$(Ku_e^2/ag)\zeta > 1 \tag{2-15}$$

where

$$\zeta = (a/\delta)(1 - e^{-a/\delta})\, e^{-a/\delta} \tag{2-16}$$

The function ζ is shown in Figure 2-2 and has a maximum value of 0.260 at $a/\delta = 1.45$. The interesting point is that for a given particle size, there exists a preferential range of boundary layer thickness for initial entrainment. That is, lift may not exist near the leading edge on a surface where the boundary layer is thin (although the shear stress is very high there) or near the tail end where the boundary layer is thick. If the flow conditions are such that Equation (2-17) is not satisfied everywhere along a surface, then no lift may occur at all. Also, in order for the particle to be lifted to a significant distance above the ground, the condition of $(Ku_e^2/ag)\zeta >> 1$ is required.

It is interesting to compare the lift force F_L with the horizontal drag force F_x. From Equations (2-10) and (2-11), the ratio is given by

$$\frac{F_L}{F_x} = \frac{1}{C_D}\frac{a}{V}\frac{du}{dy} \tag{2-17}$$

For an estimate of the value of this ratio, one may approximate V by u to obtain

$$\frac{F_L C_D}{F_x} = \frac{a}{u}\frac{du}{dy} = k = \frac{a}{\delta(e^{y/\delta} - 1)} \tag{2-18}$$

The parameter k is plotted as a function of a/δ and y/a in Figure 2-3. It is seen that k has a maximum limiting value of 1.0 which occurs when the particle is at the surface (y = a) and when $a/\delta \to 0$. Thus, the condition of $k < 1.0$ as required for the lift relation [Equations (2-3) and (2-4)] is satisfied. (However, if the particle is partially imbedded in the ground

initially, i.e., $y < a$, then $k > 1.0$ initially except for large values of a/δ.) At a distance of a few radii away (say $y/a = 10$), the ratio of vertical lift to horizontal drag becomes negligible.

Attention is now directed towards the solution of Equations (2-10) and (2-11). From these equations, it can be deduced that a particle is first accelerated off the ground by the lift force, and then decelerated vertically by drag and gravity. During its subsequent return towards the ground, the particle may get lifted again if the lift at any point within the boundary layer overcomes gravity and a few such damped oscillations may occur. However, during its descent, a particle generally has attained a horizontal velocity nearly equal to the fluid velocity and the lift due to $(u-u_p)(du/dy)$ is negligible. In fact, u_p becomes greater than u somewhere within the boundary layer, and a negative lift develops which aids gravity in returning the particle to the ground.

In order to solve Equations (2-10) and (2-11) analytically, it is necessary to make some simplifications. The drag coefficient will be taken as a constant; this is acceptable since the particle Reynolds number is generally very large. The flow is divided into two regions for solution: vertical acceleration of the particle within the boundary layer and vertical deceleration outside the boundary layer.

The boundary layer thickness will be denoted by y_e and has a value of 4.6δ at which $u = 0.99\ u_e$. For acceleration in the boundary layer, it is assumed that vertical drag and gravity are negligible compared to lift. Particles that are too small to satisfy this assumption will not be lifted significantly above the boundary layer and will not be considered. It is also assumed that u_p is negligible compared to u in computing lift. These assumptions are somewhat conservative, i.e., they would result in overpredicting the values of the vertical velocity. The boundary conditions should be $v_p = u_p = 0$ at $y = a$ if a particle is initially at rest on a flat surface. However, the boundary will be given an arbitrary value of $y = y_i$ instead of $y = a$ in the solution. With these assumptions and boundary conditions, the solution for v_p is

$$v_p = (Ku^2 - Ku_i^2)^{1/2} \qquad \text{for } y \leq y_e \qquad (2\text{-}19)$$

where u is given by Equation (2-5) and u_i is u at y_i. Equation (2-19) may be written as

$$\frac{v_p^2}{Ku_e^2} = 2\, e^{-\lambda}(1 - e^{-z}) - e^{-2\lambda}(1 - e^{-2z}) \qquad \text{for } y \leq y_e \qquad (2\text{-}20)$$

where

$$\lambda = y_i/\delta \qquad (2\text{-}21)$$

$$z = (y - y_i)/\delta \qquad (2\text{-}22)$$

Equation (2-19) shows that the maximum attainable value of v_p due to lift is only a small fraction of u_e, i.e., $v_p \to K^{1/2} u_e$ where K is on the order of 10^{-3} (when the fluid is a liquid, however, K is of order 1). Also, Equation (2-19) shows that v_p is smaller for larger particles since u_i is larger for larger particles.

In using Equation (2-11) to solve for u_p in the boundary layer, V is approximated by u and v_p by $K^{1/2}$ u. The result is

$$\frac{u_p}{u_e} = 1 - e^{-sz} + \frac{s}{1-s} e^{-\lambda}(e^{-z} - e^{-sz}) \qquad (2\text{-}23)$$

where

$$s = K^{1/2} C_D/\alpha \qquad (2\text{-}24)$$

$$\alpha = a/\delta \qquad (2\text{-}25)$$

If s = 1, the solution for u_p can be obtained by applying L'Hospital's rule to Equation (2-23).

The time a particle takes to travel from y_i to y is given by $t = \int_{y_i}^{y} v_p^{-1}\, dy$ and the horizontal distance x a particle has traveled is given by $x = \int_{y_i}^{y} (u_p/v_p)\, dy$.

After the particle has reached the edge of the boundary layer, no lift due to shear exists and the particle is considered to be decelerated vertically by drag and gravity. In this region, V can be approximated by $u_e - u_p$. It is convenient to choose a transformed time coordinate ϕ instead of z as the independent variable in this region. The solution is

$$\frac{v_p}{u_e} = \frac{1}{\phi}\left(\frac{v_{pe}}{u_e} + \frac{r}{2C_D w}\right) - \frac{r}{2C_D w}\,\phi \qquad \text{for } t > t_e \tag{2-26}$$

$$\frac{u_p}{u_e} = 1 - \frac{w}{\phi} \tag{2-27}$$

where e denotes values at y_e and

$$r = \frac{ag}{Ku_e^2} \tag{2-28}$$

$$w = 1 - \frac{u_{pe}}{u_e} \tag{2-29}$$

$$\phi = 1 + KC_D u_e w\,(t - t_e)/a \tag{2-30}$$

The distances y and x are related to t by $y = y_e + \int_{t_e}^{t} v_p dt$ and $x = x_e + \int_{t_e}^{t} u_p dt$, or

$$z = z_e + \frac{a}{KC_D w}\left[\left(\frac{v_{pe}}{u_e} + \frac{r}{2C_D w}\right)\ell n\ \phi - \frac{r}{4C_D w}\,(\phi^2 - 1)\right] \qquad \text{for } t \geq t_e \tag{2-31}$$

$$\frac{x}{s} = \frac{x_e}{\delta} + \frac{a}{KC_D w}\,(\phi - 1 - w\ \ell n\ \phi) \qquad \text{for } t \geq t_e \tag{2-32}$$

The maximum height occurs at $v_p = 0$ and can be obtained by using Equations (2-26) and (2-31). The time it takes a particle to return to the ground and the velocity components there can be obtained by setting z = 0 in Equation (2-31) and using Equations (2-26), (2-27), and (2-30).

Examination of Equations (2-19) to (2-32) shows that v_p/u_e and u_p/u_e are dependent on five dimensionless parameters: K, C_D, α, r, and z or ϕ. (The boundary of y_i = a is being used.) The five parameters encompass eight variables: ρ, ρ_s, C_D, a, δ, u_e, g, and y or t. The results of interest are shown in Figures 2-4 through 2-11 for which the values of C_D = 0.5 and K = 0.001 are used. The value of C_D = 0.5 is a good approximation since the particle Reynolds number is generally very high, and K = 0.001 is typical for blast wave conditions. In Figures 2-4 through 2-11, the subscript e denotes conditions at the edge of the boundary layer (y_e = 4.6δ) during ascent, m at the maximum height reached by the particle, and f at the point where the particle has returned to the edge of the boundary layer during descent. The normalized particle velocity components at the edge of the boundary layer, which are obtained by assuming drag and gravity to be negligible compared to lift inside the boundary layer, are shown in Figure 2-4. The maximum height reached by the particle is shown in Figures 2-5 and 2-6 where different normalization factors are used. From Figure 2-5, it is seen that the particle cannot travel far above the boundary layer unless Ku_e^2 is large (for fixed a and δ). It can also be deduced from Figure 2-5 that there is some optimum values of the ratio of particle size to boundary layer thickness for aerodynamic lift. In Figure 2-6, the nondimensional group $2g(y_m-y_e)/Ku_e^2$ is employed since it can be shown from Equations (2-26) and (2-31) that $2g(y_m-y_e)/Ku_e^2 \to 1$ as $C_D \to 0$ and $a/\delta \to 0$. The particle vertical velocity at y_m is zero, while the horizontal velocity at y_m is shown in Figure 2-7. The velocity components of the particle when it has returned to the edge of the boundary layer are shown in Figures 2-8 and 2-9 from which it can be deduced that the particle returns to the surface almost horizontally. The nondimensional total horizontal distance traveled by the particle and total time of particle stay in the gas are shown in Figures 2-10 and 2-11, respectively.

It was indicated earlier that particles for which lift is not substantially greater than drag and gravity inside the boundary layer will not achieve a substantial vertical velocity at the edge of the boundary layer. It is interesting to observe what this condition implies. Considering the order of magnitude of the various terms in Equation (2-10)

and using the approximate result of $v_p \sim K^{1/2} u$, it can be shown that the following condition must hold in order for the particle to travel far above the boundary layer:

$$1 >> \frac{K^{1/2} C_D \delta}{a} + \frac{g\delta}{Ku_e^2} \tag{2-33}$$

The ratio $K^{1/2} C_D \delta/a$, defined as s by Equation (2-24), may be considered to be a measure of the relative magnitudes of vertical drag and lift. The ratio $g\delta/Ku_e^2$, which is equal to α^{-1} times the factor r given by Equation (2-28), is a comparison between the effects of gravity and lift. Furthermore, the condition given by Equation (2-15) must be satisfied in order for a particle to be lifted off a surface.

The above results were obtained by considering the particle to be lifted by an aerodynamic force. It may be of interest to estimate the velocity of a particle as it leaves the ground if the particle is partly imbedded in the soil initially where the soil pressure is higher than the fluid pressure. For this purpose, consider the soil pressure to be p_s and the fluid pressure to be p. Let the initial distance between the particle center and the soil surface be denoted by y_i. The equation for the particle motion is given by

$$v_p \frac{dv_p}{dy} = \frac{3(p_s - p)}{4\rho_s a}\left(1 - \frac{y^2}{a^2}\right) \tag{2-34}$$

For the boundary condition of $v_p = 0$ at $y = y_i$, the solution is

$$v_p = \left[\frac{3(p_s - p)}{2\rho_s a}\left(y - y_i - \frac{y^3 - y_i^3}{3a^2}\right)\right]^{1/2} \tag{2-35}$$

The maximum v_p is obtained at $y = a$ and for $y_i = 0$ and is equal to $[(p_s - p)/\rho_s]^{1/2}$. If $(p_s - p)$ is taken to be the free-stream dynamic pressure, $\rho u_e^2/2$, the maximum v_p is $(\rho/2\rho_s)^{1/2} u_e$. This v_p is in the neighborhood of $(3\rho/8\rho_s)^{1/2} u_e$ which is the estimated maximum v_p achievable due directly to lift.

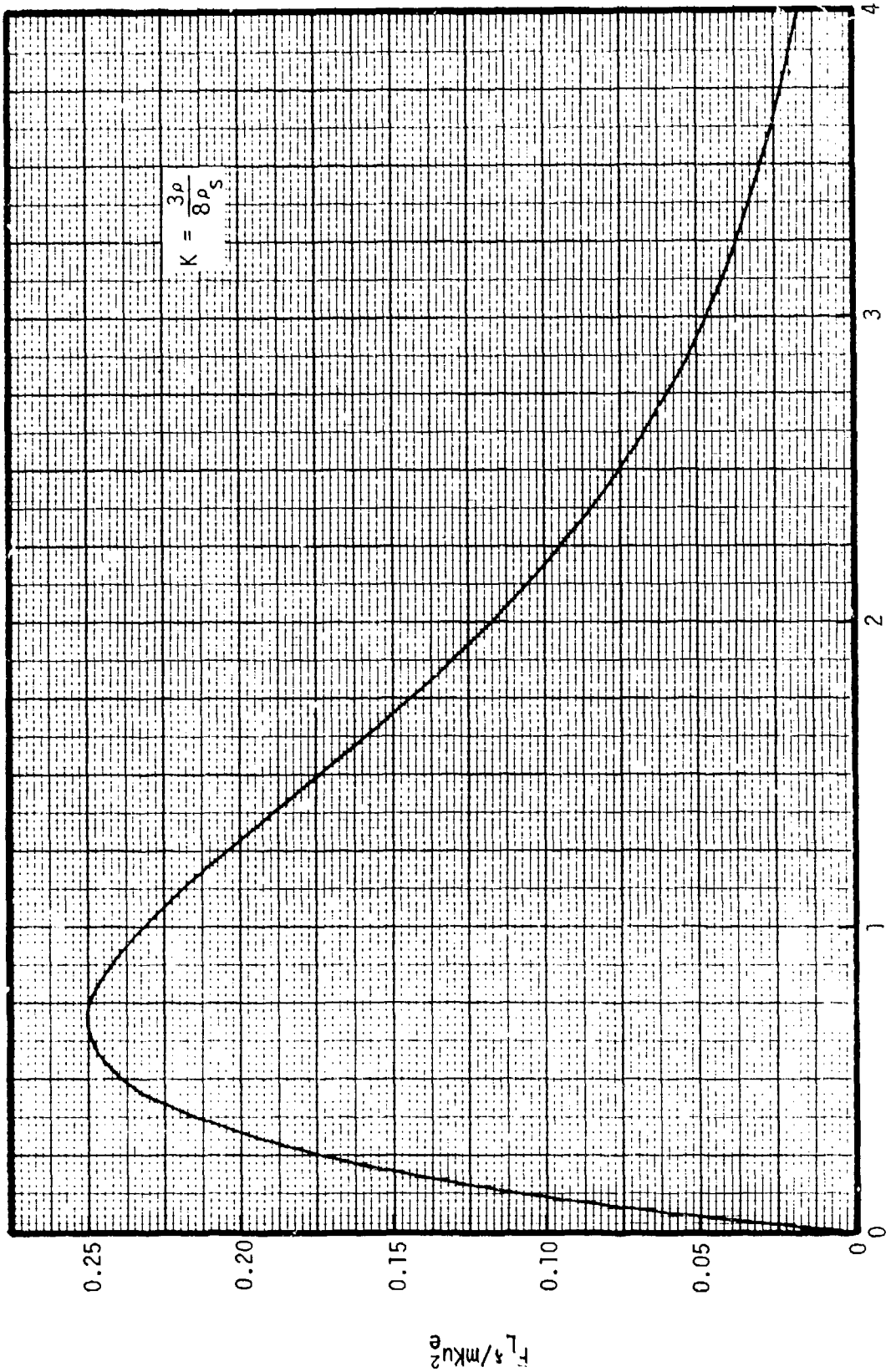

FIGURE 2-1 VARIATION OF LIFT FORCE WITH DISTANCE FROM SURFACE

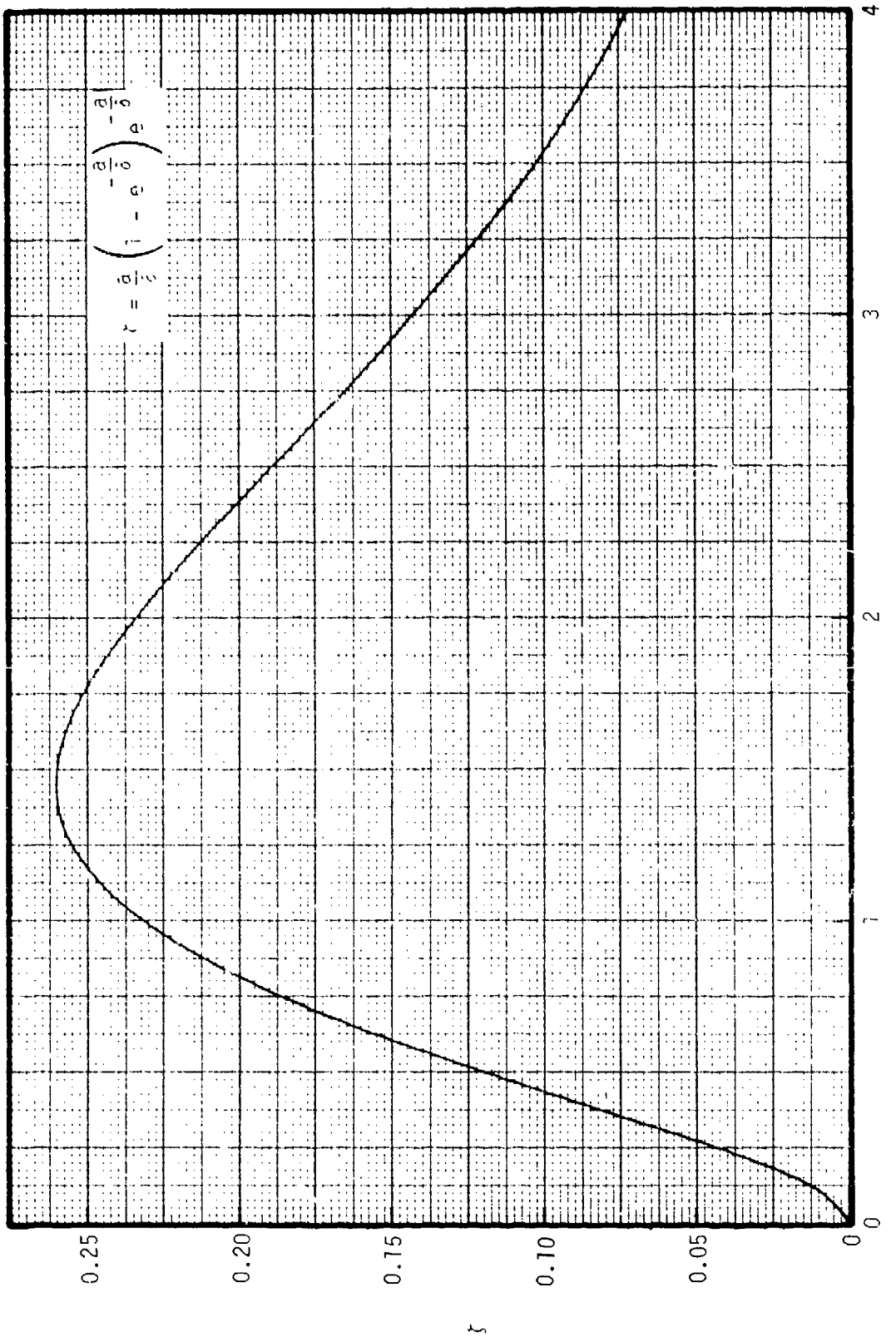

FIGURE 2-2 VARIATION OF γ WITH a/b

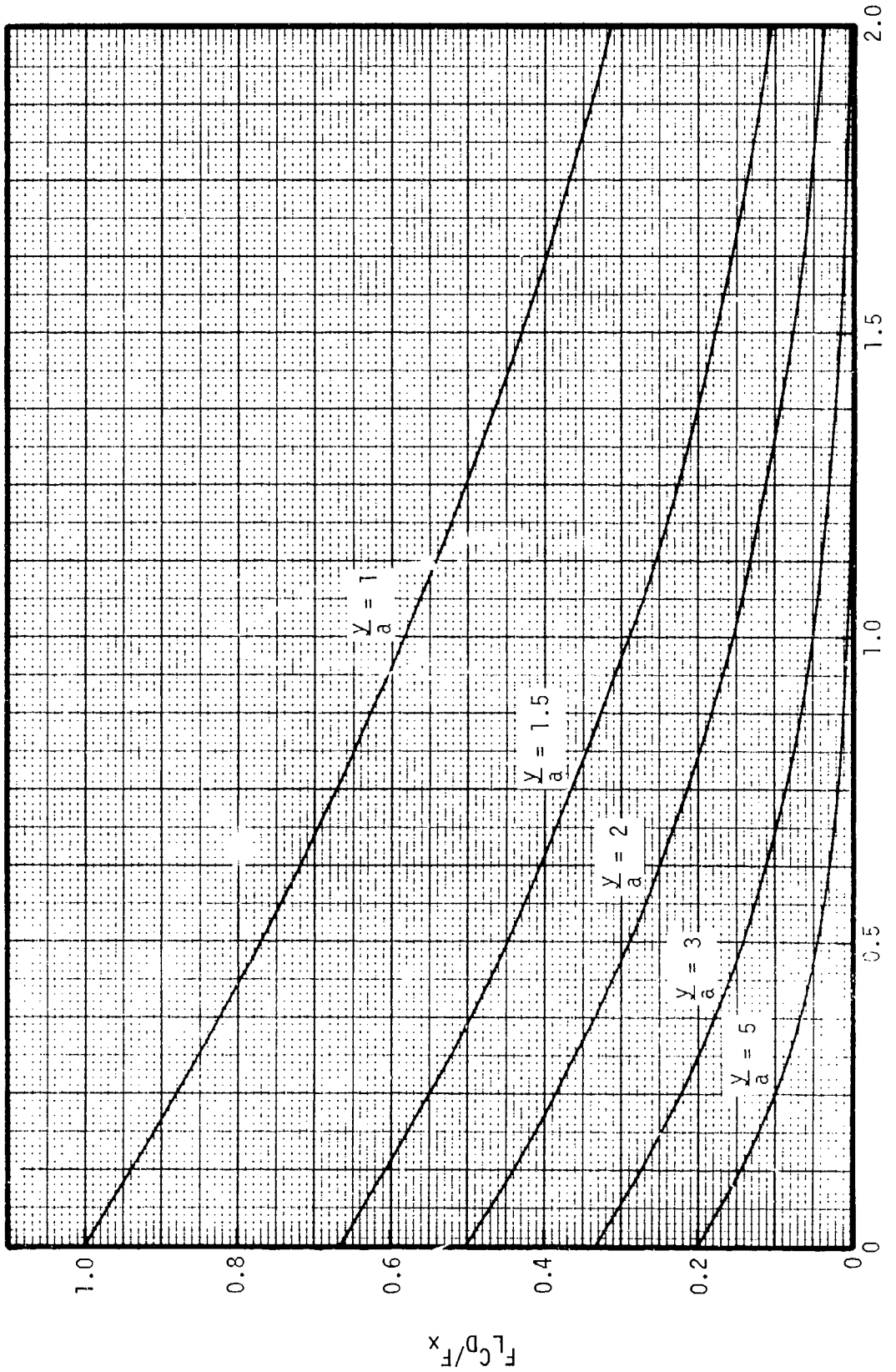

FIGURE 2-3 VARIATION OF $F_L C_D/F_x$ WITH a/δ AND y/a

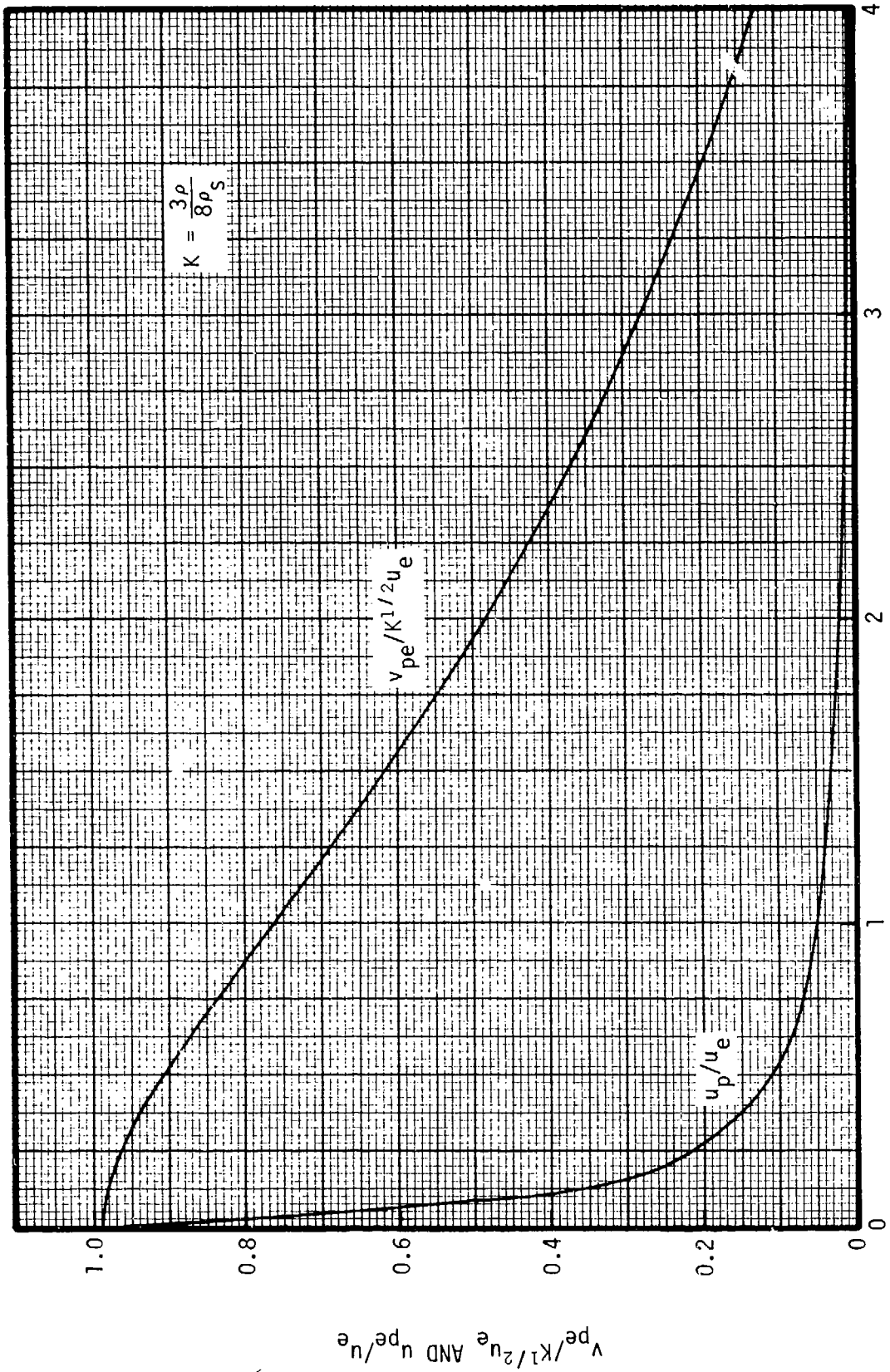

FIGURE 2-4 PARTICLE VELOCITY COMPONENTS AT EDGE OF BOUNDARY LAYER

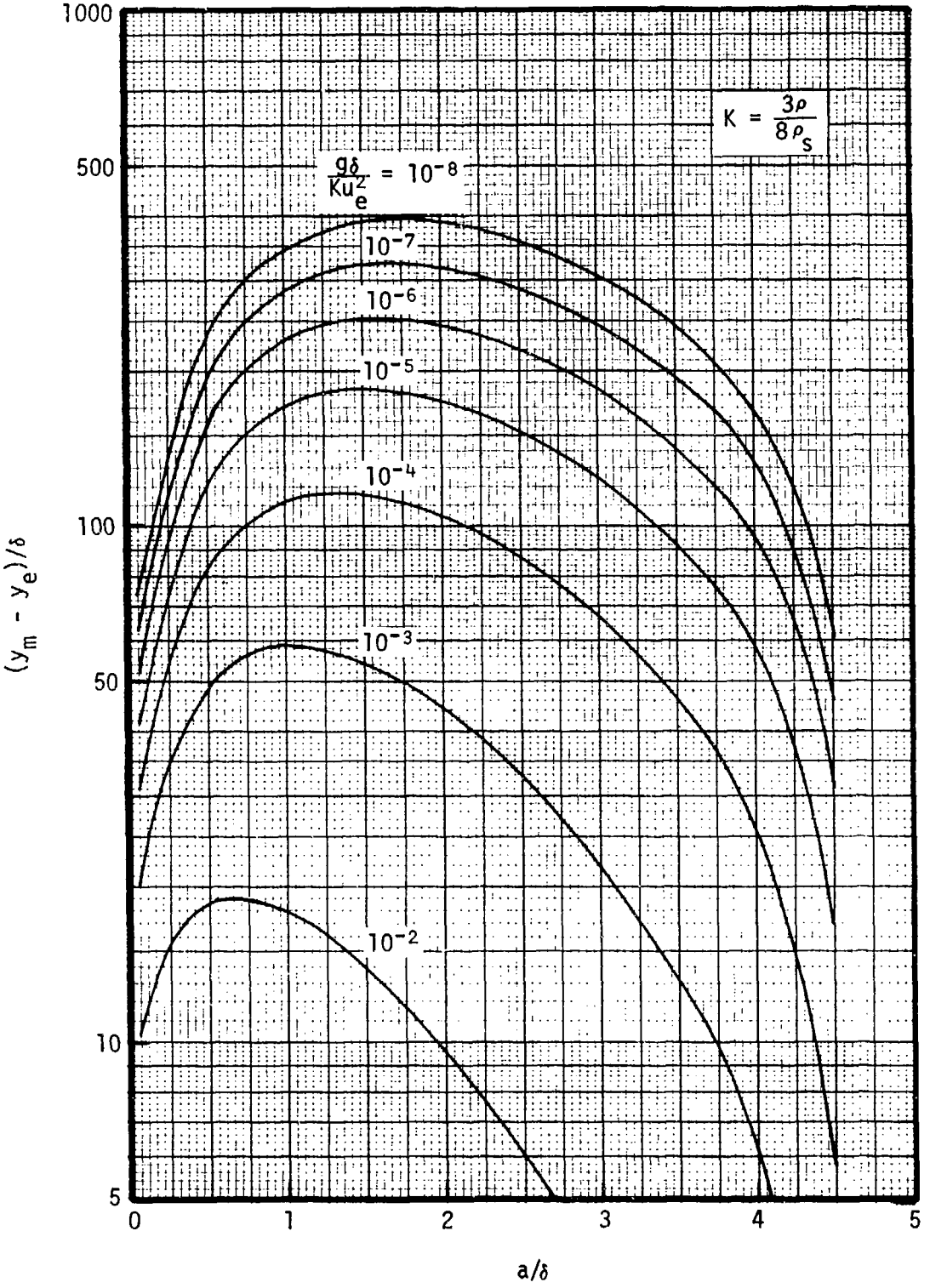

FIGURE 2-5 MAXIMUM PARTICLE HEIGHT

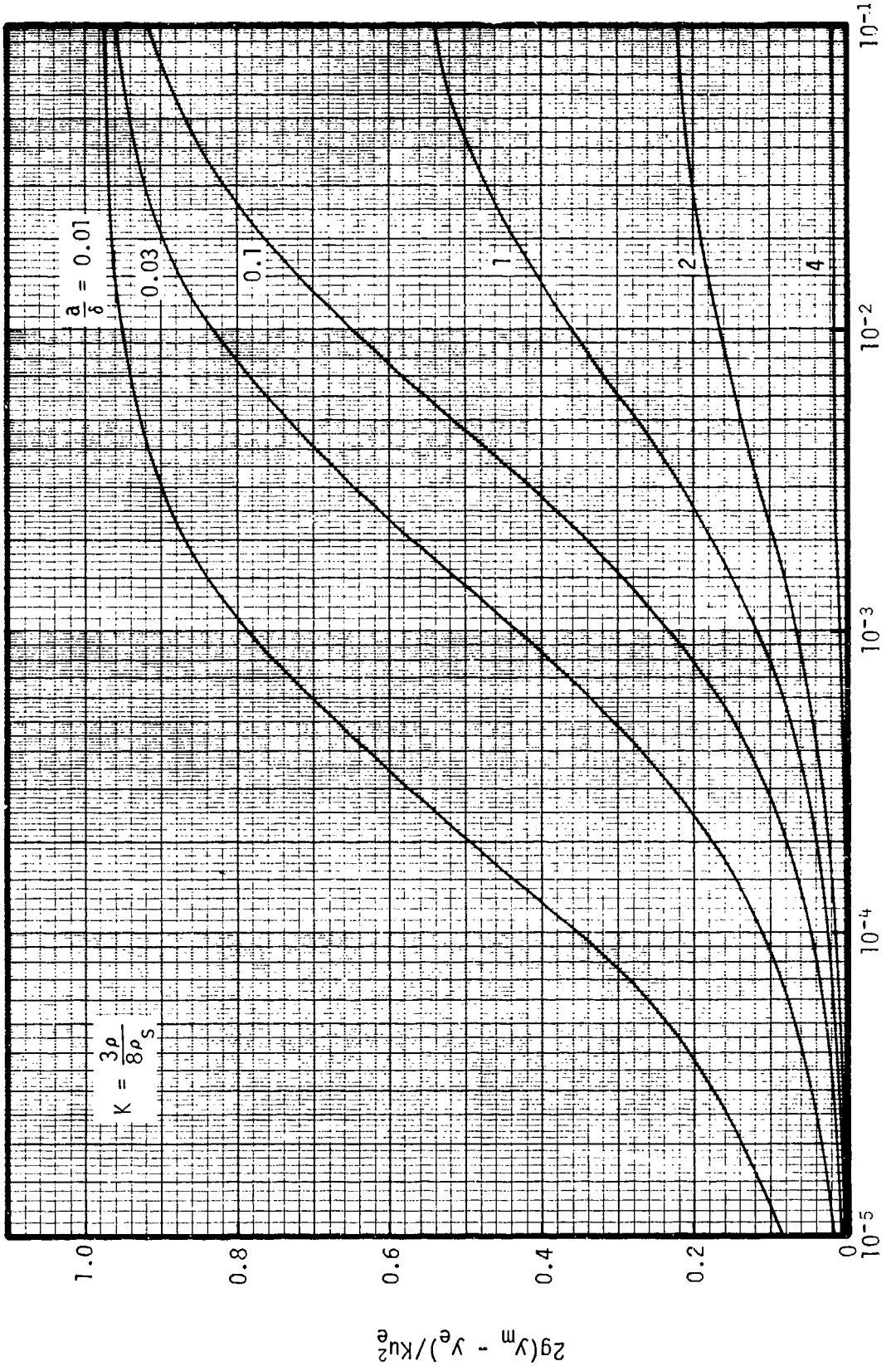

FIGURE 2-6 MAXIMUM PARTICLE HEIGHT

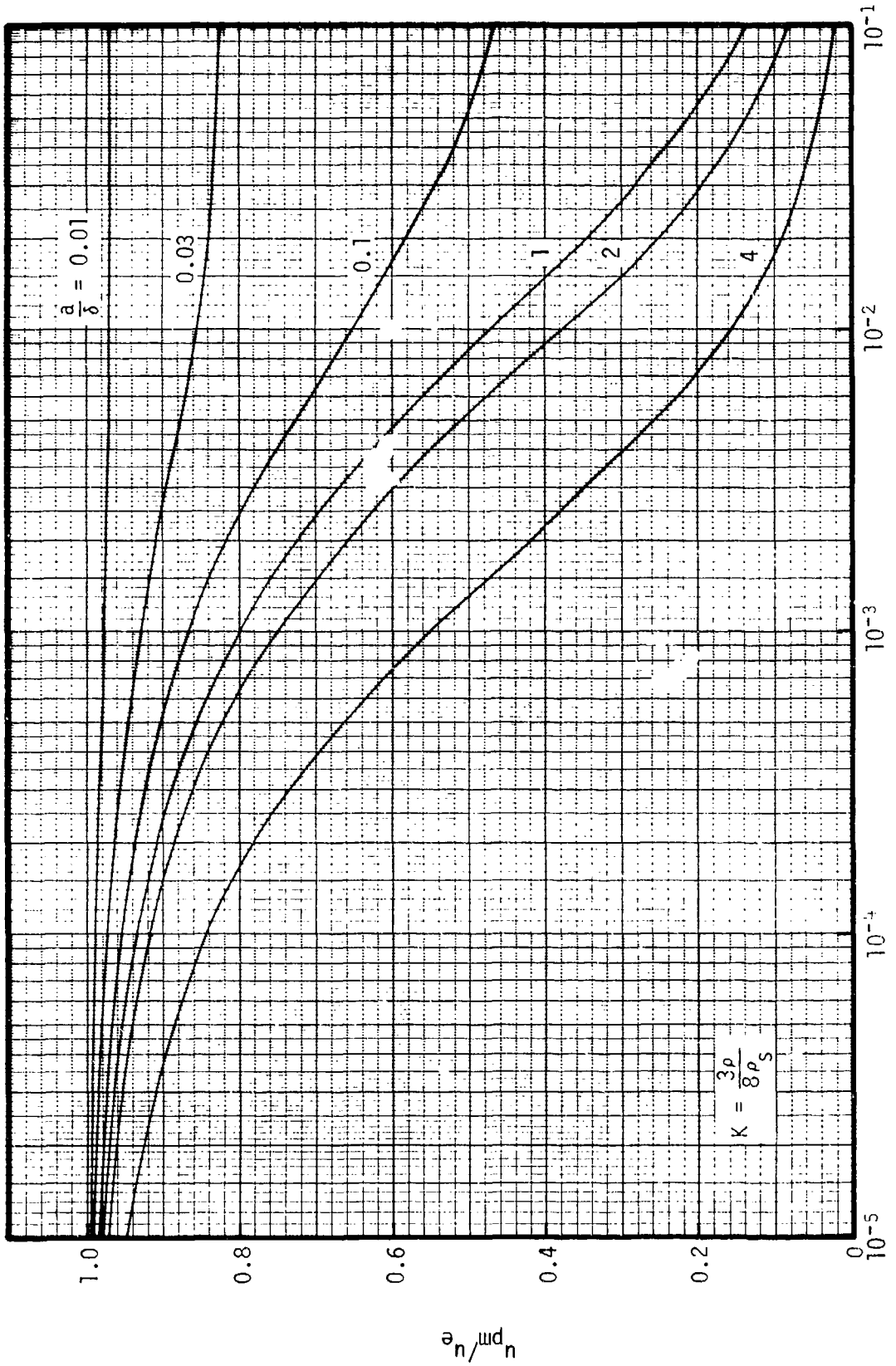

FIGURE 2-7 PARTICLE HORIZONTAL VELOCITY AT MAXIMUM HEIGHT

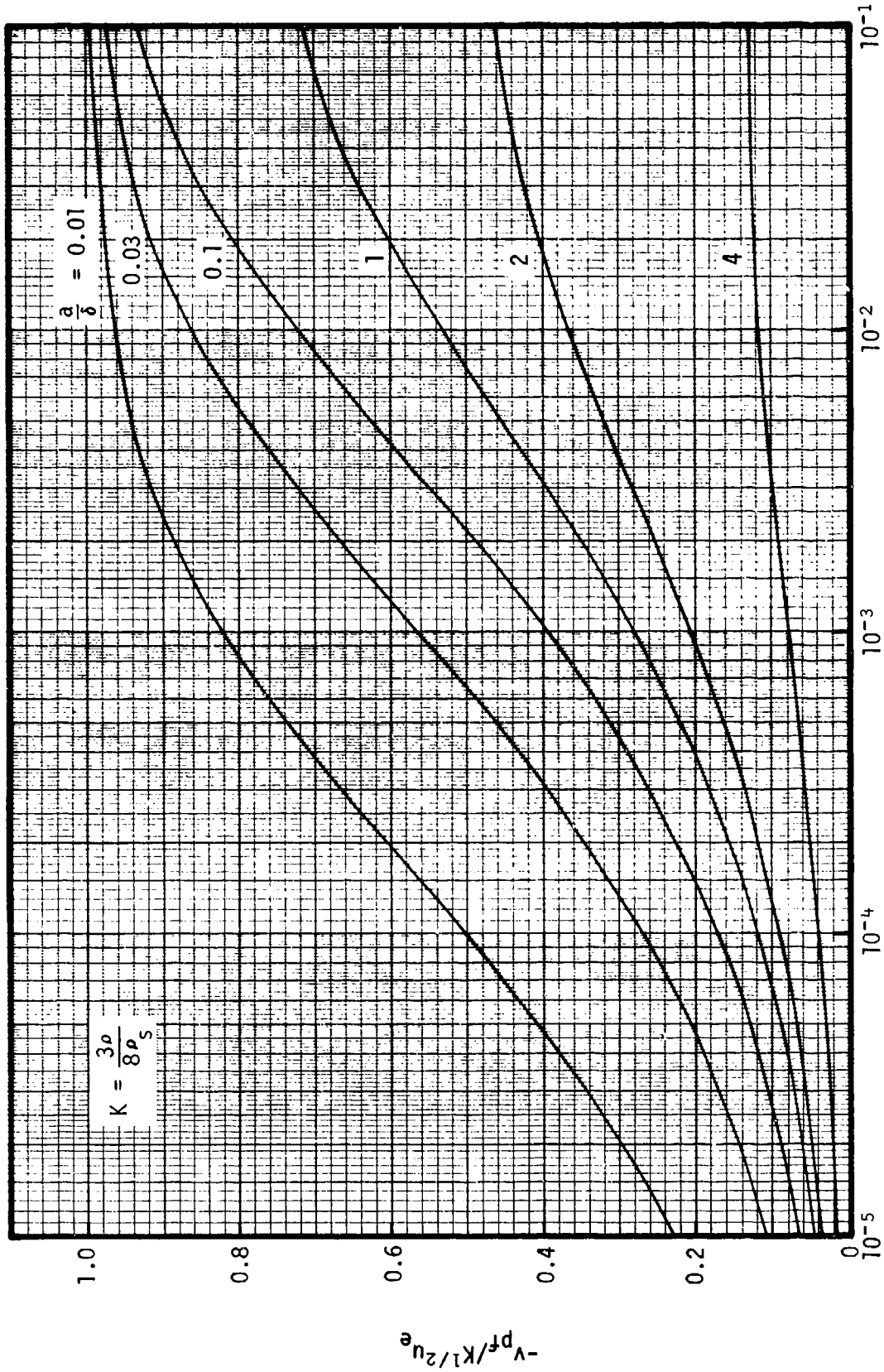

FIGURE 2-8 PARTICLE VERTICLE VELOCITY AT IMPACT

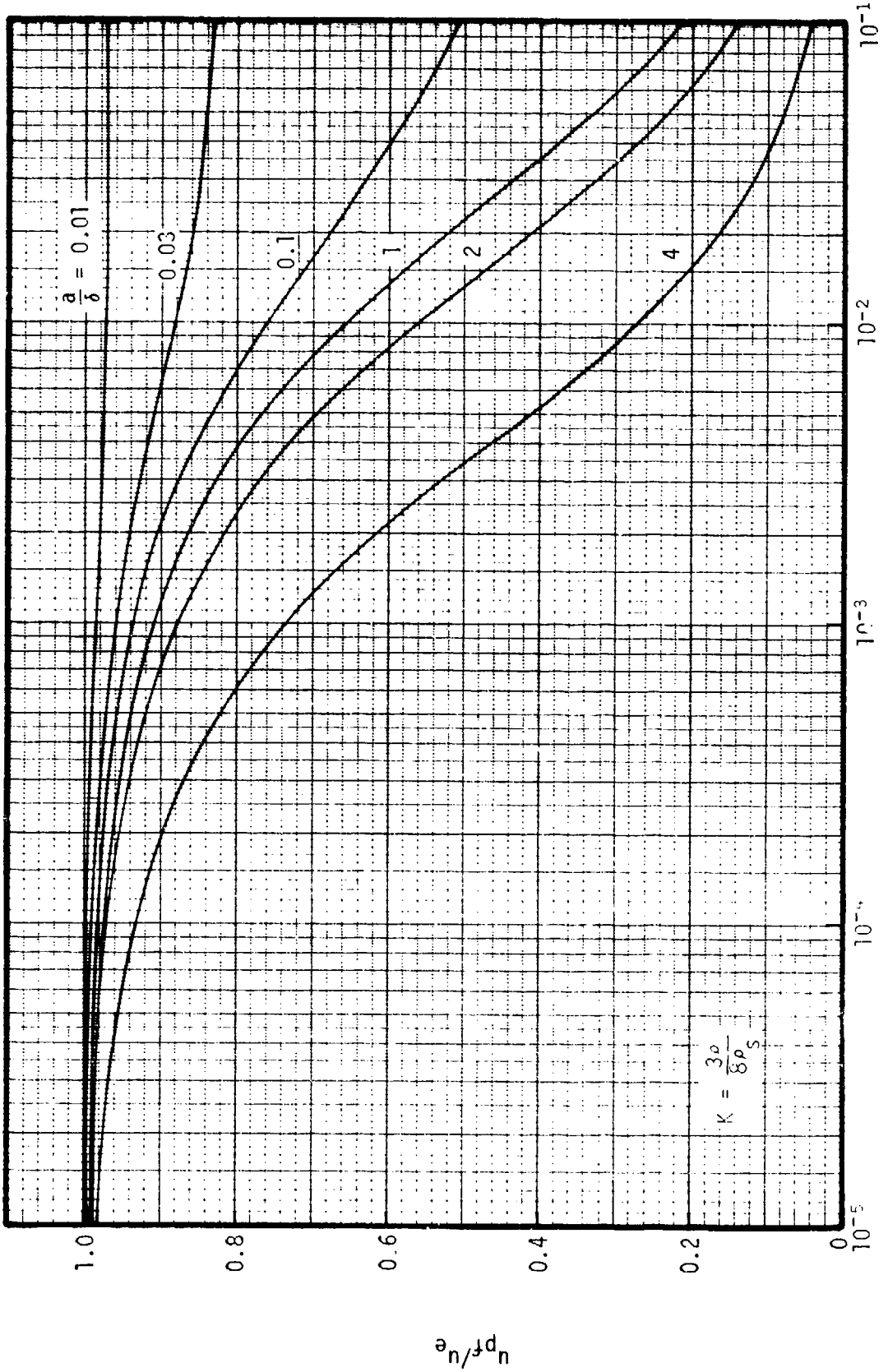

FIGURE 2-9 PARTICLE HORIZONTAL VELOCITY AT IMPACT

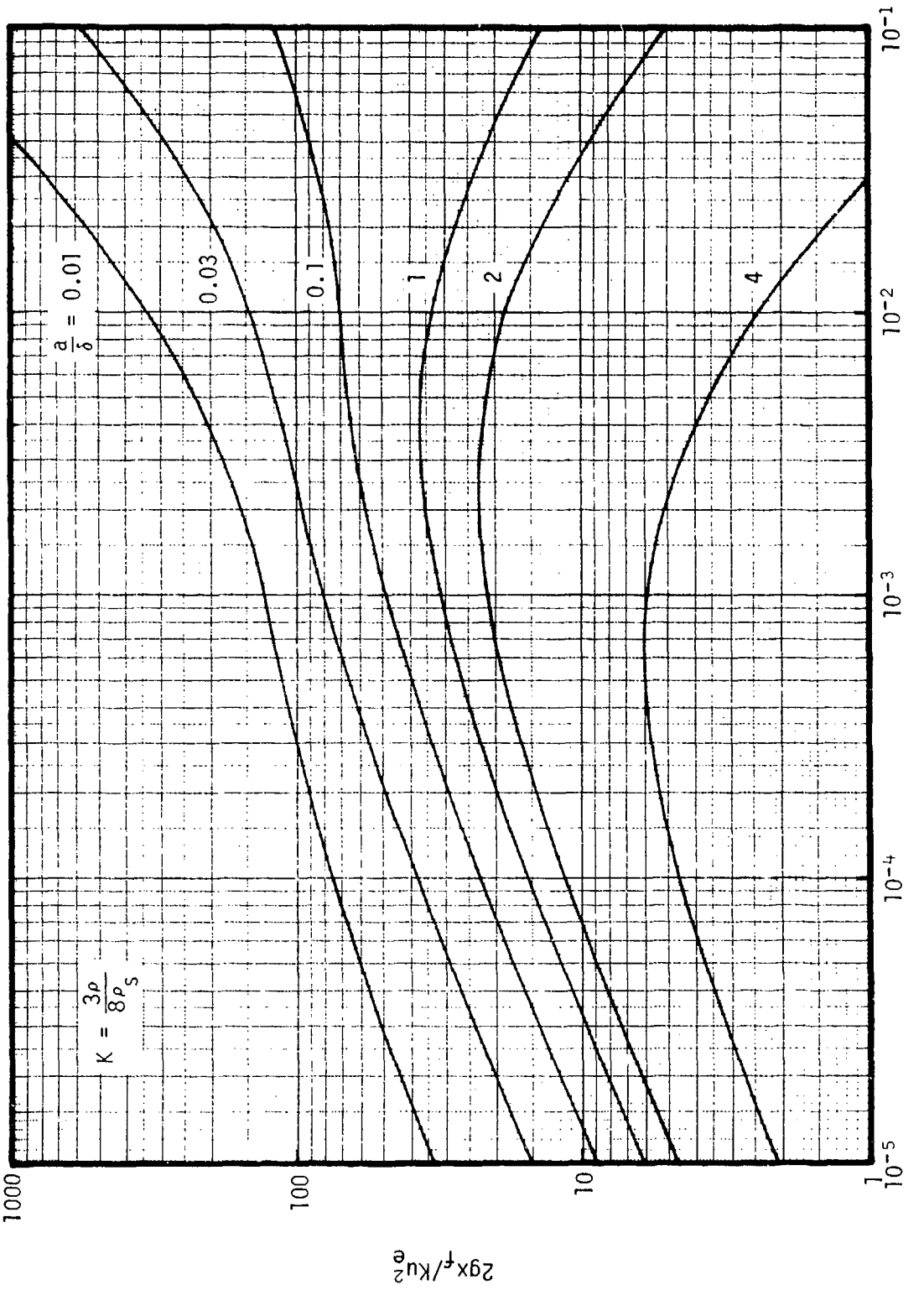

FIGURE 2-10 HORIZONTAL DISTANCE TRAVELED

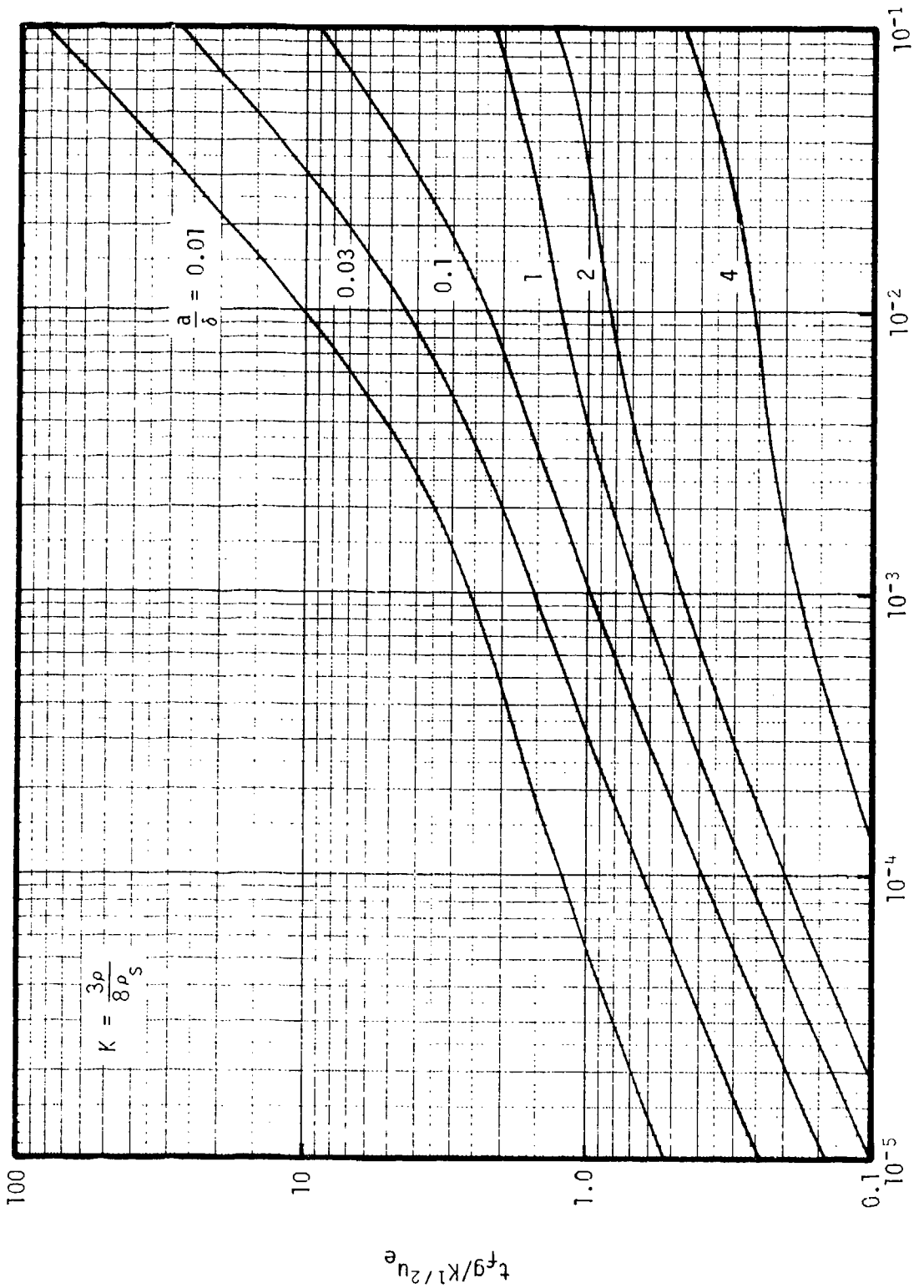

FIGURE 2-11 TIME OF STAY IN GAS

(Reverse of Page is Blank)

3. SAMPLE TRAJECTORIES

The analysis of the previous section shows analytically the effects of the various parameters on particle trajectory for a selected lift coefficient. A uniform steady flowfield with constant boundary layer thickness was assumed. In the present section, the particle trajectories in a blast flowfield transient and nonuniform, which includes the boundary layer properties obtained in Part I of this study are investigated. The equations are taken as:

$$\frac{dx}{dt} = u_p \tag{3-1}$$

$$\frac{dy}{dt} = v_p \tag{3-2}$$

$$\frac{du_p}{dt} = F\ (u-u_p) \tag{3-3}$$

$$\frac{dv_p}{dt} = F(v-v_p) + K(u-u_p)\frac{\partial u}{\partial y} - g \tag{3-4}$$

$$\frac{dT_p}{dt} = G(T-T_p) \qquad \text{for } T_p < T_{pv} \tag{3-5}$$

$$\frac{da}{dt} = 0 \qquad \text{for } T_p < T_{pv} \tag{3-6}$$

$$\frac{dT_p}{dt} = 0 \qquad \text{for } T_p = T_{pv} \tag{3-7}$$

$$\frac{da}{dt} = -\frac{c_{ps}a}{3L} G(T-T_p) \qquad \text{for } T_p = T_{pv} \tag{3-8}$$

where $K = 3\rho/8\rho_s$ and

$$F = KVC_D/a \tag{3-9}$$

$$G = Kk_\infty TNu/\rho c_{ps} a^2 T_\infty \tag{3-10}$$

$$V = \left[\left(u-u_p\right)^2 + \left(v-v_p\right)^2\right]^{1/2} \tag{3-11}$$

In the above equations, F and G are factors for drag and convective heat transfer, respectively; c_{ps} is the specific heat of the particle, T_{pv} is the vaporization or ablation temperature, L is the heat of ablation, and k_∞ is the fluid conductivity at the ambient temperature T_∞. The term involving $\partial u/\partial y$ in Equation (3-4) is used to account for lift. The effects of particles on the fluid flowfield are neglected. Since mass and heat transfers are only of secondary consideration in this study, the effects of ablation on the drag and heat transfer coefficients are also neglected. Furthermore, radiation is not considered. The drag coefficient and Nusselt number Nu are approximated by

$$C_D = \frac{24}{Re} + 0.5 \tag{3-12}$$

$$Nu = 2 + 0.459\ Re^{0.55} \tag{3-13}$$

where Re is the Reynolds number based on particle diameter.

For the fluid properties, the vertical velocity v is taken as zero. The axial velocity u, temperature T, and density ρ are approximated by $u = u_e(1-e^{-\eta/\ell})$, $T = T_w + (T_e-T_w)(1-e^{-\eta/\ell_t})$, $\rho = \rho_e(T_e/T)$, respectively, where the subscript e denotes properties for inviscid flow which are computed using the Taylor-Sedov strong shock solution. The parameters η, ℓ, and ℓ_t are taken from the laminar boundary layer integral-exponential solution given in Part I of this report, and T_w is the wall temperature. The particle is considered to be initially at rest on a flat surface.

From the numerical results, it is found that a particle of given size is not subject to direct lift in a region extremely close to the shock front where the boundary layer is thin nor in the region far away from the shock front where the boundary layer is thick. This is in agreement with the results of Section 2. It is also found that direct lift does not loft a particle to sufficient height for suspension except for a very short time after explosion when the free-stream velocity is extremely high. However, small particles that are lifted at early times vaporize soon after leaving the boundary layer because of the high gas temperature. Most of the particles that get lifted and do not ablate are confined within a few inches above the ground. They can achieve a vertical velocity of only a small fraction of the free-stream gas velocity; however, they quickly attain a high horizontal

velocity, which is comparable to the free-stream velocity, with which they return to the ground. This substantiates previous assumptions and observations[1,2,3] that particles are not directly lifted into suspension by a free-stream. Instead, a particle may bounce off the ground a few times and achieve a higher velocity with each subsequent bounce until the velocity is sufficiently high to loft the particle or bounce off another particle into suspension. However, lift does aid particle entrainment by placing the particle in the higher velocity region of the boundary layer to facilitate the acceleration of the particle by the gas stream. Also, direct lift can be partially responsible for a significant amount of dust having bouncing motions, known as saltation, within a short distance from the ground. Another mechanism responsible for saltation is horizontal drag which causes a particle to roll or slide along a surface until the particle accelerates to sufficient speed to leave the surface upon impacting another particle.

The above paragraph describes the particle trajectories qualitatively. Some numerical results are presented in Figures 3-1 through 3-5 for illustration. The blast properties correspond to a 1.0 megaton spherical surface explosion. The physical properties used are: $T_\infty = T_w = 530°R$, $\rho_\infty = 0.076 U/ft^3$, $C_p = 0.24$ BTU/lb-°R, $\mu_\infty = 1.23 \times 10^{-5}$ lb/ft-sec, $k_\infty = 4.1 \times 10^{-6}$ BTU/sec-ft-°R, $\gamma = 1.4$, $\rho_s = 145$ lb/ft^3, $c_{ps} = 0.2$ BTU/lb-°R, $T_{pv} = 6400$ °R, and L = 3700 BTU/lb. Figure 3-1 shows the trajectories (y vs x) of particles of various sizes; the particles have been assumed to be initially at rest and get lifted at 0.01 second after explosion and at a distance of 10 feet behind the shock. Note that drastically different scales have been used for the x and y coordinates. The smaller particles become ablated by the hot gas soon after they leave the boundary layer and are indicated in Figure 3-1. The larger particles are lifted to higher altitudes (there is an increase in boundary layer thickness as the particle is being lifted), but there is a cutoff diameter (roughly 20,000 microns for the conditions of Figure 3-1) above which a particle does not get lifted at all because its weight becomes larger than the lift at the ground position.

Figures 3-2 to 3-4 are similar to Figure 3-1 except that the time of 0.1 second after explosion is used. Also, the locations at which the particles become lifted are 1 foot, 10 feet, and 100 feet behind the shock for Figures 3-2, 3-3, and 3-4, respectively. At 0.1 second after explosion, it is

*This is calculated based on 1.0 megaton free air burst which corresponds roughly to 1/2 megaton surface burst.

found that the particles do not reach ablation temperature (except for small particles at locations beyond 100 feet from the shock). The initial free-stream gas velocity u_{ei} and the initial velocity boundary layer thickness y_{ei} ($u = 0.99\ u_e$ at $y = y_e$), along with the velocity components v_{pg} and u_{pg} when the particles impacts the ground and the length of time Δt in which the particle stays in the gas, are tabulated in the figures. In Figure 3-2, the location of the shock, x_{sg}, when the particle returns to the ground and the velocity boundary layer thickness, indicated by y_{eg}, experienced by the particle when it returns to the ground are also indicated. It can be observed that a particle accelerates more rapidly towards the ground as it returns to the boundary layer region; this is due to a negative lift which develops since u_p becomes greater than u inside the boundary layer. However, v_{pg} is still very small compared to u_{pg}, and a particle is expected to strike the ground almost horizontally.

From Figures 3-1 to 3-4, it is seen that the particles are lifted not more than a few inches above the ground except for early time after explosion or from regions of large boundary layer thickness. It is also seen from the figures that for a given boundary layer thickness, there is some optimum particle size for entrainment. Particles can be lifted to higher altitudes if their diameter is roughly equal to the boundary layer thickness, i.e., $D/y_{ei} \simeq 1$. It is interesting to note that the analysis of Section 2 predicts a similar result: in Figure 2-5, y_m is largest for $a/\delta \simeq 1.5$; since $a = D/2$ and $\delta = y_e/4.6$, the maximum y_m corresponds to $D/y_e \simeq 0.7$.

After returning to the ground at high speed, the particles are expected to rebound from the ground. The rebound speed and direction depend on the soil properties such as elasticity and surface smoothness. Some rebound trajectories are illustrated in Figure 3-5. The position from which a particle rebounds corresponds to the end of the particle's lift trajectory shown in Figure 3-3. The rebound speed is taken to be the impact speed, and the rebound angle is taken to be 0, 45, or -45 degree from the normal direction to surface. As expected, the larger particles can rebound to much greater heights than the smaller particles because of lower drag forces. Figure 3-5 also shows that the particle trajectories are similar for all three rebound angles chosen for illustration. The end of each trajectory corresponds to 2.0 seconds after explosion. Thus, a particle that is lifted

off a surface may travel only a short vertical distance and return quickly to the ground; but after first bounce, it may remain in the gas for several seconds which is sufficiently long for the particle to be carried aloft by the rising fireball thermal. Furthermore, the larger particles can achieve a height of several hundred feet simply by rebound.

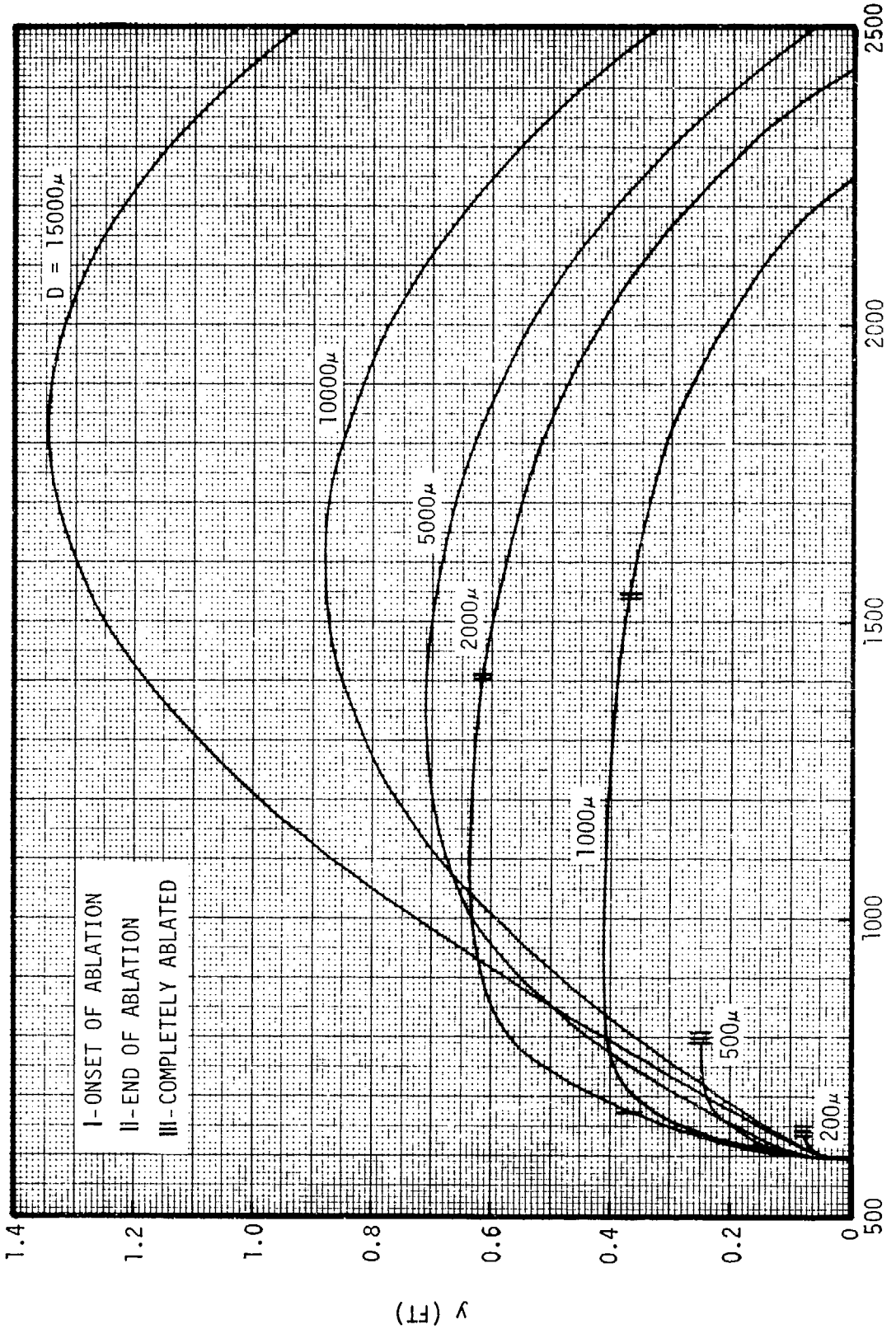

FIGURE 3-1 PARTICLE TRAJECTORY FOR A 1.0 MEGATON EXPLOSION WITH INITIAL TIME 0.01 SECOND AFTER EXPLOSION AND INITIAL DISTANCE 10 FEET BEHIND SHOCK

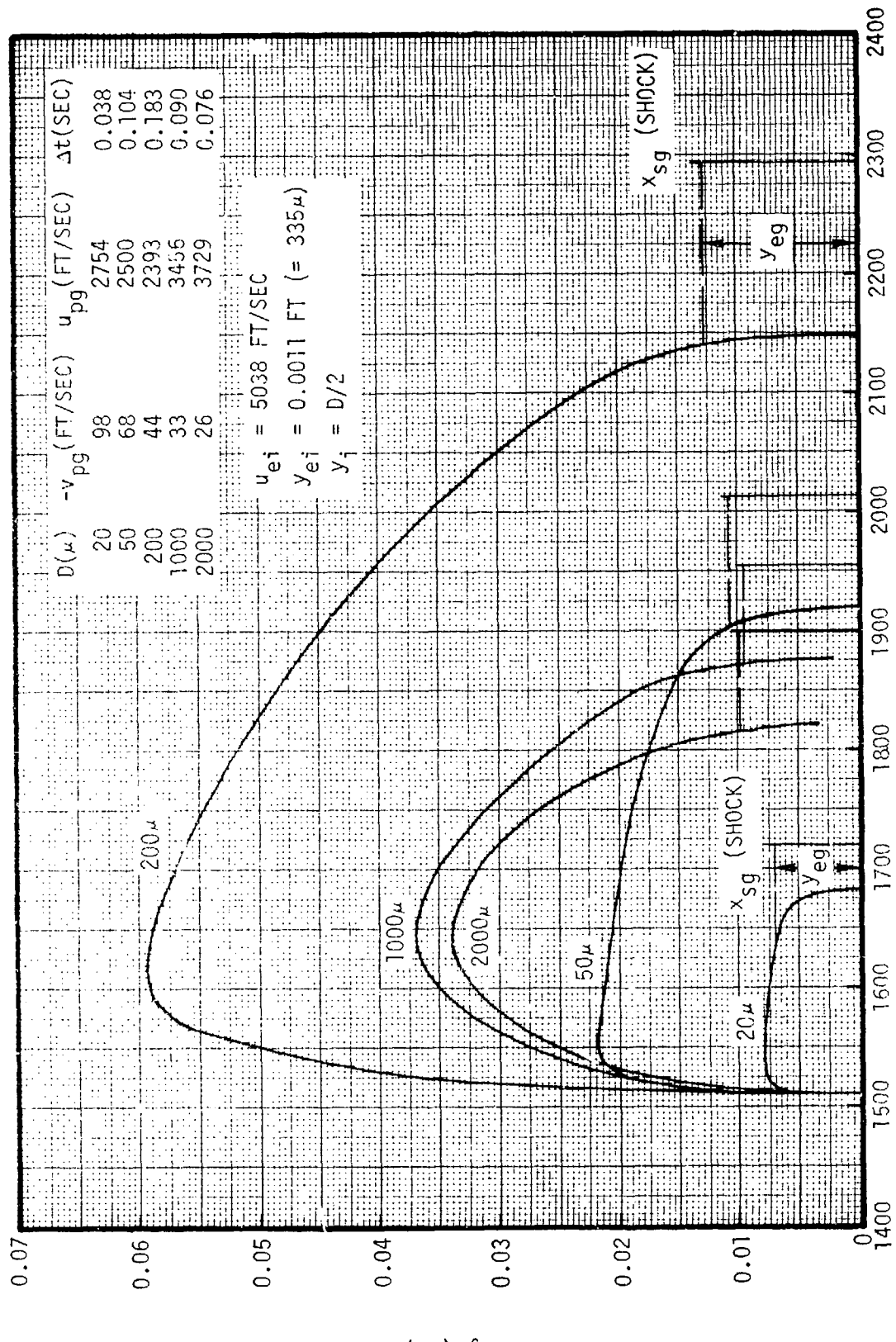

FIGURE 3-2 PARTICLE TRAJECTORY FOR A 1.0 MEGATON EXPLOSION WITH INITIAL TIME 0.1 SECOND AFTER EXPLOSION AND INITIAL DISTANCE 1 FOOT BEHIND SHOCK

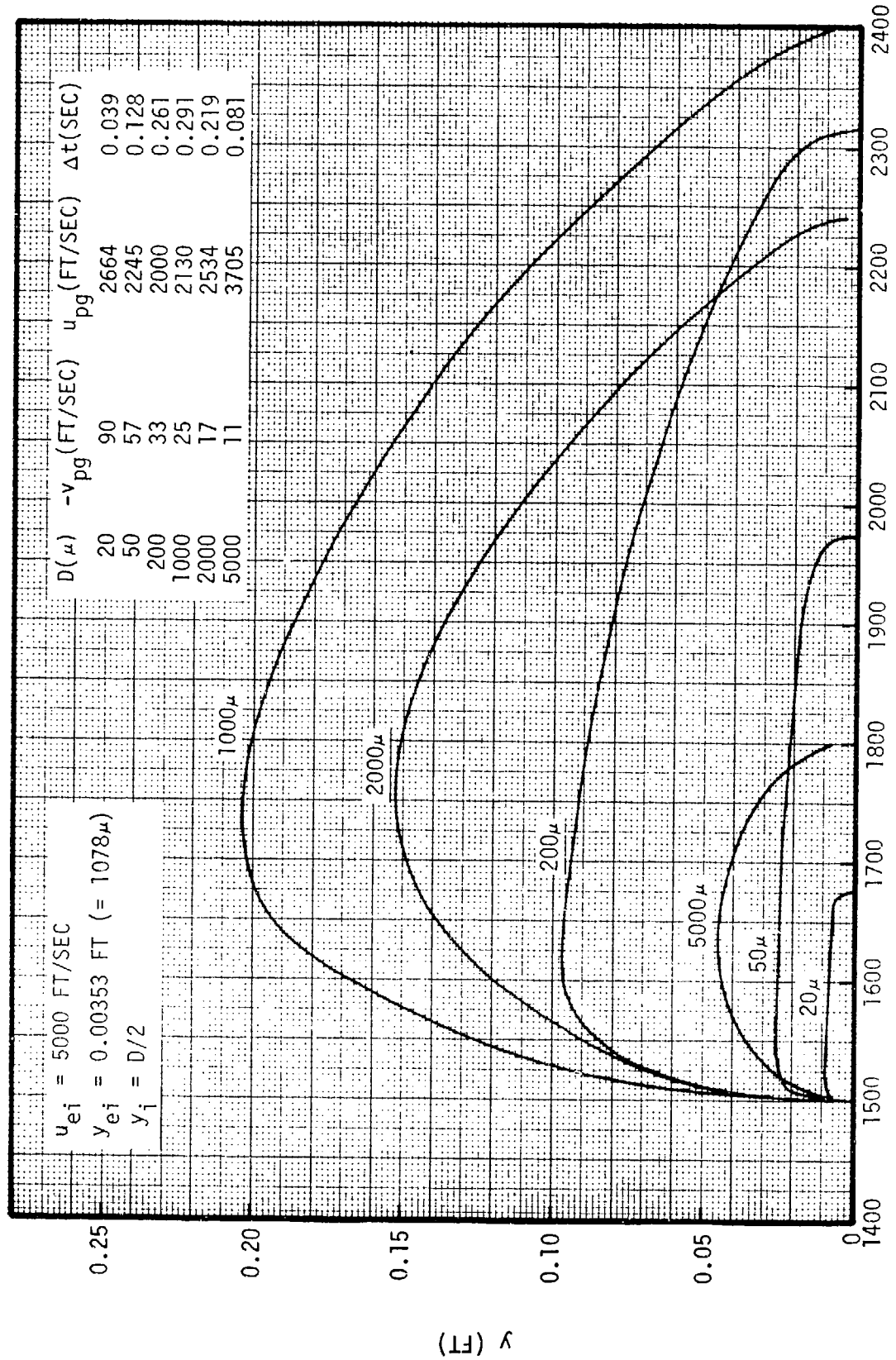

FIGURE 3-3 PARTICLE TRAJECTORY FOR A 1.0 MEGATON EXPLOSION WITH INITIAL TIME 0.1 SECOND AFTER EXPLOSION AND INITIAL DISTANCE 10 FEET BEHIND SHOCK

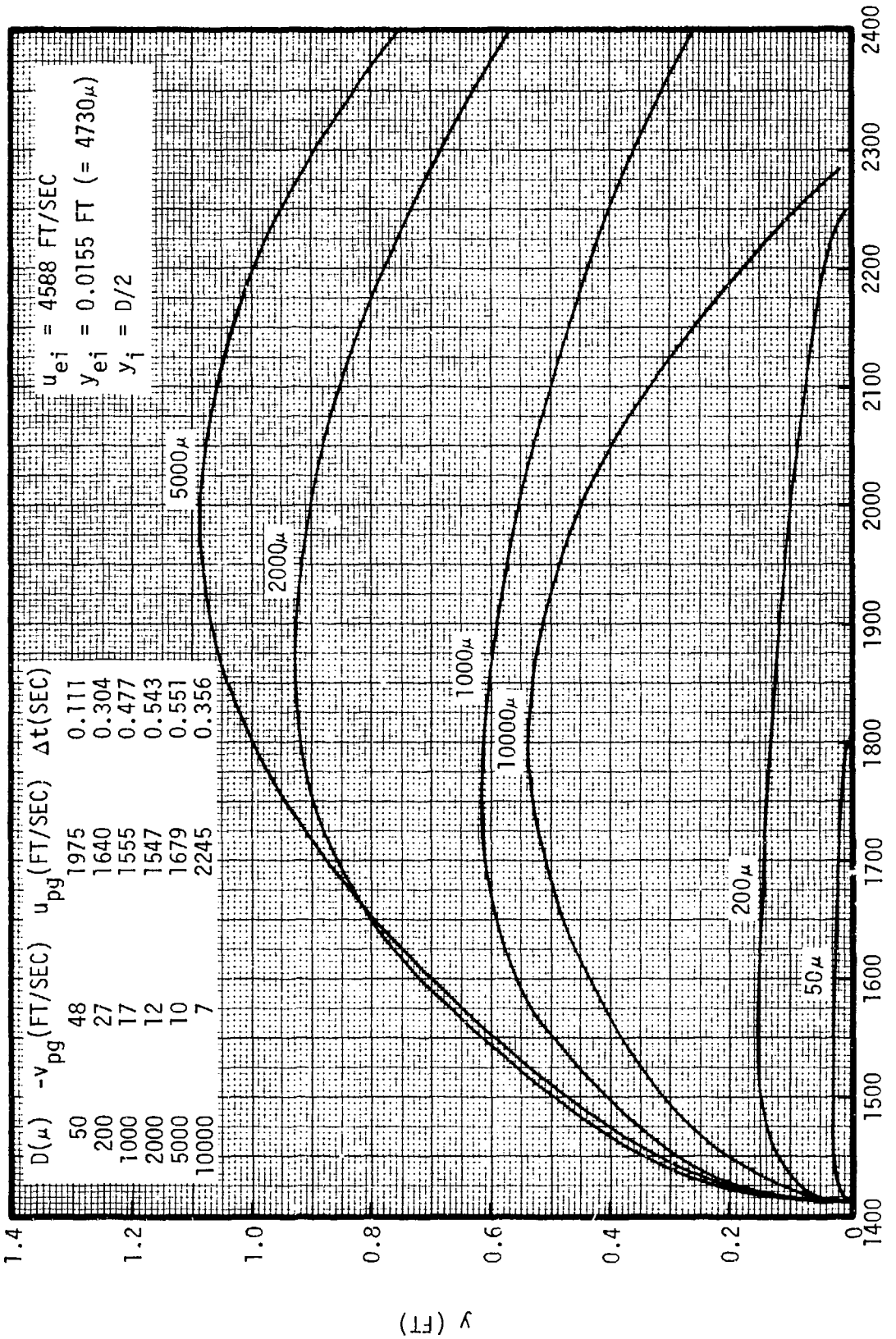

FIGURE 3-4 PARTICLE TRAJECTORY FOR A 1.0 MEGATON EXPLOSION WITH INITIAL TIME 0.1 SECOND AFTER EXPLOSION AND INITIAL DISTANCE 100 FEET BEHIND SHOCK

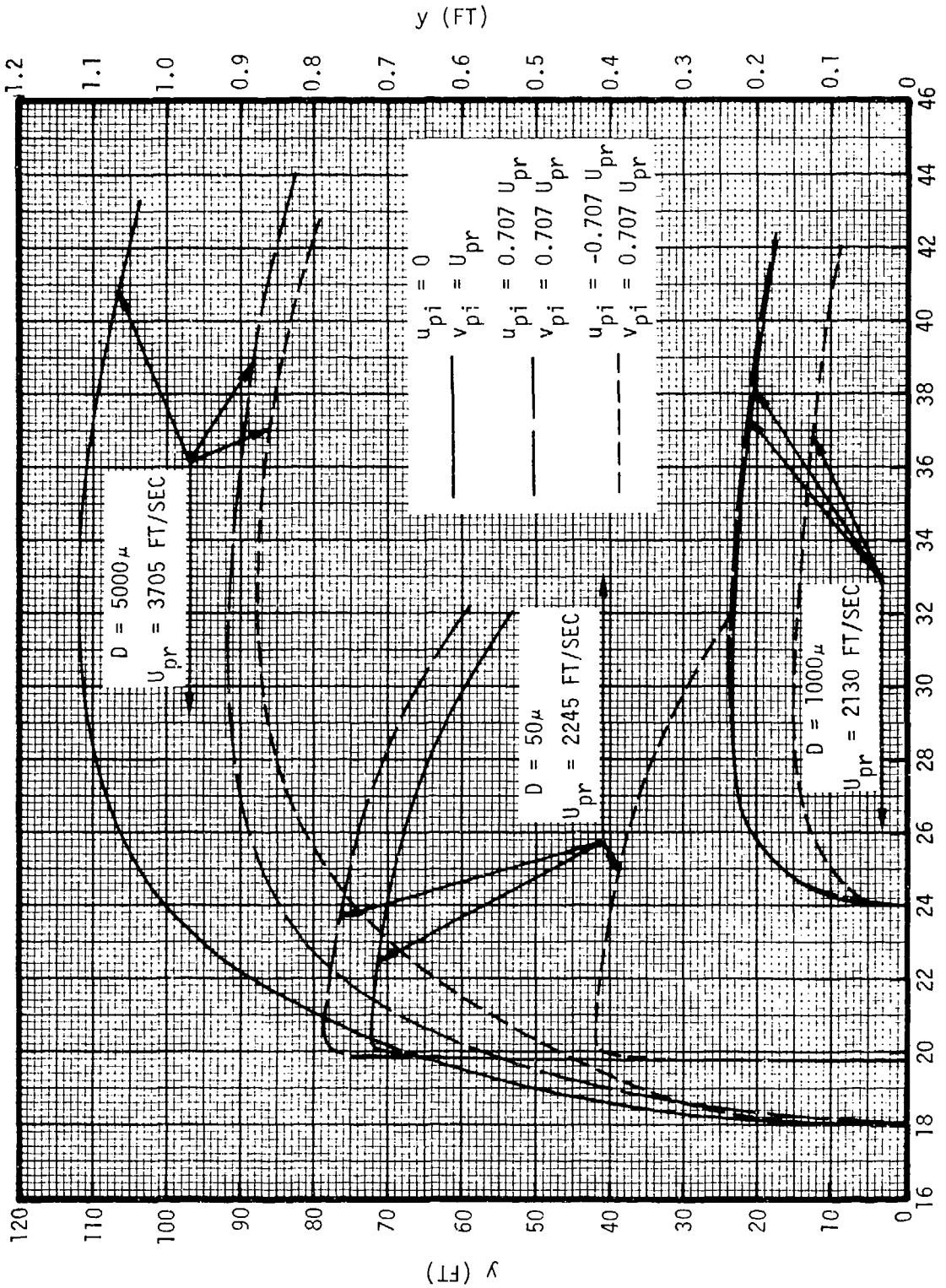

FIGURE 3-5 PARTICLE REBOUND TRAJECTORY

4. EROSION ESTIMATES

In order to analyze rigorously the amount of soil erosion due to aerodynamic entrainment, it is necessary to solve the coupled two-phase (particles-gas) Navier-Stokes equations. The development of such a solution for the blast flowfield appears prohibitive at present, however, since even the simple case of erosion over a flat plate has not been solved. Here, only an extremely simple model is used to estimate erosion. The model is similar to the one first employed by Roberts[5] in regard to soil erosion by a lunar landing vehicle, and it can be written as

$$fu \frac{dm}{dt} = \tau_o - \tau^* \tag{4-1}$$

where f is interpreted as a dimensionless average momentum of the entrained particles, u is a gas velocity, dm/dt is the rate of mass entrained per unit area, τ_o is the shear stress on the surface without dust entrainment, and τ^* is the reduced shear stress due to the presence of dust entrainment. Equation (4-1) states that the impulse due to shear $[(\tau_o - \tau^*)dt]$ is converted into particle momentum with the particle velocity being fu. The value τ^* represents the soil's resistive shear stress to erosion, and depends on the soil properties such as particle size, cohesiveness, etc. The value of f is difficult to analyze; in fact it partly depends on the definition of mass erosion. If only those particles that reach high altitude are considered, then f should be close to 1.0 since only the particles with initial velocities that are comparable to the gas velocity can be lifted to significant height. On the other hand, a great many particles that are lifted off a surface according the results of Section 2 are confined within a short distance from the surface; these particles have lower velocities as they leave the boundary layer and f should be substantially less than 1.0. In this section, f is taken as an arbitrary constant and τ^* is neglected when it is compared to τ_o. The total mass M eroded is then given by

$$M = \frac{1}{f} \int_t \int_A \frac{\tau_o}{u} \, dA dt \tag{4-2}$$

Using the results of Part I of this study (laminar boundary layer integral polynomial solution) for τ_o and Sedov's strong shock expression for u, it is

found that for a spherical explosion

$$M = \frac{1.16}{f}\left(\frac{\gamma+1}{2}\frac{\mu_\infty}{p_\infty}\right)^{1/2}\rho_\infty C^3 t^{0.7} \qquad (4\text{-}3)$$

where γ is the ratio of the gas specific heats, C is a constant which depends on the explosion strength, and u_∞, p_∞, and ρ_∞ denote the gas viscosity, pressure, and density, respectively, at ambient conditions. Since C varies with the explosion energy E to the 0.2 power, Equation (4-3) shows M to vary with E to the 0.6 power. Also, M varies with time t to the 0.7 power. Here, t is bounded by the time when the shock is no longer strong or when the soil τ^* exceeds τ_o. Consider a 1.0 megaton explosion (i.e., $C \simeq 3800$ ft/sec$^{0.4}$) in ambient air and take t = 1.0 second. Then $M = 35\ f^{-1}$ tons. Hence if f is close to 1.0, M is very small (compared to mass ejected due to cratering). However, if the particle velocity is taken as the vertical velocity due to boundary layer lift, then $f \simeq K^{1/2}$ where $K \simeq 0.001$. This yields M = 1,100 tons for laminar boundary layer shear.

It may be mentioned that the total impulse delivered to the surface due to aerodynamic shear is found to be (for laminar boundary layer):

$$\int_t \int_A \tau_o dA dt = 1.82\left(\frac{\gamma+1}{2}\frac{\mu_\infty}{p_\infty}\right)^{1/2} \rho_\infty C^{0.4}\ t^{0.1} \qquad (4\text{-}4)$$

For a 1.0 megaton explosion in ambient air and t = 1.0 second, the total impulse is equal to 4.15×10^8 lb-ft/sec. If the mass eroded, M, is taken to be equal to this impulse divided by some effective average particle velocity, then M is proportional to $E^{0.8}$ (since $C \sim E^{0.2}$) and $t^{0.1}$; whereas in Equation (4-3), M is proportional to $E^{0.6}$ and $t^{0.7}$.

The numbers given in the two preceeding paragraphs are for laminar flow. For turbulent flow, the values for M is expected to increase by at least one order of magnitude. Although the assessment of soil erosion behind the turbulent blast wave should probably be performed only after the turbulent boundary layer solution is obtained, it may be interesting to make a prediction by employing a simple model and available experimental data. Consider the model

$$\frac{dm}{dt} = \beta\ \rho_s \left(\frac{\rho}{\rho_\infty}\right) u \qquad (4\text{-}5)$$

where β is a constant. Equation (4-5) states that the mass erosion rate is proportional to the free-stream velocity. This model is similar to that employed in Reference 6, except particle size and terminal particle velocity are not considered and a factor ρ/ρ_∞ is inserted to account for the varying density behind a blast wave. The mass eroded, M, then becomes

$$M = \beta \rho_s \int_A \int_t \left(\frac{\rho}{\rho_\infty}\right) u \, dAdt \tag{4-6}$$

Using the Sedov solution for ρ and u for a spherical explosion, it is found that

$$M = 0.55\beta\rho_s C^3 t^{1.2} \tag{4-7}$$

Here, M is proportional to C^3 (or $E^{0.6}$) and $t^{1.2}$. Refering to the experimental data of Reference 6, one may suspect that β is far from being a constant and may vary between, say, 10^{-5} and 10^{-3}. In fact, β for loose soil is about one order in magnitude higher than that for compact soil. For a given soil, β varies with u. One may suspect that the scatter in data for β is at least partly due to the data correlation in which the direct effects of boundary layer growth are not taken into account. Taking $\beta = 6 \times 10^{-5}$ and $\rho_s = 145$ lb/ft^3, it is found that $M = 1.32 \times 10^5$ tons for a 1.0 megaton explosion and t = 1.0 second.

(Reverse of Page is Blank)

5. DISCUSSION AND CONCLUSIONS

Using a lift coefficient of $C_L = a(u - u_p)^{-1}$ (du/dy) for boundary layer aerodynamic lift, it is found in the present study that a particle initially at rest can attain a vertical velocity of only $K^{1/2}$ times the free-stream gas velocity where K is equal to $3\rho/8\rho_s$. A similar vertical velocity is attained if a particle is initially imbedded in the soil and if the pressure difference between the soil and the free-stream is equal to the dynamic pressure. Also, spinning of a particle may generate a Bernoulli force for which the lift coefficient is similar to that due to shear.

The analytical results of Section 2, which are for constant flow conditions, may be applied to obtain rough estimates of particle motion due to boundary layer lift behind blast waves. The reason for this is that a particle stays in the gas, especially inside the boundary layer, for only a short time within which the fluid properties, including the boundary layer thickness, experienced by the particle do not change drastically.

For given flow conditions and a given particle size, the aerodynamic lift is not sufficient to overcome the particle weight to lift the particle if the boundary layer thickness is either too small or too large. Particles that are more readily entrained are those with diameters of the order of the boundary layer thickness.

In general, particles are not lifted more than a few inches above the ground except for early times after explosion when the gas velocity is high and/or at locations far away from the shock (but not too far) where the boundary layer is thick and the gas velocity and density are still high. However, at early times after explosion or at distances near the explosion point, the temperature is extremely high and the lifted particles (especially the small ones) soon vaporize.

As a particle is lifted off a surface, it attains a very high horizontal velocity. Although it reaches a vertical height of only a few inches and stays in the gas for only a fraction of a second, it may travel a horizontal distance of a few hundred feet before returning to the ground. It impacts the ground about horizontally at a high speed. The height reached by the particle after rebounding from the ground is still small for small particles (say less than 100 microns in diameter) because of drag

effects, but the height can be on the order of a few hundred feet for large particles (say 1000's of microns in diameter). The particles after rebounding can remain in the gas for several seconds. Thus, although lift may not directly contribute significantly to particle density in a nuclear cloud, it can aid the particle in acquiring a high rebounding velocity. The particles after rebound can stay in the gas sufficiently long to be carried to great heights by a rising nuclear cloud.

In the present study on particle lift, the vertical component of the gas velocity has been neglected. This vertical velocity may substantially increase the particle vertical velocity, especially for small particles, in the regions of thick boundary layers. Turbulent diffusion also aids entrainment of small particles.

The amount of soil erosion due to laminar boundary layer entrainment is estimated to be small, say about one thousand tons for a one megaton explosion. However, for turbulent boundary layers, an increase by two orders of magnitude appears possible.

REFERENCES

1. Bagnold, R. A., The Physics of Blown Sands and Desert Dunes, Methuen and Co., London, 1941.

2. Chepil, W. S., "Dynamics of Wind Erosion," Soil Sci., Vols. 60 and 61, 1945.

3. Owen, P. R., "Saltation of Uniform Grains in Air," J. Fluid Mech., Vol. 20, 1964, pp. 225-242.

4. Vidal, R. J., "Aerodynamic Processes in the Downwash-Impingement Problem," J. Aerospace Sci., Vol. 29, 1962, pp. 1067-1076; and AIAA Journal, Vol. 1, 1963, pp. 726-727.

5. Roberts, L., "The Action of a Hypersonic Jet on a Dust Layer," IAS Paper No. 63-50, 1963.

6. Swatosh, J. J. Jr., and Wiedermann, A. A., "Nuclear Weapons Effects: Dust and Air-Temperature Environmental Studies (U)," Summary Final Technical Report J6012-2A, Illinois Institute of Technology Research Institute, April 1970, (Secret).

7. Trulio, J. G., McKay, M. W., and Carr, W. E., "Lofting of Solid Material by Vaporization, Thermal Expansion and Crater Splash in a Near-Surface Burst," DASA Report Number 2270, February 1969.

8. Quan, V., "Blast Wave Turbulent Boundary Layers," IOC 70.4333.2-104, TRW Systems, 31 August 1970.

9. Vennard, J. K., Elementary Fluid Mechanics, 4th Edition, John Wiley and Sons, Inc., 1961.

10. Torobin, L. B., and Gauvin, W. H., "Fundamental Aspects of Solid Gas Flow," Canadian J. of Chem. Engin., 1959 and 1960.

11. Carlson, D. J., and Hoglund, R. F., "Particle Drag and Heat Transfer in Rocket Nozzles," AIAA Journal, 1964, pp. 1980-1984.

12. Crowe, C. T., "Drag Coefficient of Particles in a Rocket Nozzle," AIAA Journal, 1967, pp. 1021-1022.

13. Eickhorn, R., and Small, S., "Experiments on the Lift and Drag of Spheres Suspended in a Poiseuille Flow," J. Fluid Mech., Vol. 20, 1964, pp. 513-527.

14. Saffman, P. G., "The Lift on a Small Sphere in a Slow Shear Flow," J. Fluid Mech., Vol. 22, 1965, pp. 385-400.

15. Hall, I. M., "The Displacement Effect of a Sphere in a Two-Dimensional Shear Flow," J. Fluid Mech., Vol. 1, 1956, pp. 142-162.

TRW, INC.
DISTRIBUTION LIST

	Copy/s No.
DEPARTMENT OF DEFENSE	
Director Advanced Research Projects Agency Architect Building 1400 Wilson Blvd. Arlington, Virginia 22209	1
Assistant to the Secretary of Defense (Atomic Energy) Washington, D.C. 20301	
Attn: Document Control	1
Director Defense Atomic Support Agency Washington, D.C. 20305	
Attn: APSI (Archives)	1
Attn: SPSS	2
Attn: J-3	1
Attn: DDST	1
Attn: APTL (Technical Library)	2
Administration Defense Documentation Center Cameron Station - Building 5 Alexandria, Virginia 22314	
Attn: Document Control	2
Director Defense Intelligence Agency Washington, D.C. 20301	
Attn: DI-7B, Phys. Vul. Div., Mr. Edward O. Farrell	1
Attn: DT-2 Weapons and Systems Division	1
Director of Defense Research & Engineering Washington, D.C. 20301	
Attn: Asst. Dir. (Nuclear Programs), Dr. William W. Carter	1
Attn: Asst. Dir. (Strategic Weapons), Mr. Ben T. Plymale	1
Commander Field Command Defense Atomic Support Agency Sandia Base Albuquerque, New Mexico 87115	
Attn: FCWD-C	1
Attn: Technical Library, FCWS-SC	1

Copy/s No.

DEPARTMENT OF DEFENSE (Continued)

Commandant
Industrial College of the Armed Forces
Fort Lesley J. Mc Nair
Washington, D.C. 20315
Attn: Document Control — 1

Director Joint Strategic Target Planning Staff
Offutt AFB
Omaha, Nebraska 68113
Attn: JLTW — 1

Chief
Livermore Division, Field Command Dasa
Lawrence Radiation Laboratory
P.O. Box 808
Livermore, California 94550
Attn: FCWD-D — 1
Attn: Document Control — 2

Commandant
National War College
Fort Lesley J. Mc Nair
Washington, D.C. 20315
Attn: NWCLB-CR — 1

Commander
Test Command
Defense Atomic Support Agency
Sandia Base
Albuquerque, New Mexico 87115
Attn: Document Control — 2

Director
Weapons Systems Evaluation Group, ODDR&E
Office, Secretary of Defense
400 Army-Navy Drive
Washington, D.C. 20305
Attn: Capt. Donald E. McCoy, USN — 1

Commanding Officer
901st MI
Sandia Base
Albuquerque, New Mexico 87115
Attn: Document Control — 1

Copy/s No.

DEPARTMENT OF THE ARMY

Director
Advanced Ballistic Missile Defense Agency
Commonwealth Bldg.
1320 Wilson Blvd.
Arlington, Virginia 22209
Attn: CRDABM-NE, LtC James H. Sloan 1
Attn: John Shea 1

Commanding General
Army Engineer Center
Fort Belvoir, Virginia 22060
Attn: ATSEN-SY-L 1

District Engineer
Army Engineer District, Omaha
215 N. 17th Street
Omaha, Nebraska 68102 1

Division Engineer
Army Engineer Division, Huntsville
P.O. Box 1600, West Station
Huntsville, Alabama 35807
Attn: HNDSE-R, Mr. Michael M. Dembo 1

Division Engineer
Army Engineer Division, Ohio River
P.O. Box 1159
Cincinnati, Ohio 45201
Attn: Document Control 1

Commanding Officer
Army Engineer Nuclear Cratering Group
Lawrence Radiation Laboratory
Livermore, California 94550
Attn: Document Control 1

Director
Army Engineer Waterways Experiment Station
Box 631
Vicksburg, Mississippi 39180
Attn: Mr. W. Flathau 1
Attn: Mr. J. G. Jackson 1
Attn: Research Center Library 1

Commanding Officer
Army Mobility Equipment R and D center
Fort Belvoir, Virginia 22060 1

Copy/s No.

DEPARTMENT OF THE ARMY (Continued)

Chief
Army Nuclear Effects Laboratory
Edgewood Arsenal, Maryland 21010
Attn: AMXRD-BNL, Technical Library 1

Commandant
Army War College
Carlisle Barracks, Pennsylvania 17013
Attn: Library 1

Assistant Chief of Staff for Force Development
Department of the Army
Washington, D.C. 20310
Attn: Director of Chemical and Nuclear Operations 1

Director
Ballistic Research Laboratories
Aberdeen Proving Ground, Maryland 21005
Attn: Document Control 2

Chief of Engineers
Department of the Army
Washington, D.C. 20314
Attn: ENGMC-ED 1
Attn: ENGME-RD 1

Chief of Research & Development
Department of the Army
Washington, D.C. 20310 1

Director of Civil Defense
Department of the Army
Washington, D.C. 20310
Attn: Staff Director, RE(SR), Mr. George N. Sisson 1

Safeguard System Manager
Safeguard System Office
1320 Wilson Blvd.
Arlington, Virginia 22209
Attn: Dr. John Shea 1

Commanding Officer
U.S. Army Combat Developments Command
Institute of Nuclear Studies
Fort Bliss, Texas 79916
Attn: CDINS-E 1

Copy/s No.

DEPARTMENT OF THE ARMY (Continued)

Commanding Officer
U.S. Army Materials & Mechanics Research Center
Watertown, Massachusetts 92172
Attn: Dr. Arfon Jones 1

Commanding General
U.S. Army Materiel Command
Washington, D.C. 20315
Attn: AMCRD-BN 2

DEPARTMENT OF THE NAVY

Chief of Naval Operations
Navy Department
Washington, D.C. 20350
Attn: OP-03EG 1
Attn: OP-75 2

Chief of Naval Research
Department of the Navy
Arlington, Virginia 22217 1

Commanding Officer
Naval Civil Engineering Laboratory
Port Hueneme, California 93041
Attn: Mr. J. Allgood 1
Attn: Code L31 1

Commander
Naval Facilities Engineering Command
Headquarters
Washington, D.C. 20390
Attn: Code 04B, Chief Engineer, Mr. William J. Bobisch 1
Attn: Code 03A, Chief Research Eng., Mr. Stanley Rockefeller 1

Commander
Naval Ordnance Laboratory
Silver Spring, Maryland 20910
Attn: Code 240, Mr. C. J. Aronson 1
Attn: Code 243, Mr. Frederick J. Gleason 1
Attn: Code 242, Mr. Irving Kabik 1

Commander
Naval Ordnance Systems Command
Headquarters
Washington, D.C. 20360
Attn: ORD-91313, Library 1

Copy/s No.

DEPARTMENT OF THE NAVY (Continued)

Superintendent
Naval Postgraduate School
Monterey, California 93940
Attn: Code 2124, Technical Reports Librarian 1

Director
Naval Research Laboratory
Washington, D.C. 20390
Attn: Code 1065, Classified Material Control Branch 1

Commanding Officer
Naval School
Civil Engineer Corps Officers
Naval Construction Battalion Center
Port Hueneme, California 93041
Attn: Document Control 1

Commander
Naval Ship Engineering Center
Center Building
Prince Georges Center
Hyattsville, Maryland 20782
Attn: Document Control 1

Commander
Naval Ship Research and Development Center
Washington, D.C. 20034
Attn: Code L42.3, Library 1

President
Naval War College
Newport, Rhode Island 02840
Attn: Document Control 1

Commander
Naval Weapons Center
China Lake, California 93555 1

Director
Strategic Systems Project Office
Navy Department
Washington, D.C. 20390
Attn: SP-272, CDR Robert J. Stinner, Section Head 1

DEPARTMENT OF THE AIR FORCE

Commander
Aerospace Defense Command
Ent AFB, Colorado 80912
Attn: XPOW, Advanced Planning Division 1
Attn: XP, DCS/PLANS 1

	Copy/s No.
DEPARTMENT OF THE AIR FORCE (Continued)	
AF Armament Laboratory, AFSC Eglin AFB, Florida 32542 Attn: ADLRW, Mr. W. H. Dittrich	1
AF Weapons Laboratory, AFSC Kirtland AFB, New Mexico 87117	
Attn: Dev, Dr. M. A. Plamondon	1
Attn: DE-I	1
Attn: Dev, Dr. Henry Cooper	1
Attn: DOGL, Technical Library	1
Headquarters Air Force Systems Command Andrews AFB Washington, D.C. 20331	
Attn: DLTW	1
Attn: SDME	1
Commander Armament Development & Test Center Eglin AFB, Florida 32542	
Attn: ADBRL-2	1
Chief of Staff U.S. Air Force Washington, D.C. 20330	
Attn: PRE (Director of Civil Engineering)	1
Attn: RDQPN (S/V & Nuclear Programs Division)	1
Attn: RDPM (Missile Systems Div., Dir. of Dev. & Acq.)	1
Attn: INATA (Dissemination Request Research Branch)	1
Detachment 37 (ORA) AFSC Holloman AFB, New Mexico 88330	
Attn: RRRD	1
Commander Rome Air Development Center, AFSC Griffiss AFB, New York 13400	
Attn: EMTLD, Documents Library	1
Attn: EMREC, Mr. R. W. Mair	1
Commander Space and Missile Systems Organization (SAMSO) Los Angeles, California 90045	
Attn: CCD	1

Copy/s No.

DEPARTMENT OF THE AIR FORCE (Continued)

Space and Missile Systems Organization, AFSC
Norton AFB, California 92409
- Attn: MMN, Engineering Division — 1
- Attn: RNS, Systems Definition Division — 1
- Attn: SYSN, Survivability Program Manager — 1
- Attn: MMH, Hard Rock Silo Development — 1

Commander
Strategic Air Command
Offutt AFB, Nebraska 68113
- Attn: OAI — 1
- Attn: XPFS — 1

ATOMIC ENERGY COMMISSION

Los Alamos Scientific Laboratory
P.O. Box 1663
Los Alamos, New Mexico 87544
- Attn: Document for Report Library — 1

Sandia Laboratories
P.O. Box 5800
Albuquerque, New Mexico 87115
- Attn: Document Control for Dr. Walter Herrmann — 1
- Attn: Document Control for Dr. M. L. Merritt — 2

U.S. Atomic Energy Commission
Albuquerque Operations Office
P.O. Box 5400
Albuquerque, New Mexico 87115
- Attn: Document Control — 1

U.S. Atomic Energy Commission
Nevada Operations Office
P.O. Box 14100
Las Vegas, Nevada 89114
- Attn: Document Control for Technical Library — 1

U.S. Atomic Energy Commission
Washington, D.C. 20545
- Attn: Document Control for Classified Technical Library — 1
- Attn: Document Control for Classified Tech. Info. Serv. — 1

University of California
Lawrence Radiation Laboratory
Technical Information Division
P.O. Box 808
Livermore, California 94550
- Attn: Dr. J. T. Cherry, L-47 — 1
- Attn: Dr. Lawrence S. Germain, L-18 — 1

Copy/s No.

OTHER GOVERNMENT

Department of the Interior
Bureau of Mines
Bldg. 20, Denver Federal Center
Denver, Colorado 80225
Attn: Science Advisor-Mining Research, Dr. Leonard A. Obert 1

DEPARTMENT OF DEFENSE CONTRACTORS

Aerospace Corp.
P.O. Box 5866
San Bernardino, California 92408
Attn: Mr. Warren Pfefferle 1
Attn: Dr. Mason B. Watson 1

Aerospace Corporation
P.O. Box 95085
Los Angeles, California 90045
Attn: Technical Information Services 2

Agbabian-Jacobsen Associates
8939 South Sepulveda Blvd.
Los Angeles, California 90045
Attn: Dr. J. Isenberg 1
Attn: Document Control 1

Analytic Services, Inc.
5613 Leesburg Pike
Falls Church, Virginia 22041
Attn: George Hesselbacher 1

Applied Theory, Inc.
1010 Westwood Blvd.
Los Angeles, California 90024
Attn: Security Officer 1

Avco
Government Products Group
201 Lowell Street
Wilmington, Massachusetts 01887
Attn: Research Library, A830, Room 2201 1

Battelle Memorial Institute
505 King Avenue
Columbus, Ohio 43201
Attn: Mr. R. W. Klingesmith 1

The Boeing Company
P.O. Box 3707
Seattle, Washington 98124
Attn: Mr. John Blaylock 1
Attn: Dr. R. Hager 1

Copy/s No.

DEPARTMENT OF DEFENSE CONTRACTORS (Continued)

Computer Sciences Corporation
P.O. Box 530
6565 Arlington Blvd.
Falls Church, Virginia 22046
Attn: Mr. O. A. Israelsen 1

EG&G, Inc.
P.O. Box 227
Bedford, Massachusetts 01730
Attn: Document Control Center for Mr. Donald F. Hansen 1

Engineering Physics Company
12721 Twinbrook Parkway
Rockville, Maryland 20852
Attn: Dr. Vincent J. Cushing 1

General American Transportation Corporation
General American Research Division
7449 N. Natchez Avenue
Niles, Illinois 60648
Attn: Dr. G. L. Neidhardt, Manager of Engineering 1

General Electric Company
Tempo-Center for Advanced Studies
816 State Street
Santa Barbara, California 93102
Attn: DASA Information & Analysis Center, W. Chan 2

General Electric Company
Space Division
Valley Forge Space Center
P.O. Box 8555
Philadelphia, Pennsylvania 19101
Attn: Dr. M. H. Bortner, Space Sci. Lab. 1

General Motors Corporation
Manufacturing Development
Manufacturing Staff
12 Mile and Mound Roads
Warren, Michigan 48090
Attn: Supervisor-Physics Engineering, Mr. William M. Isbell 1

General Research Corporation
P.O. Box 3487
Santa Barbara, California 93105
Attn: Technical Information Office for Mr. Benjamin Alexander 1

Copy/s No.

DEPARTMENT OF DEFENSE CONTRACTORS (Continued)

General Research Corporation
1501 Wilson Blvd.
Arlington, Virginia 22209
Attn: Dr. Giles F. Crimi 1

Gulf Energy & Environmental Systems, Inc.
P.O. Box 1111
San Diego, California 92112
Attn: Manager, TISD for Dr. Howard Kratz 1

IIT Research Insittute
10 West 35th Street
Chicago, Illinois 60616
Attn: Mr. Milton R. Johnson, Assistant Director of Research 1
Attn: Technical Library 1
Attn: Dr. R. E. Welch 1

Institute for Defense Analyses
400 Army-Navy Drive
Arlington, Virginia 22202
Attn: Technical Information Office 1

Kaman Sciences Corporation
Kaman Nuclear Division
1700 Garden of the Gods Road
Colorado Springs, Colorado 80907
Attn: Mr. Paul A. Ellis 1

Lockheed Missiles and Space Company
3251 Hanover Street
Palo Alto, California 94304
Attn: Dr. Roland E. Meyerott, Dir of Sci., Dept 50-01, Bldg 201 1

Lockheed Missiles and Space Company
Division of Lockheed Aircraft Corporation
P.O. Box 504
Sunnyvale, California 94088 1

The Mitre Corporation
Route 62 and Middlesex Turnpike
P.O. Box 208
Bedford, Massachusetts 01730
Attn: Document Control 1

Nathan M. Newmark
1114 Civil Engineering Bldg.
University of Illinois
Urbana, Illinois 61801 1

Copy/s No.

DEPARTMENT OF DEFENSE CONTRACTORS (Continued)

Physics International Company
2700 Merced Street
San Leandro, California 94577
Attn: Document Control for Mr. Fred M. Sauer, Dept. Manager 1
Attn: Document Control for Dr. Charles Godfrey, Vice President 1
Attn: Document Control for Mr. Michael McKay 1
Attn: Document Control for Dr. Steven Gill 1

The Rand Corporation
1700 Main Street
Santa Monica, California 90406
Attn: Dr. C. C. Mow 1
Attn: Dr. Albert L. Latter 1
Attn: Dr. Harold L. Brode 1
Attn: Mr. William B. Wright, Jr. 1

Research Analysis Corporation
McLean, Virginia 22101
Attn: Documents Library 1

Science Applications, Inc.
P.O. Box 2351
La Jolla, California 92037
Attn: Dr. Charles Stevens 1

Science Applications, Inc.
1901 North Fort Myer Drive
Suite 808
Arlington, Virginia 22209
Attn: Dr. William M. Layson 1

Shock Hydrodynamics, Inc.
15010 Ventura Blvd.
Sherman Oaks, California 91403
Attn: Mr. K. Kreyenhagen 1

Stanford Research Institute
333 Ravenswood Avenue
Menlo Park, California 94025
Attn: Dr. Donald R. Grine 1

Systems Science and Software, Inc.
P.O. Box 1620
La Jolla, California 92037
Attn: Document Control 1

Copy/s No.

DEPARTMENT OF DEFENSE (Contractors)

TRW Systems Group
One Space Park
Redondo Beach, California 90278
Attn: Dr. Peter Dai 1
Attn: Dr. Benjamin Sussholz 1
Attn: Mr. H. Jerry Carpenter (Bl. Rm 2211) 1

TRW Systems Group
San Bernardino Operations
P.O. Box 1310
San Bernardino, California 92402
Attn: Dr. J. L. Merritt, Manager, Facilities Engineering 1

URS Research Company
155 Bovet Road
San Mateo, California 94402
Attn: Mr. Harold Mason 1

Weidlinger, Paul, Consulting Engineer
110 East 59th Street
New York, New York 10022
Attn: Dr. Melvin L. Baron, Partner & Director of Research 1

DOCUMENT CONTROL DATA - R & D

(Security classification of title, body of abstract and indexing annotation must be entered when the overall report is classified)

1. ORIGINATING ACTIVITY *(Corporate author)*
TRW Systems Group
One Space Park
Redondo Beach, California 90278

2a. REPORT SECURITY CLASSIFICATION
Confidential

2b. GROUP
3

3. REPORT TITLE
AN ANALYSIS OF BLAST WAVE LAMINAR BOUNDARY LAYERS AND PARTICLE ENTRAINMENT

4. DESCRIPTIVE NOTES *(Type of report and inclusive dates)*
Final Report — 12 May 1970 to 11 December 1970

5. AUTHOR(S) *(First name, middle initial, last name)*
Victor Quan, Richard M. Traci, and John L. Farr, Jr.

6. REPORT DATE	7a. TOTAL NO. OF PAGES	7b. NO. OF REFS
11 December 1970	127	33

8a. CONTRACT OR GRANT NO.
DASA01-70-C-0135

b. PROJECT NO.
NWER XAXS

c.
Task and Subtask A001

d. Work Unit 10

9a. ORIGINATOR'S REPORT NUMBER(S)
16118-6002-R7-00

9b. OTHER REPORT NO(S) *(Any other numbers that may be assigned this report)*

10. DISTRIBUTION STATEMENT

11. SUPPLEMENTARY NOTES

12. SPONSORING MILITARY ACTIVITY
Director
Defense Atomic Support Agency
Washington, D. C. 20305

13. ABSTRACT

Part I. In the first part of this report, the laminar boundary layer flowfields generated by plane, cylindrical, and spherical strong blast waves are studied. Solutions are obtained using two different methods. In the first method, the governing equations are reduced to ordinary differential equations by using a similarity transformation and a parametric integral technique. In the second method, the assumptions of quasi-steady state and local similarity are invoked. Results obtained using each method are presented. A method of solving the turbulent boundary layer equations is also outlined in detail in this report.

Part II. The second part of the report is on particle entrainment. Using a lift force generated by the boundary layer velocity gradient, the particle velocity is estimated. Sample particle trajectories in strong blast wave flowfields are illustrated, and the amount of soil erosion due to aerodynamic entrainment is assessed.

Defense Threat Reduction Agency
45045 Aviation Drive
Dulles, VA 20166-7517

CPWC/TRC May 6, 1999

MEMORANDUM FOR DEFENSE TECHNICAL INFORMATION CENTER
ATTN: OCQ/MR WILLIAM BUSH

SUBJECT: DOCUMENT REVIEW

The Defense Threat Reduction Agency's Security Office has reviewed and declassified or assigned a new distribution statement:

- AFSWP-1069, **AD-341090**, STATEMENT A ~~AD~~ waiting for reply
- DASA-1151, AD-227900, STATEMENT A
- DASA-1355-1, **AD-336443**, STATEMENT A OK
- DASA-1298, AD-285252, STATEMENT A
- DASA-1290, AD-444208, STATEMENT A
- DASA-1271, AD-276892, STATEMENT A
- DASA-1279, AD-281597, STATEMENT A
- DASA-1237, AD-272653, STATEMENT A
- DASA-1246, AD-279670, STATEMENT A
- DASA-1245, AD-419911, STATEMENT A
- DASA-1242, AD-279671, STATEMENT A
- DASA-1256, AD-280809, STATEMENT A
- DASA-1221, AD-243886, STATEMENT A ~~AD~~
- DASA-1390, **AD-340311**, STATEMENT A
- ~~DASA-1283, AD-717097~~, STATEMENT A OK
- DASA-1285-5, AD-443589, STATEMENT A
- DASA-1714, AD-473132, STATEMENT A
- DASA-2214, AD-854912, STATEMENT A
- DASA-2627, AD-514934, STATEMENT A
- DASA-2651, AD-514615, STATEMENT A
- ~~DASA-2536, AD-876697, STATEMENT A~~
- DASA-2722T-V3, AD-518506, STATEMENT A
- DNA-3042F, AD-525631, STATEMENT A
- DNA-2821Z-1, AD-522555, STATEMENT A

If you have any questions, please call me at 703-325-1034.

Ardith Jarrett

ARDITH JARRETT
Chief, Technical Resource Center